Ultrasound Technique for the Dynamic Mechanical Analysis (DMA) of Polymers

vorgelegt von
B.Eng; MSc
Jarlath Mc Hugh
aus Longford, Irland

von der Fakultät III- Prozesswissenschaften
der Technischen Universität Berlin
zur Erlangung des akademischen Grades

Doktor der Ingenieurwissenschaften
- Dr.-Ing. -

genehmigte Dissertation

Promotionsausschuss:

Vorsitzender: Prof. Dr. rer. nat. H.-J. Hoffmann
Berichter: Prof. Dr.-Ing. M. H. Wagner
Berichter: Dr. rer. nat. habil. W. Stark

Tag der wissenschaftliches Aussprache: 24. Mai 2007

BERLIN 2007
D 83

To my Parents and Family
- *Thanks for your Support*

Abstract

The objective of this work is to demonstrate practical application and sensitivity of ultrasound as a high frequency Dynamic Mechanical Analysis DMA technique. Conventional DMA techniques typically employ dynamic shear or tensile loading at frequencies between 0.1 to 50 Hz and are commonly used to determine thermo-mechanical behaviour of polymers. In principle, wave propagation techniques for example using ultrasound sensors can also be employed for DMA of materials. Depending on type of wave propagated, shear $G´$, $G´´$, longitudinal $L´$, $L´´$ storage or loss modulus and $\tan(\delta)$ may be determined from the measured acoustic parameters sound velocity and attenuation. In contrast to conventional DMA for wave propagation techniques the influence of several additional factors need to be taken into account before accurate interpretation and quantitative evaluation of the results is possible. Factors considered include influence of high measurement frequency, dispersion, hysteresis, reflections at material boundaries, and change in material density as well as the influence of temperature on the experimental set-up. A wide range of experimental data was obtained by using different acoustic sensors operating in the frequency ranges from 400 to 800 kHz and 3 to 6 MHz. All experiments take place in a temperature range from 20 to 200°C on a fully cured epoxy. The ultrasound results are compared to the tensile moduli $E´$, $E´´$ and $\tan(\delta)$ measured using a conventional DMA technique operating at 0.1 to 33 Hz. Using different evaluation strategies such as the Williams Landel Ferry WLF equation it was possible to interpret the information available providing a unique opportunity to study the sensitivity of wave propagation to variations in the viscoelastic behaviour of a polymer.

Secondly using this background knowledge, experimental results are presented showing the sensitivity of ultrasound parameters to the polymerisation reaction and to the material state transformations gelation and vitrification. For these investigations an uncured epoxy material is used and cured over a range of temperatures. To support and verify conclusions information relating to the chemorheology of the resin system both Differential Scanning Calorimeter DSC and rheological techniques are employed. The results for all measurement techniques are summarised and presented as a function of degree of cure and with the aid of the Arrhenius relationship it is possible to evaluate the sensitivity of ultrasound as a DMA technique used to monitor the curing reaction.

Acknowledgements

Contents

Notation

<u>Symbols (by order of appearance)</u>

f	Frequency; functionality
λ	Wavelength (acoustics); adjustable parameter in Di Benedetto's equation
M^*	Complex modulus
$M'; M''$	Real and imaginary parts of the complex modulus
L^*	Complex longitudinal wave modulus
$L'; L''$	Real and imaginary parts of the complex longitudinal modulus
K^*	Complex bulk compression modulus
$L'; L''$	Real and imaginary parts of the complex bulk modulus
G^*	Complex shear modulus
$G'; G''$	Real and imaginary parts of the complex shear modulus
δ	Phase angle
$\tan(\delta)$	Loss Factor
A	Amplitude; Pre-exponential factor in Arrhenius equation
x	Direction of wave propagation
ρ	Density
ω	Angular frequency
α	Attenuation; degree of Cure (Conversion)
τ	Relaxation time; Transmission time (Acoustics)
c, c_p, c_g	Sound velocity, phase velocity and group velocity
a_T	Shift factor
k	Wave number; reaction rate
$Q_t; Q_\infty$	Partial and total heats of reaction
$C_1; C_2$	Parameters in WLF equation
s	Slope of a line
i	intercept of a plotted function
E_a	Activation energy
E_d	Activation energy for diffusion controlled reaction
λ	Wavelength (acoustics); Adjustable parameter in Di Benedetto's equation
T_g	Glass rubber transition temperature
T	Tension force; Temperature

d	Thickness
Z	Acoustic impedance
D	Transmission factor
R	Reflection factor; gas constant ($8.314 \, JK^{-1}mol^{-1}$)
τ_{Total}	Transmission time from sender to receiver
k_1, k_2	Chemical reaction rate constants
p_c	Critical point of epoxy conversion for gelation
$c_{p0}; c_{p\infty}$	Heat capacities of initial mixture and fully cured resin
n, m	Reaction orders
T_g	Glass transition temperature
T_{g0}	Glass transition temperature of the uncured resin
$T_{g\infty}$	Glass transition temperature of the fully cured resin
$_{gel}T_g$	Glass transition temperature at gel point
T_{cure}	Cure temperature
F_x	Segmental mobility for crosslinked polymer
F_m	Segmental mobility for uncrosslinked polymer
c	Concentration
N	Number of sample points
$\phi_{s1}; \phi_{s2}$	Phase angle for sample 1 and sample 2
τ	Shear stress
τ_0	Maximum shear stress
M_t	Torque
A	Stress factor
r	Radius
$\dot{\gamma}$	Strain rate
γ	Amplitude or displacement
γ_0	Maximum amplitude
σ	Stress
η	Steady state viscosity
η^*	Complex viscosity
$\eta'; \eta''$	Real and imaginary parts of the complex viscosity
η_{crit}	Critical value for viscosity
$\Delta H_{res}; \Delta H_T$	Residual and total heat of reaction

Abbreviations

A-Scan	Amplitude Scan or Oscillogram
BAM	Bundesanstalt für Materialforschung und –prüfung
	English translation: Federal Institute for Material Research and Testing
DMA	Dynamic Mechanical Analysis
DMTA	Dynamic Mechanical Thermal Analysis
DSC	Differential Scanning Calorimetry
US	Ultrasound
DEA	Di-Electric Analysis
DETA	Di-Electric Thermal Analysis
RTM	Resin Transfer Moulding
FFT	Fast Fourier Transformation
WLF	William Landel Ferry
TTT	Time Temperature Transformation
RTD	Resistance Temperature Detector (e.g. Pt 100)
DGEBA	Diglycidyl Ether of Bisphenol A
PMMA	Polymethylmethacrylate
PE	Polyethylene
IIW	International Institute of Welding
ASCII	American Standard Code for Information Interchange
DIN	Deutsches Institut für Normung
A/D	Analog to Digital Converter
VFT	Vogel Fulcher Tammann

Chapter 1

1 Introduction

Characterisation of mechanical properties of polymer materials using acoustics dates back to the late 1940's whereby A.W. Nolle was one of the first authors to discuss in detail the propagation of sound waves in rubber materials and also provide a solution to the wave equation taking into consideration damping of waves in polymers. It has been well documented (Ferry `53, `80; Papadakis `72) that by using longitudinal and shear wave propagation techniques the corresponding complex dynamic modulus of polymers may be determined. Considering the large amount of literature published over the last 50 years, it may seem surprising that research in this field still remains very important. Early studies cited in this chapter were mainly concerned with demonstrating the feasibility of various acoustic techniques for characterising the viscoelastic properties of polymers and were unsuited to practical implementation. In the last decade the renewed interest in acoustic techniques most likely results from advancements in sensors, hardware and evaluation technologies making the application of compact equipment a practical financial option for commercial production technologies. In the mid to late nineties an ultrasound transmission technique was developed at the BAM Berlin for the industrial process monitoring of thermosetting moulding compounds (Stark `97). To my awareness it is the only commercial acoustic equipment available at present (software, hardware and sensors) that has this capability. The instrument is presently in its third generation with several modifications in software and hardware mainly facilitating adaptations for commercial applications (Döring `01). The development of high temperature stable sensors capable of being mounted behind the mould wall and thus leaving no impression or markings on moulded components have opened new doors in terms of the potential to analyse polymers under adverse conditions (temperature and pressure) and in

confined spaces. Several examples can also be found relating to industrial applications in moulds for a range of materials and applications (Rath `00, Starke `05). More modern analytical publications (Lionetto `04a, `04b; Challis `00 and Döring `01) go a step further and compare several analysis techniques facilitating improved interpretation of acoustic parameters. However, the conclusions rely heavily on general correlations between often unrelated analysis techniques e.g. Differential Scanning Calorimetry DSC and Di-Electric Analysis DEA. This makes it difficult to assess the sensitivity of ultrasound parameters to changes in physical material properties such as the elastic modulus or transformations in curing epoxies such as gelation and vitrification.

The necessity for continued research in this field is reflected by the level of funding at BAM in the last 5 years for themes concerning, in foremost, the acoustic characterisation of polymer materials (including rubbers and polymer composites). Research grants (independent of my PhD funding) in this area totalled in the region of 400 k€. The vast majority of funding was spent on manpower mainly involved in the testing and analysis work (e.g. interpretation of acoustic results) using a variety of thermosetting materials and usually in combination with the development of application software. It is expected that the application of intelligent process control techniques such as ultrasound will gain in importance as the demand for complex engineering components constructed from fibre reinforced composites increases. The aerospace industry is an obvious market for sophisticated carbon fibre composite materials particularly as the use of lighter materials in aircraft construction allows for larger fuel savings or greater payloads. At present the Airbus A380 commercial aircraft employs an estimated 35 tonnes of CFRP (carbon fibre reinforced plastic) normally in combination with a thermosetting polymer matrix e.g. epoxy. For newer aircraft models in planning such as the Airbus A350 volume/weight ratios are guaranteed to increase. According to market forecasts[*] a rise in the worldwide production of carbon fibre from 25 to over 50 thousand tonnes per year is predicted in the next 5 years. One of the main reasons for this large prediction is the expected trend towards carbon fibre applications in the automobile branch which is the biggest growth industry in this sector. The versatility of the presented ultrasound technique and in particular the sensor has proved to be a huge advantage as it can be adapted to virtually all polymer moulding processes or laboratory applications. Additionally, as demonstrated in a recent EU project (McHugh `05) characterisation of polymers using ultrasound is not limited to reactive thermoset polymers. In the a forenamed project loaded/filled epoxies were developed for application in ultrasound phased array sensors employed at depths up to 10 km

---

[*] http://www.toray.com/ir/library/pdf/lib_a136.pdf: Market research forecasts from Toray Inc., Tokyo

in oil boreholes. The array sensors are currently being developed to detect corrosion or porosity in steel borehole piping. A major challenge in this project was to characterise and improve the acoustic and mechanical properties of epoxy based systems used in the array sensor at temperatures and pressures up to 180 °C and 1400 bar (caused by the large depths). To make decisions on the suitability of new and advanced epoxy polymer composites for such applications the mechanical properties were determined in this working range using a modified ultrasound technique and sensors integrated into a testing device placed in a high pressure autoclave.

This wide research spectrum provided a unique opportunity to study both the curing reaction and the influence of temperature on the mechanical properties of a fully cured epoxy. The common link between research projects is that a large change in viscoelastic properties will be observed. Although this background was extremely helpful, methodical and conclusive analysis of results could only realistically have been achieved in the framework of a funded PhD. This is mainly because of time constraints, project deadlines or restrictions such as disclosure agreements or choice of materials. In line with the above research projects, the overall goal of this work is to demonstrate the application and sensitivity of ultrasound as a high frequency Dynamic Mechanical Analysis DMA technique for analysis of polymer materials. To achieve this objective, experiments were performed on both a cured and a reactive epoxy system. The results on the cured epoxy as a function of temperature tend towards fundamental interpretation of acoustic parameters in terms of elastic modulus, taking factors such as measurement frequency, choice of parameters and evaluation of complex modulus type etc. into account. Secondly, by using this background knowledge the sensitivity of ultrasound parameters to the polymerisation reaction and for example transformations such as gelation and vitrification are investigated. The same epoxy polymer is employed throughout this work so that a correlation of results from experiments on the fully cured resin and the polymerisation (curing) reaction is possible, which as will be shown is very helpful in supporting conclusions. In the following two pages a more detailed breakdown of objectives is provided.

1.1 Objectives

Experimental results in Chapter 5.1 deal with fundamental questions relating to the application of ultrasound as a high frequency DMA technique for the characterisation of polymers. A fully cured epoxy with a glass to rubber transition at approximately 80 °C that is taken as tan(δ) maximum at 1 Hz is employed for these investigations. The advantage of using a cured epoxy is that its properties are thermally reversible so that consistent heating and cooling runs up to 200 °C are possible without adverse effects (e.g. degradation). Secondly, the glass transition region of the selected epoxy lies within the measurement range of all analysis techniques employed so that its influence on the elastic modulus may be studied over a large frequency range. Following topics are of major interest:

- Influence of measurement frequency on interpretation of results. This is investigated as function of temperature in the frequency range 0.1 to 50 Hz using conventional DMA with a dual cantilever setup. Using the Williams Landel Ferry WLF equation it is possible to predict the influence of measurement frequency on the ultrasound results.

- Determination of complex longitudinal and shear modulus as well as tan(δ) from sound velocity and attenuation measurements. Expression of acoustic parameters in terms of their representative moduli or tan(δ) is necessary to compare ultrasound measurements with conventional DMA at measurement frequencies between 0.1 and 33 Hz. All acoustic parameters are evaluated as a function of frequency and temperature using a specifically developed software package based on Fast Fourier Transformation FFT principles. Using this analysis technique, factors such as the influence of frequency on the measured sound velocity and attenuation are considered. Signal amplitude losses at material boundaries, for example due to reflection are also accounted for by employing a two sample measuring technique.

- Clarification of the relationship between ultrasound parameters and the complex modulus. For example, are measured attenuation values sufficient or should the results be expressed in terms of longitudinal loss L″ or tan(δ)? Furthermore, the longitudinal storage modulus L′ is typically evaluated from the measured sound velocity. However, L′ is a rather unfamiliar quantity. To determine the sensitivity of L′ it is compared to other more commonly used storage moduli as a function of temperature e.g. Shear G′, Bulk K′, and Tensile E′ modulus.

The measurement set-up and evaluation techniques presented needed to be adapted for experiments performed on a curing epoxy. In Chapter 5.2 a brief description relating to the accuracy and limitations of this new technique is provided. This technique is employed in Chapter 5.3 to measure the variations in ultrasound parameters that are related to changes in viscoelastic properties of epoxy polymers as a result of the curing reaction. Only isothermal cure is monitored over a range of temperatures using transducers operating in transmission mode at a middle frequency of 4 MHz. Interpretation of ultrasound results is possible when qualified information about the chemical reaction as well as the resulting changes in viscoelastic properties in terms of complex modulus is available. Two macroscopic phenomena gelation and vitrification usually mark the progress of this polymerisation process. The point at which growth and branching of polymer chains leads to a transition from a liquid state to a rubbery state is called gelation. At or about this transition an abrupt change in viscosity or complex modulus will be observed. As the reaction continues it typically slows as the glass transition temperature nears the set mould temperature. This gradual cessation of the reaction marks the transition from the rubbery to the glassy state of the curing material. The resin eventually solidifies unless further reaction is triggered by increasing the cure temperature. This transition is referred to as vitrification. From the perspective of a material processor it is important to follow the progression of the reaction and if possible identify the two phenomena, for example on the variation of a complex modulus curve. Taking the Resin Transfer Moulding RTM process as an example, fibre wetting must be completed well before gelation otherwise the viscosity of the resin will be too high to ensure optimal fibre impregnation whereas knowledge of vitrification times may be employed to optimise cure cycle times. Experiments are performed using a Differential Scanning Calorimeter DSC and a rheometer which are employed to obtain information relating to the degree of cure or progression of the polymerisation reaction and the resulting changes in viscoelastic properties and state transitions. The analysis techniques are based on different physical operating principles making a direct comparison very difficult. The Arrhenius relation that is valid for all techniques is employed to compare results. By combining results it is possible to determine the sensitivity of the ultrasound parameters to changes in the viscoelastic properties of the epoxy during the curing reaction and specifically to the material transformations at gelation and vitrification.

Chapter 2

2 Characterisation of the elastic properties of polymers using ultrasound

2.1 Literature Review and Background

2.1.1 Fundamental Development

Ultrasound as a non-destructive testing technique is normally associated with the detection of defects, cracking, pores etc. Acoustic techniques are also well suited for determining the effective values of elastic and viscous coefficients for polymer materials. All acoustic phenomena involve the vibrations of particles of a medium moving back and forth under the combination of stiffness and inertial forces. For crystalline materials a simple relationship describing elastic recovery exists: $M=\rho c^2$, whereby M represents the mechanical modulus, ρ the density and c is transversal or longitudinal sound velocity. On the other hand, viscoelastic materials such as polymers dissipate energy (anelastic behaviour) and wave propagation is attenuated. Therefore equations used to describe the relationship between wave propagation and modulus are expressed using a complex modulus M*. M* is a general term commonly used by authors in mathematical equations (Challis `02; Ferry `80; Hueter and Bolt `55) to represent various modulus types that will dependent on type of loading stress and include tensile E*; shear G*, bulk compression K* and longitudinal modulus L*. M* is described on the next page and is composed of two frequency dependent components $M'(\omega)$ is the real part

or storage modulus describing elastic components and M′′(ω) the imaginary part or loss modulus describing viscous components.

$$M^*(\omega) = M'(\omega) + iM''(\omega)$$

where the angular frequency ω=2πf and i=-1$^{1/2}$. A more detailed description is provided in Chapter 2.2.3 and this explanation is only used to promote a discussion of available background literature. Nolle (Nolle `47) formulated an equation that describes the relationship between the measured acoustic parameters sound velocity c and attenuation α and M′ or M′′ by *(ρ* is density):

$$M' = \rho c^2 \quad \text{and} \quad M'' = \frac{2\rho c^3 \alpha}{\omega} \qquad \text{(see Chapter 2.2.3)}$$

The general wave theory in combination with experimental evidence for propagation of bulk waves in polymers was mainly developed by the following authors Nolle `46-`52; Cunningham `56; Ivey `49 and Witte `49 as well as strong complimentary works from Maeda `55 and Kolsky `63. The mathematical derivation of the above formula is explained in Chapter 2.2.3 and as illustrated is only valid in this form if the term r = αc/ω<<1, otherwise more complex equations will have to be employed (see Eqs. 2.9 and 2.11). In standard textbooks it is automatically assumed that this statement is true on the basis of these early papers. However, a few points should be considered before accepting that this reduced equation is universally valid for polymers, which was not the conclusion of the forenamed authors. The early experiments from Nolle (Nolle `47) and Ivey (Ivey `49) were performed in transmission mode using longitudinal waves at frequencies ranging from kHz to MHz on different rubber mixtures. Generally measurements took place in a bath which depending on the required temperature was either filled with alcohol (T<0 °C) or water (T>0 °C). The liquids performed a double function, working as heating- as well as coupling medium between sensor and sample. Nolle and Ivey made the following general assumptions to simplify experiments:

- Attenuation is calculated from the amplitude ratio of the experimental apparatus with and without a sample according to Eq. 4.5. Sound velocity is measured by considering transmission times and sample thickness. This setup assumes no loss in amplitude as the sound wave passes from the coupling liquid into the sample. However, this statement is only valid if liquids of approximately the same acoustic

impedance of rubber are used and that the impedance relationship remains constant over the whole temperature measurement range (-40 to 70 °C). According to table values (Kräutkramer `89) a 10 dB loss in amplitude due to reflections is to be expected at a rubber/glycerine boundary. Different impedance values are also expected for water/rubber boundary.

- Scattering effects (on particle boundaries, Chapter 2.2.4) that may lead to both a variation in attenuation and sound velocity are not considered. The standard rubber employed contains several very different ingredients including filler, accelerator, sulphur etc. and the range of particle size is unknown.

- Changes in density are assumed to be negligible. From experience change in density would be expected to be less than 5 % in the temperature range employed.

Taking the above points into consideration there is at least reasonable doubt in regard to the accuracy of the above measurements. The cited authors typically quote peak values of $r = \alpha c/\omega$ of approx. 0.1 or slightly higher. Other authors (Maeda `55) quote attenuation values for PVC at $T_g$ of up to 20 dB/mm at 1600 m/s [$\lambda = 0.2$ mm] i.e. $r = 0.8$. From Kono (Kono, `60) maximum r values for Polystyrene of 0.11 are estimated (using $c = 1650$ m/s, $f = 2.25$ MHz and 8 dB/mm). Maximum values of $r > 0.11$ are very unusual in the literature and are only expected at high attenuation at temperatures in the vicinity of a molecular relaxation process such as the α relaxation. The published values are only valid for longitudinal wave propagation. It has been shown for shear wave propagation in rubber materials (Cunningham `56), that it is not unusual for r values to reach unity for soft rubber. The same author assumes that for r values greater than unity, shear waves will not propagate for example in soft materials or liquids (see Chapter 2.2.1). From the literature studied it remains uncertain if the statement $r << 1$ *is valid* for all polymers especially over a large temperature range e.g. 200 °C or in the region of molecular relaxations.

2.1.2 Characterisation of a Polymer's Elastic Properties using Ultrasound

The acoustic parameters relating to material elastic properties are obtained from the signal transmission times τ and amplitudes A through the sample. When the sample thickness is known, sound velocity c and attenuation α can easily be calculated (see Eqs. 4.6 and 4.7) and provide the basis for the calculation of a complex dynamic modulus. In the case of

longitudinal waves the following terms are employed to describe the complex storage L′ and loss L′′ modulus. The loss factor tan(δ) is also commonly used to describe material losses and is defined by the relationship L′′/L′. In general no standard parameters are employed to describe the material properties using ultrasound. For example several authors just use sound velocity and attenuation (Ferry `80) to describe the elastic modulus whereas others prefer the longitudinal modulus, real part of the complex Poisson's ratio (Kono `61; Waterman `63, `77), phase and group velocities (Sutherland `72; Freemantle `98), relaxation times (Sahoune `96; Challis `03), attenuation per wavelength (Ivey `49; Cunningham `56), real and imaginary part of the complex modulus (Nolle `46; Maeda `55; Richeton `05; Alig `94; Kroll `06) and tan($\delta$) (Parthun `95). It is interesting to note from the publishing years that up to the present day this wide distribution concerning the choice of acoustic parameters employed still exists. Each author is correct in his own right as this choice is often closely related to the actual application. For example, to compare the ultrasound technique with a technique based on other measurement principles a parameter common to both techniques is often employed. To facilitate comparison with Di-electric Thermal Analysis DETA results on a curing epoxy, Challis (Challis `00) chose to formulate the acoustic results in terms of relaxation times. Commonly, where comparisons between various analysis techniques occur, most authors are largely satisfied with empirical correlation of the results. Lionetto (Lionetto `04) went a step further and compared the results from DMA, DEA and ultrasound to investigate post cure on an unsaturated polyester resin. Using the Williams Landel Ferry WLF (Ferry `80) equation which roughly fits a six point scatter diagram (although 4 points are taken from DEA) curve obtained from experimental data, the author concluded that all techniques are sensitive to the α relaxation process. The results are however not convincing considering that a frequency range over almost 8 decades is covered with techniques based on different physical measurement principles. This is reflected by the author's estimates for the WLF constants C_1 and C_2 with respective values of 22 and 111.9 K. According to estimates from Strobl (Strobl `96) using the glass transition temperature $T_g$ as a reference temperature the constants should only vary between 14 to 18 for $C_1$ and 30 K to 70 K for $C_2$. If experimental data is not available the constants are often taken as universal (Aklonis `72 and Eisele `90) with C_1 taken as 17.44 and C_2 as 51.6 K. Therefore the statement from the author that "he has proven without ambiguity" that the attenuation peak in acoustic measurement is caused by the α relaxation, especially considering experimental evidence and the estimated values for C_1 and C_2 employed in the WLF fit are not convincing. More detailed analysis was completed by Maeda (Maeda `55) who employed both ultrasound techniques and

DEA in a similar frequency range to study PVC plasticiser compositions. The author's results are in strong contrast to Lionetto (above) as he revealed that the tan(δ) loss peak maximum associated with α relaxation is observed at completely different temperatures (almost 40 °C apart) depending on analysis technique used independent of measurement frequency. He concluded that ultrasound measurements are based on mechanical principles and directly related to the elastic modulus and loss, whereas dielectric measurements are based on electronic properties related mainly to dipole mobility and therefore only indirectly related to the mechanical properties. Therefore the results will depend very strongly not only on actual physical properties but also material composition (dipole content). This indicates as the author states that DEA is very dependent on the actual material employed (dipole content) and not just viscoelastic changes in material properties. Ferry (Ferry `53), also confirms discrepancies between dielectric and DMA results for investigations on two PVC compositions. Comparison between techniques based on different measurement principles should be treated carefully as the results are very dependent on material composition. Alig (Alig `98) investigated the formation of acrylic-styrene based copolymer films using both rheological and ultrasound techniques. His results and discussion indicate that the loss peak observed is caused by the α relaxation process. Only two frequencies at 1 Hz and 4 MHz were illustrated and the loss peak associated with the α relaxation was observed at approximately 50 °C higher temperature at 4 MHz than at 1 Hz. Although only very limited experimental evidence is provided, the results do support a general rule of thumb based on DEA data (Cowie `91, Sperling `92) which states that the loss peak will be observed at approximately 7 K higher temperatures for each decade increase in measurement frequency. However, deviations from this linear rule that is based on Arrhenius principles (see Chapter 2.3.2) are common. For this reason the WLF relation is preferred to predict the frequency dependence of the α relaxation and a fit of experimental data normally follows an exponential function. As described by (Aklonis `72) an Arrhenius plot is better suited to describe the frequency dependence of secondary relaxations.

Attenuation α, loss modulus L'', and tan(δ) are all employed to describe damping losses in polymer materials. For acoustic measurements on polymers, the relationship between the three parameters attenuation α, loss modulus L'', and tan(δ) is not clear. For example, as stated by Pethrick (Pethrick `83) without further explanation *tan(δ) = $\alpha\lambda$.* This has the appearance of a very simple relationship and is slightly misleading as both α and λ are calculated independently and are both frequency dependent variables. Furthermore, as shown in Eq. 2.14, *tan(δ) = $\alpha\lambda/\pi$* is only valid if the term r<<*1* as discussed in the last subsection.

This equation is of large practical value as both attenuation α and wavelength λ are variables that can be obtained directly from experimental measurements.

2.1.3 Characterisation of Reactive Thermoset Polymers using Ultrasound

The bulk of modern research work on acoustic cure monitoring of thermosetting resins has been published by the authors Alig (Alig `88, `89, `94), Challis (Challis `98, `03) as well as Maffezoli and co-workers (Frigione `00; Lionetto `04a and Maffezoli `99) and researchers at the BAM in Berlin (Döring `02, `03; Mc Hugh `03, `06 and Stark `97, `99). In nearly all cases the authors use sound velocity as the main parameter and a plot of sound velocity as a function of time (cure profile) forms a sigmoidal shape for a curing resin. Secondly, the attenuation goes through a maximum (forms a broad relaxation peak) at isothermal cure temperatures. Alig (Alig `89) was one of the first authors to attribute the attenuation peak to the dynamic glass transition and not as suspected by earlier publications to gelation. Both Alig (Alig `94) and Challis (Challis`03) independently compared relaxation times calculated from dielectric analysis DEA and ultrasound. The authors estimated gelation times from conductivity data (slight inflection in curve) and compared these times with the ultrasound data, gelation was reached shortly after the large increase in sound velocity. However, as no inflection point or other anomaly is observed in the acoustic data in this region it is difficult to conclude as the authors do that ultrasound is sensitive to gelation, especially as viscosity or gelation can only be determined indirectly using DEA techniques.

Challis (Challis `98, `03) combined shear and longitudinal wave measurements using a single measurement set-up. Such techniques have the advantage that both the complex shear and longitudinal modulus may be determined during epoxy cure. This is a particularly interesting paper because it is known that shear waves do not propagate in liquids. The author demonstrated that the curing epoxy could first sustain shear wave propagation after gelation. Phase velocity c_p (Chapter 2.2.4) throughout curing showing that the sound velocity remains stationary as a function of frequency in the 2 to 12 MHz range if evaluated at selected times during cure i.e. dispersion does not play a significant role. Other authors (Alig `88; Lionetto `04) have shown that small changes in the degree of cure at the end of the reaction although barely distinguishable using the DSC analysis technique can be detected by monitoring the sound velocity. Because of these results the authors state that ultrasound is very sensitive to vitrification. No physical evidence in the form of models or further explanation is provided that supports this view and vitrification is broadly defined as the

cessation of the curing reaction and not a specific transition point. It is difficult from the information available to make a conclusive decision on its sensitivity of ultrasound as a cure monitoring technique particularly in relation to the transformations gelation or vitrification. Chow (Chow `92) is the only author found that demonstrated on a curing epoxy resin that simultaneous sound velocity and shear modulus measured using a rheometer will have a similar profile. He also tries to account for the large difference in measuring frequencies between techniques. No further papers on this topic could be found from this author although the technique showed great potential.

2.2 Wave Propagation and Dynamic Mechanical Analysis

2.2.1 Propagation of Sound Waves

Ultrasonic testing is based on time varying deformations or oscillations in materials. All materials are comprised of atoms which may be forced into vibrational motion about their equilibrium position. Acoustics focuses on particles that contain atoms that move in unison to produce a mechanical wave. When the particles are displaced from their equilibrium positions, internal restoration forces arise. It is these restoration or binding forces, combined with inertia of the particles that leads to oscillatory motions of the medium. The individual particles or oscillators do not progress through the medium with the waves. Their motion is simple harmonic and limited to oscillations about their equilibrium position. Waves in elastic bodies can be characterized in space by oscillatory patterns that are capable of maintaining their shape and propagating in a stable manner. The propagation of these waves are described in terms of "wave modes" with this work being constrained to waves travelling through the material bulk or volume i.e. longitudinal and transversal waves. Waves on surfaces and interfaces or various types of elliptical or complex vibrations of the particles which make possible propagation of other wave types such as Rayleigh, Lamb or Love waves are not considered. Longitudinal wave propagation involves particle oscillations that occur in the direction of the wave propagation as shown in the schematic Fig. 2.1 (on next page). Since dilatational forces are active in these waves they are often referred to as compression or pressure waves. Compression waves can be generated in both liquids and solids because the energy travels through the atomic structure by a series of comparison and expansion movements. For transverse or shear waves the particles oscillation of particles takes place at a

right or transverse angle to the direction of propagation. The particle displacement shown in this figure is approx. 10 % of the wavelength, which is rather high and chosen for illustration purposes. In a steel sample the particle displacement is about $1.8*10^{-6}\,\lambda$ or 2 millionth of a wavelength (Krautkrämer `86). Shear waves require an acoustically solid material for effective propagation and therefore are not effectively propagated in materials such as liquids or gases. The basic motion relationship "distance = velocity c * time t" is the key to the basic wave relationship. Taking wavelength λ as distance, this relationship becomes $\lambda = ct$. By using $f = 1/t$ (where f = frequency) the standard wave relationship is formed $c = f\lambda$, whereby c is the sound velocity in an elastic body with no dispersion (i.e. the phase and group velocities are equal; see Chapter 2.2.4).
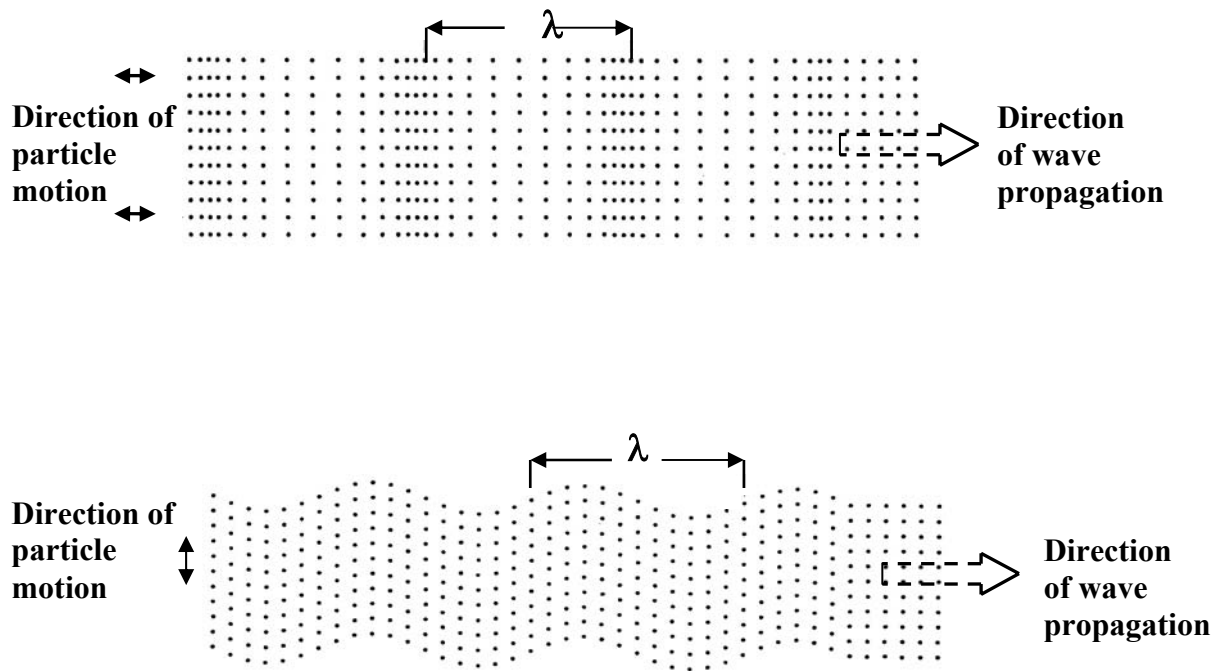
Fig. 2.1: *Longitudinal Wave Propagation (Top) and Transversal Wave Propagation (Bottom)*

2.2.2 Mechanical Oscillations and Wave theory

Mechanical waves require a medium for the transfer of energy to occur. As such both ultrasound wave motion and dynamic mechanical analysis are governed by laws based on harmonic oscillations, in this case based on an applied force varying sinusoidally with time.

Simple harmonic motion is typified by the motion of a mass on a spring when it is subject to a linear elastic force governed by Hooke's law. Motion equations are usually defined using a sine or cosine wave of singular frequency or wavelength. Visualisation of ultrasound behaving as a mechanical wave from which elastic material constants (e.g. tensile modulus) may be calculated is a rather abstract concept. For this reason the actual derivation of ultrasound modulus from the wave equation is highlighted concentrating particularly on physical explanation rather than mathematical theory. Derivation of the wave equation using an elastic model can be found in most standard textbooks. Several books helpful in this field and in particular relating to wave propagation in polymer materials are listed (Kolsky `69, Hueter and Bolt `55 and Pain `93). The actual wave equation of motion is usually derived by considering transverse motion of a wave on a string. A section of the string will perform vertical simple harmonic motions; i.e. a simple oscillator with displacement y is used to represent the variable which is changing as the wave passes through the material i.e. the displacement of an element in the direction x at a particular time t. This means that y is a function of (x,t). The wave equation of a string will relate the displacement y of a single oscillator to distance x and time t. This equation can be expressed in terms of Newton's second law $F = ma$ (F = Force, m = Mass, a = Acceleration) using the derivative form (Hueter `55; Pain, `93) as shown.

$$T \frac{\partial^2 y}{\partial x^2} = \rho \frac{\partial^2 y}{\partial t^2} \qquad\qquad\qquad Eq.\ 2.1$$

The right hand side is the linear density ρ (mass per length) of the elementary segment of the string times the acceleration of that segment. The required restoring force or tension T is proportional to the curvature of the string. It is sometimes useful to express the above wave equation in terms of sound velocity. The term T/ρ has the same units as sound velocity squared c^2 (see below):

$$\frac{\partial^2 y}{\partial x^2} = \frac{\rho}{T} \frac{\partial^2 y}{\partial t^2} \qquad \text{where } c^2 = \frac{T}{\rho} \left[\frac{\frac{mkg}{s^2}}{\frac{kg}{m}} = \frac{m^2}{s^2} \right]$$

$$\Rightarrow \frac{\partial^2 y}{\partial x^2} = \frac{1}{c^2} \frac{\partial^2 y}{\partial t^2} \qquad\qquad\qquad Eq.\ 2.2$$

Simple harmonic motion of an oscillator y of amplitude a at position x and time t can be expressed using the typical formulation for harmonic oscillation:

$$y = a \sin(\omega t - \theta)$$

Eq. 2.3

θ represents the phase lag, with respect to the oscillator at position x_0. Two points are said to be in-phase if they behave exactly the same; that is, if they are a multiple of a wavelength apart. Therefore θ will have values between 0 and 2π (complete vibration of the oscillator). Acoustic measurement parameters are sound velocity and attenuation and therefore the above solution for a harmonic oscillation needs to be rewritten to include these variables.

$$\text{Phase Lag } \theta = \frac{2\pi x}{\lambda} \text{ and } \omega = \frac{2\pi c}{\lambda} = 2\pi f; \text{ also } k = \frac{2\pi}{\lambda}$$

$$y(x,t) = a\sin(\omega t - \theta)$$
$$= a\sin k(ct - x)$$
$$= a\sin\frac{2\pi}{\lambda}(ct - x)$$

Eq. 2.4

Any relation in which x and t are combined in the form *(ct+x)* or *(ct-x)* in which c is the velocity of the wave can be employed to solve the wave equation (Pain `93). The term in brackets *(ct-x)* has the dimensions of length and for the function to be a sine or cosine its argument must have the dimensions radians. For this reason *(ct-x),* the minus sign denotes a wave moving to the right, must be multiplied by a factor k referred to as wave number.

$$y(x,t) = a\sin\frac{2\pi}{\lambda}(ct - x)$$
$$= a\sin(\omega t - kx)$$

Eq. 2.5

This equation in radians may be employed to solve the wave equation in Eq. 2.1 so that a relationship can be formed expressing wave parameters in terms of an elastic modulus. Another solution uses both sine and cosine functions also presented in exponential form below in Eq. 2.6.

$$y = a(\sin(\omega t - kx) + i\cos(\omega t - kx)) = ae^{i(\omega t - kx)}$$

Eq. 2.6

This provides a simple solution sufficient for an elastic material i.e. one which obeys Hooke's law i.e. *-KY =Ma* where *K* is the spring constant and *Y* the displacement of a mass at the end of a spring. In the case of plastic materials we are dealing with viscoelastic materials, commonly represented by a combination of spring and dashpot (viscous) models. For such materials the modulus is complex M* and represented by the real and imaginary parts (in-phase and out of phase parts) M*=M′+ iM′′. The terms M′ and iM′′ describe the real (elastic) and imaginary (viscous) parts of the complex modulus (see Chapter 2.1.1). These terms have to be integrated into the wave equation (Eq. 2.1) giving:

$$\rho \frac{\partial^2 y}{\partial t^2} = M * \frac{\partial^2 y}{\partial x^2}$$

$$\rho \frac{\partial^2 y}{\partial t^2} = M' \frac{\partial^2 y}{\partial x^2} + iM'' \frac{\partial^2 y}{\partial x^2} \qquad\qquad Eq.\ 2.7$$

This decay in oscillation amplitude is typically described by an exponential factor *(e^{-αx})* to express the rates at which the amplitude in material is reduced. The larger the material damping coefficient α or attenuation the more rapid the rate of amplitude decay. The term α is measured directly from the ratio of ultrasonic wave amplitude entering and leaving the sample as shown in Eq. 4.1 and Eq. 4.2 and has the units Neper/mm (Np/mm). By integrating this term into Eq.2.6, the solution to the wave equation for viscoelastic materials becomes:

$$y = a(\sin(\omega t - kx) \ + \ i\cos(\omega t - kx))e^{-\alpha x} \qquad\qquad Eq.\ 2.8$$

This solution is also presented in the work of McSkimin (McSkimin `64) although different symbols, terms and explanations are provided. By substituting into Eq 2.7 and on performing following mathematical manipulation (taking place in three primary steps), equations describing the complex modulus in terms of measured ultrasound parameters may be formed.

1. The differential components in Eq. 2.7 are evaluated.

2. The real *M′* and imaginary terms *iM ′′* for the full equation are evaluated.

3. Two simultaneous equations can be formed and it is then possible to solve for the real and imaginary parts each in terms of the four parameters, ρ, c, α, ω.

The following equations result:

$$M' = \rho c^2 \left(\frac{1 - \left(\alpha c / \omega \right)^2}{\left(1 + \left(\alpha c / \omega \right) \right)^2} \right)$$

Eq. 2.9

$$M' = \rho c^2 \quad \text{when} \quad \alpha c / \omega \ll 1$$

Eq. 2.10

$$M'' = \rho c^2 \left(\frac{\alpha c / \omega}{\left(1 + \left(\alpha c / \omega \right) \right)^2} \right)$$

Eq. 2.11

$$M'' = \frac{\rho c^3 \alpha}{\omega} \quad \text{when} \quad \alpha c / \omega \ll 1$$

Eq. 2.12

As shown the Eqs. 2.10 and 2.12 can be simplified under the condition that the term $r = \alpha c / \omega \ll 1$ that may also be rewritten as follows:

$$r = \frac{\alpha c}{\omega} = \frac{\alpha \lambda}{2\pi} \ll 1$$

Eq. 2.13

Actual values of *r* are only rarely provided in literature. Some authors (Nolle `48 and Ivey `49) estimate maximum values of *r* of about 0.1 or slightly above. Accurate determination of *r* requires considerable experimental preparation as well as complicated evaluation procedures (see Chapter 5.1). Therefore the assumption from most recent authors (Parthun `94; Sahoune `96 and Alig `94) that r<<1 is valid for all polymers can save considerable time and effort. As the following example shows, this is a reasonable assumption for the majority of applications, especially as most authors are satisfied with relative attenuation values. One can <u>estimate the attenuation required to achieve *r* values of 0.1 or higher</u> i.e. leading to increased error in calculations if Eqs. 2.10 and 2.12 are used. A typical rounded off value for sound velocity *c* for a polymer material is about 2000 m/s and wavelength $\lambda = 0.5$ mm at a frequency *f* of approx. 4 MHz. Attenuation α as derived from the wave equation has the units Neper/mm. The factor 8.686 is used to convert units of attenuation from Neper (Np) to decibel (dB). Attenuation values are provided in dB measurement units as they are more commonly employed (than Np) for acoustic applications.

$$r = \frac{\alpha c}{\omega} = \frac{\alpha \lambda}{2\pi (8.686)} = \frac{\alpha \lambda}{54.6}$$

Eq. 2.14

$$\Rightarrow \quad 0.1 = \frac{0.5 \alpha}{54.6} \quad \text{and} \quad \alpha = 11 \, dB/mm$$

The resulting high value for attenuation of 11 dB/mm would describe a material with good damping properties such as employed in the development of backing materials for ultrasound transducers (Mc Hugh `05). Realistically, such high damping properties for neat polymers (no fillers) can only be expected in the vicinity of primary or secondary relaxations. Little information could be found in relation to absolute attenuation values of *r* at temperatures in the vicinity of the α relaxation. Some authors including Maeda (Maeda `53) quote attenuation values for PVC at $T_g$ (α relaxation at 4 MHz) of up to 20 dB/mm at 1600 m/s for a wavelength  λ of 0.2 mm] i.e. r = 0.8. Kono  reports  (Kono `60) maximum values for Polystyrene of *r* =0.11 (c = 1650, *f* = 2.25 MHz at 8 dB/mm). These publications provide evidence that *r<<1* should not be universally assumed for all polymers at temperatures especially in a relaxation region.

The imaginary part of the modulus M´´ is a quantity measuring the amount of energy dissipated as heat when the material is deformed. Another parameter commonly used to describe the materials damping properties is tan(δ) which is a measure of the internal friction of the system. tan(δ) is defined as the ratio of the energy dissipated per cycle to the maximum potential energy stored during a cycle i.e. tan(δ) = M´´/M´. In the field of acoustics damping loss is also described by the Quality Factor or simply "*Q*" value, which is employed as a measure of the rate at which energy decays (Pain `93). *Q* is simply the reciprocal of tan(δ) i.e. Q=1/tan(δ). For acoustic measurements tan(δ) is quite easy to perceive as it can be determined directly from the acoustic parameters as follows:

$$\tan(\delta) = \frac{M''}{M'} = 2c\alpha \frac{\omega}{\omega^2 - c^2\alpha} \quad \text{and when} \quad \alpha c/\omega << 1 \qquad \textit{Eq. 2.15}$$

$$\tan(\delta) = 2\,\alpha c/\omega = \alpha\lambda/\pi \qquad \textit{Eq. 2.16}$$

Interestingly, from Eqs. 2.13 and 2.15 it is observed that tan(δ) ≈ 2*r*. In practice *r* is usually less than 0.1 apart from a few exceptions explained above. Application of tan(δ) as a measurement parameter for describing a material's damping properties has following advantages (context of DMA):

- does not require density values (compare to M´´) which can only be determined from a separate experiment
- can be evaluated directly from the acoustic parameters wavelength and attenuation.
- can be easily compared with tan(δ) ascertained from other measurement techniques

2.2.3 Interrelation of Elastic Modulus

The velocity of longitudinal waves in a solid depends upon the dimensions of the specimen in which the waves are travelling. The complex modulus term M* has been defined in Chapter 2.1. If one takes a bar shaped specimen (lateral dimensions are small in comparison to the wavelength) under tensile loading then the complex dynamic modulus M* can be replaced by a complex tensile modulus E*. On the other hand a longitudinal wave in a medium compresses it and distorts it laterally. Because a solid can develop a shear force in any direction such a lateral distortion is accompanied by a transverse shear. However, in the case of bulk solids the longitudinal and transverse wave modes can be considered separately. If a large (dimensions large compared to wavelength) flat poker shaped specimen is placed under tension or compression then the complex modulus M* can be replaced by a complex longitudinal L* or complex shear modulus G* depending on which wave mode is propagated. The specimens employed in this project were typically a minimum of 6 times larger than the actual wavelength of a longitudinal wave. Therefore following formulations are valid for M* and can each be derived from the wave equation as shown.

$$M^* = M' + iM''$$ *Eq. 2.17*

where M^* can represent

L* - Longitudinal Modulus; G* - Shear Modulus

K*- Bulk Modulus; E* - Youngs Modulus

The various moduli can typically be interrelated using the Poisson's ratio μ_p. Using the example of a bar shaped specimen under tensile loading μ_p describes the relationship between changes in length per unit length to changes in width per unit length. Poisson's ratio can be derived from this tensile experiment (Ferry, `80). Interrelation of G*, E* and K* and $\mu_p$* is as follows (Cowie, `91) :

$$E^* = \frac{9G^*K^*}{G^*+3K^*} \text{ giving } \mu_p^* = \frac{E^*}{2G^*} - 1$$ *Eq. 2.18*

A three-way equation may be written relating the four basic mechanical properties.

$$E^* = 3K^*(1 - 2\mu_p^*) = 2(1 + \mu_p^*)G^*$$ *Eq. 2.19*

Any two of these properties may be varied independently, and, conversely knowledge of any two may be employed to calculate the remaining unknown parameters. For example, when E* and G* in Eq. 2.19 are known then B* and μ_p* can be calculated. To a good approximation Poisson's number is $\mu_p{}^* \approx 0.5$ for soft rubbers and therefore *E*=3G**. The modulus for longitudinal waves is given by Loves Mathematical Theory of Elasticity (Love `27).

$$\text{Love's Theory:} \quad L^* = K^* + \frac{4}{3}G^* \qquad\qquad Eq.\ 2.20$$

$$L' = K' + \frac{4}{3}G' \quad and \quad L'' = K'' + \frac{4}{3}G'' \ (Nolle\ `52) \qquad Eq.\ 2.21$$

This was also confirmed mathematically by rewriting Eq. 2.19 in terms of its real and imaginary components and evaluating. Such formulations are particularly useful as one can relate terms evaluated from experimental measurements (L′ and L′′) to various other moduli. It is evident that K′ and K′′ can only be evaluated when sound velocity and attenuation are available for both longitudinal and shear waves. It is easy to appreciate that in liquids where it is not possible for shear waves to propagate then *L*=K**. In other words the longitudinal modulus in liquids is equal to the bulk compression modulus (Eq. 2.19). A plot of the various moduli for the same material will have following intensity relationship *L*>K*>E*>G** whereby *G** is roughly 1/5 *L** (Vogel `66). For acoustic characterisation of materials bulk properties the interrelation of moduli is of interest, particularly as is the case here, when comparing different measurement techniques. From the Eqs. 2.18 to 2.21 the interrelation of L*, G* and E* can be formulated:

$$L^* = G^* \frac{E^* - 4G^*}{E^* - 3G^*} = \frac{4G^* - E^*}{3 - \dfrac{E^*}{G^*}} \qquad\qquad Eq.\ 2.22$$

Similar to Eq. 2.21, the complex modulus in Eq. 2.22 may also be replaced either by the respective storage or loss modulus term. This was also confirmed mathematically. In the field of material science the longitudinal modulus is a rather unfamiliar term and tensile or shear modulus values are more common. The tensile modulus can be also obtained by longitudinal wave propagation in thin strips or rods but this technique breaks down when the wavelength becomes comparable to the cross-sectional dimension of the strips at higher frequencies. In this case the longitudinal waves yield not E′ but the quantity K′+4/3G′ or simply the

longitudinal modulus L′ as in Eq. 2.20. As it is difficult to guarantee slim geometries over a range of temperature longitudinal modulus is a much more practical value. Similarly shear modulus can be determined using shear wave propagation but it has the distinct disadvantage that it is very difficult to obtain accurate values in liquids or soft polymers because of their inability to support transverse (shear) excitations.

2.2.4. Phase Velocity and Dispersion

The discussion so far has been limited to monochromatic waves, waves of a single frequency and wavelength. However, it is much more common for waves to occur as a number or group of frequency components. In the field of wave motion two main velocities that are quite distinct although mathematically connected are of practical importance(Pain `93).

1. The phase velocity c_p of a wave is the rate at which the phase of the wave propagates in the material. This is the velocity at which the phase of any one frequency component of the wave will propagate. You could pick one particular phase of the wave (for example the crest) and it would appear to travel at the phase velocity. The phase velocity c_p is given in terms of the wavelength at a specific frequency or as in Eq. 2.4 in terms of the wavenumber k: $c_p = f\lambda = \omega/k$. In mechanics a perfectly elastic material is normally represented by a spring and the complex modulus M*=M′ as no viscous effects (M′′ or out of phase components, see Eq. 2.7) have to be considered. In such cases wave form will be independent of frequency ($f\lambda$ is a constant) and the phase velocity c_p is equal to the group velocity c_g (refer to point 2).

2. A number of waves of different frequencies, wavelengths and velocities may be superposed to form a group. The group velocity c_g of a wave is the velocity with which the variations in the shape of the wave's amplitude (known as the modulation or envelope of the wave) propagate through space. Publications in which results are presented show that a large difference on phase and group velocities may be observed in polymer materials (Ping `98; Challis `00) within a limited MHz frequency range at isothermal temperatures.

A brief insight into superposition of waves and Fourier analysis principles is provided in more detail in Chapter 4.2. Distinction of group and phase velocities is of particular interest in dispersive medium such as polymers because the absorption properties or attenuation α (defined in Eq. 2.8) can often change dramatically as a function of temperature. Attempts have been made to determine suitable mathematical relations between the respective damping for $\alpha(\omega)$ and $c_p(\omega)$ phase functions using the Kramers-Konig relations (O'Donnell `81;

Zellouf `96; Wintle `99). However such relationships are not trivial particularly in regard to viscoelastic materials and the results are, as admitted by the last two authors cited sometimes contradictory. Propagation of sound waves in dispersive media may distort the time domain signal leading to a possible shift of resonance frequency, change in wavelength or signal form. This leads to different phase shifts in different frequency components. Dispersion refers to the fact that the phase velocity c_p of a propagating wave in dispersive media will vary with frequency or wavelength as formulated below:

$$c_g = \frac{\partial}{\partial k}\omega = \frac{\partial}{\partial k}(kc_p) = c_p + k\frac{\partial c_p}{\partial k} = c_p - \lambda\frac{\partial c_p}{\partial \lambda} \qquad\qquad Eq.\ 2.23$$

Dispersion may also be caused by geometry effects or scattering when heterogeneities such as voids or crystallites occur. The frequency spectrum of the ultrasonic pulses scattered reveal information about the scatterer's size, shape and orientation. For heterogeneities with sizes ranging from 1/1000 to 1/100 of the wavelength scattering is non-influential. Larger heterogeneities if not considered in the calculations can lead to large errors in determining modulus values using wave propagation (Krautkrämer `86). Therefore care was taken that the epoxy samples or mixtures were homogenous enough to neglect this effect.

2.3 Time, Temperature and Frequency Effects

In the previous section the theoretical relationships between measured acoustic parameters and the complex dynamic modulus for polymer materials, was discussed. The concepts discussed are strictly independent of the existence of molecules; the results of those concepts fall into the realm of continuum mechanics. The emphasis in the following is the interpretation of the viscoelastic behaviour on a molecular scale and discussion of glass transition phenomenon. Molecular mechanisms at least in terms of mechanical analogues are discussed in the following which will aid in understanding time/frequency and temperature correspondence for polymer materials. Viscoelastic materials as the name suggests exhibit a combination of elastic and viscous behaviour. Using an amorphous polymer as an example most textbooks describe five distinct regions of viscoelastic behaviour. The regions are marked in Fig. 2.4 (used to demonstrate superposition principles) for a thermoplastic (polyisobutlyene) material. Using a continued heating regime starting at low temperatures the

Glassy region refers to stiff polymer properties. Region 2 is the *glass transition* and describes the transition zone from glass to rubber. Region 3 is the *rubbery plateau* region. As the temperature is raised past the rubbery plateau region the polymer is marked by both rubber elasticity and flow properties – this zone is called the *rubbery flow* region (4). At still higher temperatures the *liquid flow* region 5 is reached. For a crosslinked polymer such as the cured epoxy used in this work, only the first 3 regions are of interest as to a first approximation the modulus will remain constant in the rubbery plateau region (see Fig. 2.2). Liquid flow will not occur. The complex modulus is a function of time as well as temperature. Therefore, the same viscoelastic behaviour can be observed by measuring the modulus as a function of time at constant temperature or by measuring the modulus as a function of temperature at a constant frequency. Modulus plotted as a function of temperature or as a function of time/frequency at constant temperature will yield the same viscoelastic profile. The second region describes the glass to rubber transition and results in large drop in modulus of approx. 3 orders in magnitude and a peak in the loss modulus. This considerable variation in properties makes it one of the most important parameters in characterising the mechanical behaviour of a cured epoxy resin. Changes associated with the glass transition include volume and expansion coefficients, enthalpy and mechanical properties. Experiments performed in this work take place using different techniques but always on samples prepared in exactly the same manner and also at low cooling rates. In the following, the influences time/frequency effects on the determination of the glass transition are discussed from an analytical perspective.

2.3.1 Time Dependence in Mechanical (DMA) Relaxation Studies

In Fig 2.2, the dynamic tensile storage E′, loss modulus E′′, and tan(δ) for a 3 point bending experiment performed at 1 Hz on a fully cured epoxy are illustrated. DMA measurement principles are explained in Chapter 4.3. The first 3 regions of viscoelastic behaviour for a crosslinked polymer are clearly marked, (discussed above). At low temperatures (0 to 40 °C), the polymer is stiff/frozen and has a high storage modulus E′ and low loss modulus E′′. The chains are frozen in fixed positions because insufficient energy for translational and rotational motions of the polymer segments is available. As the temperature increases, the polymer obtains sufficient thermal energy to enable its chains to move more freely. At temperatures larger than 100 °C the modulus decreases to about 10 MPa, a typical value for rubberlike materials. In analogy with this process a transition occurs at temperatures between 60 to

100 °C and the loss modulus E″ goes through a maximum. This region is referred to as the glass rubber transition or glass transition T_g and can be qualitatively interpreted as the onset of large scale conformational rearrangements of the polymer chain backbone (Mc Crum `67). Frictional interaction between polymer chain segments leads to energy being dissipated as heat and a corresponding maximum will be observed in the loss factor E″ or tan(δ). The temperature at which this peak maximum is observed is conventionally defined as T_g. Below T_g only 1 to 4 chain atoms are involved in movement while above T_g 10 to 50 chain atoms attain sufficient thermal energy to move in a co-ordinated manner. This indicates that segmental mobility is strongly time dependent and will depend on the rate of applied load or measurement frequency. On a molecular scale, the relaxation time τ of a polymer indicates the order of magnitude of time required for a certain proportion of the polymer to relax; respond to the thermal stress by thermal motion.
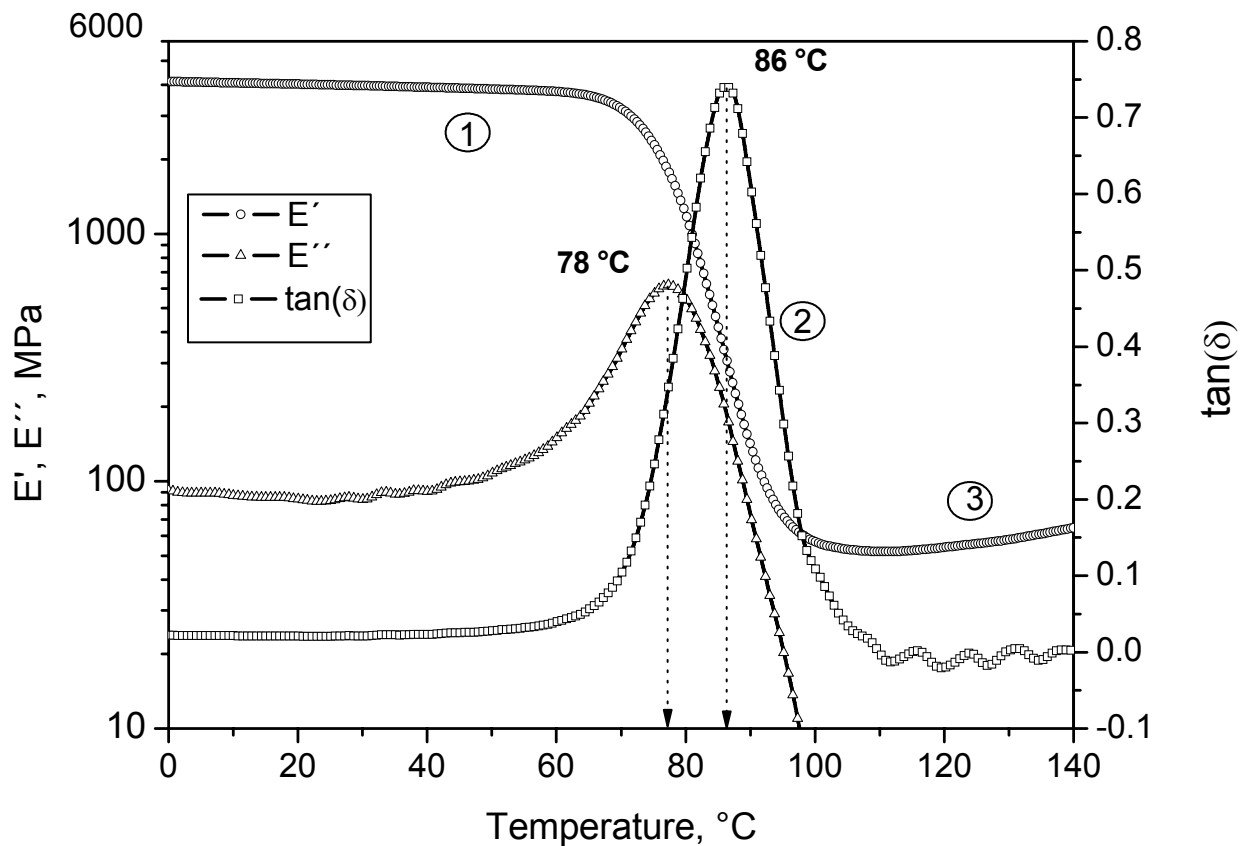
Fig. 2.2. *Behaviour of elastic modulus E′ and E″ and tan(δ) as a function of temperature for a fully cured epoxy. The loss peaks result from the α relaxation.*

To permit a mathematical analysis of relaxation phenomenon spring and dashpot models are frequently used. The spring represents an elastic solid such as a metal and the dashpot a purely viscous liquid. A simple Maxwell model is employed in Fig.2.3 for illustration purposes to help explain this relaxation behaviour. If the spring in the Maxwell model corresponds to the tensile rigidity E and the dashpot to the viscosity η of a polymer, then the relaxation time τ of this element is defined as $\tau = \eta/E$ and is a measure of time required for stress relaxation.
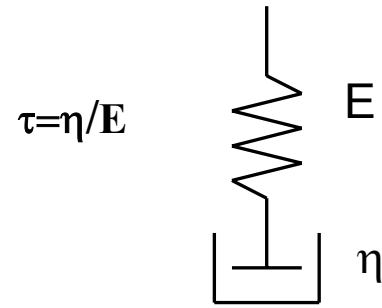
Fig. 2.3 *Maxwell Model*

To observe a relaxation process, dynamic experiments must be performed at an angular frequency (ω) in the region $\omega = 1/\tau$. For example to observe molecular relaxation times in the range of 10^{-3} sec at a fixed temperature then experiments must be performed at a frequency of $\omega = 10^3$ sec^{-1}. The various molecular relaxations are labelled with the Greek letters α, β, γ etc. in order of occurrence and the corresponding relaxation temperatures are typically determined from the peak maxima in E″ or tan(δ) measured using DMA methods as shown in Fig. 2.2. The glass rubber transition T_g (Mc Crum `67) is also referred to as the primary relaxation labelled as α (Strobl `96; Sperrling `92). Frequency dependence of the α relaxation may be explained using the DMA experiment for example purposes (Fig. 2.2). In the glassy region well below the glass transition at constant frequency the relaxation times $\tau \gg 1$ are high and the polymer segments cannot respond to the applied stress. The material behaves rigidly and has low damping. At temperatures above the glass transition, molecular segments can respond easily to the applied force and $\tau \ll 1$ and there is little loss of energy due to frictional interaction. E″ or tan(δ) will have an accordingly low magnitude. At or in the vicinity of the α relaxation segmental motion can respond to the frequency of the applied force and $\omega\tau = 1$ correlating with a maximum in the loss factor E″ or tan(δ). In this work both the terms α relaxation and T_g will be employed depending on relevance. For experiments performed over a large time or frequency range then the term α relaxation is used as it is more relevant to relaxation or time domain phenomena. For experiments where the variation of mechanical properties as a function of temperature at constant frequency has priority then the term T_g will be employed as the actual temperature at which the material transition occurs is more relevant than the actual molecular relaxation times. This differentiation is common procedure in standard literature related to polymer science (Murayama `78; Ferry `86).

2.3.2 TTS Theory: Time Temperature Superposition

As stated, determination of the modulus for a viscoelastic material will depend on frequency or timescale and temperature of a given experiment. However, only a small range of viscoelastic response manifests itself during an experimentally accessible time range. The accessible time scale for stress relaxation experiments lies in the 10^1 to 10^6 sec range but obviously a wider range would be desirable. Observations on viscoelastic materials showed that changing stress relaxation times is equivalent to changing temperature (Leaderman `43). Using this information a composite isothermal curve covering the required temperature range can be constructed from data collected at different temperatures (Fig. 2.4). This is accomplished by translation of small curves along the logarithmic time axis until they are all superimposed to form a large master curve. Stress relaxations data at one temperature can be superimposed on data taken at a different temperature merely by shifting the creep curves. The time scale (relaxation time) at each individual measurement temperature is multiplied by a shift factor a_T. The shift factor is estimated by shifting each individual component curve so that it can be superimposed on a reference curve at time t_{ref}. The component curves represent measurements at different constant temperatures. The factor a_T is chosen so that the component curves can be joined onto the reference curve at t_{ref} forming a smooth profile. The curve obtained at each temperature is shifted by an amount a_T:

$$\log t - \log t_{\text{ref}} = \log a_T \quad \Rightarrow \quad a_T = \frac{t}{t_{\text{ref}}} \qquad\qquad Eq.\ 2.24$$

The so-called master curve formed illustrates the relaxation behaviour over the generated time scale at the chosen reference temperature. The relaxation rate equals the rate of transitions between two conformational states. The observed activation energy E_a has to be identified with the height of the energy barrier which has to be passed over during this change. In Fig. 2.4 a logarithmic plot of the shift factor against temperature is illustrated. Over a small temperature interval such a plot will often be linear indicating a thermally activated process, with a relaxation time being given by the Arrhenius law:

$$\tau \sim \exp\frac{E_a}{RT} \quad \text{or} \quad \ln\tau \sim \frac{E_a}{RT} \qquad\qquad Eq.\ 2.25$$

R is the universal gas constant
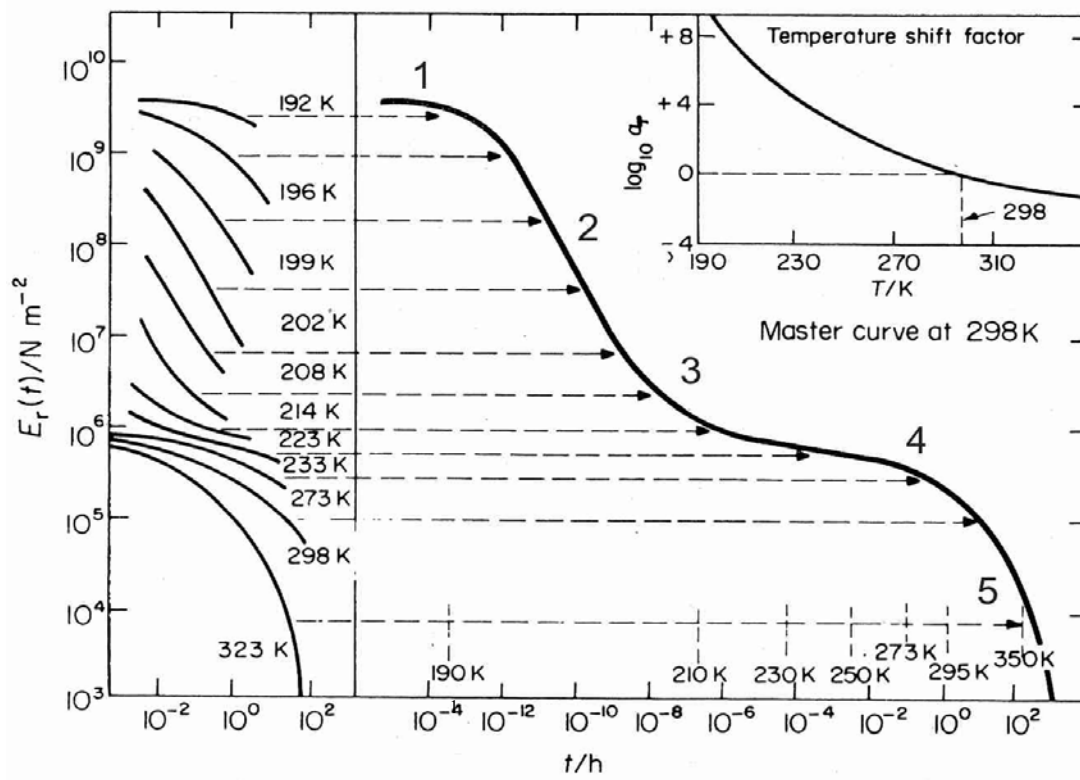
Fig. 2.4. *Making of a master curve (adapted from Tobolsky `56) using stress relaxation data for Polyisobutylene. The numbers mark the various region of viscoelastic*

Graphical analogue to this equation is the Arrhenius plot (log shift factor a_T vs. reciprocal temperature in Kelvin). A linear shift plot indicates that the ratio of the relaxation or retardation times at the temperatures T_1 and T_2 obey an Arrhenius equation in the form:

$$a_T = \frac{\tau_2}{\tau_1} = \exp\frac{E_a}{RT} \qquad\qquad Eq.\ 2.26$$

If the above equation is combined with the relation $\omega = 1/\tau$, the average relaxation time at which a loss peak maximum occurs at the temperatures T_1 and T_2 then:

$$a_T = \frac{\tau_2}{\tau_1} = \frac{\omega_1}{\omega_2} = \exp\frac{E_a}{R}\left(\frac{1}{T_1} - \frac{1}{T_2}\right) \qquad\qquad Eq.\ 2.27$$

Using this equation the influence of high measurement frequencies (ultrasound - MHz) on the determination of T_g can be estimated. As an example, if one considers an increase in frequency of one decade ($e^{2.303}$) then the above equation can be reformulated as follows:

$$e^{2.303} = \exp \frac{E_a}{R}\left(\frac{1}{T_1} - \frac{1}{T_2}\right)$$

$$and \quad \left(\frac{1}{T_1} - \frac{1}{T_2}\right) = \frac{2.303R}{E_a}$$

Eq. 2.28

Estimated values of E_a = 84 kcal/mol (355 kJ/mol) for the α relaxation process in polystyrene can be found in the literature (Sperling `92). Also an approximate value of $T_g$ = 373 K for polystyrene that was obtained using low frequency techniques (Brydson `90) can be placed into Eq. 2.28 by letting $T_2 = T_g$. In this manner T_1 is determined and yields a value of 7.5 or in other words T_g will be observed at a temperature approx. 7.5 K higher for every decade increase in frequency. This value is also commonly quoted in textbooks on the basis of DEA measurements (Sperling `92 and Cowie `91). However, following points should be considered before using accepting that such a general rule is valid for the majority for polymers:

1. This rule will be very dependent on the actual activation energy of the individual polymer (see Eq. 2.27).
2. For the majority of polymers if T_g is plotted against the reciprocal of frequency it will not exhibit linear behaviour but will be slightly curved. In this case the Williams Landel Ferry WLF equation is better suited for modelling the frequency behaviour. Some authors (Aklonis `72) suggest using such plots to differentiate between primary and secondary relaxations. The former exhibiting WLF behaviour and the latter Arrhenius dependence Polystyrene is one of the few exceptions where the Arrhenius equation is better suited to describe frequency dependence of observed T_g.

The derivation of this WLF equation is based on free volume principles (Ferry `80) and is illustrated in Eq. 2.28. According to Ferry (Ferry `80) the constants C_1 and C_2 can be calculated experimentally by plotting (T-T_{ref})/log a_T against T-T_{ref} whereby T refers to temperature and T_{ref} is a constant reference. From the slope *s* and the intercept *i* of the resulting line the constants are calculated: C_1 = 1/*s* and C_2=*i*/*s*.

$$\log a_T = \frac{-C_1(T - T_{ref})}{C_2 + T - T_{ref}}$$

Eq. 2.29

According to investigations performed by the WLF author if a temperature approx 50 K above the T_g is chosen then C_1 = 8.86 and C_2 =101.6 K are constants independent of polymer.

It is more common is to reduce relaxation, temperature or creep data to the glass transition temperature T_g. In such experiments $T_g = T_{ref}$ and if no experimental data is available then C_1 and C_2 are chosen as 17.44 and 51.6 °K respectively. Nowadays, these values are normally taken as universal for polymers (prerequisite $T_g = T_{ref}$). According to Strobl, (Strobl `96) this is not true and the constants C_1 and C_2 are material dependent parameters that will normally vary in the ranges $C_1 = 14$ to 18 and $C_2 = 30$ to 70 K. For the example illustrated in Fig. 2.4, the T_g of Polyisobutylene is given as 202 K (at low frequencies). If C_1 and C_2 are chosen as 17.44 and 51.6 °K then a shift factor of approx. 5 °C for every decade increase in frequency can be estimated. Therefore the rule of thumb describing the influence of measurement frequency on T_g should just be taken as a rough estimate as it typically varies somewhere between 5 and 8 K per decade and will depend on whether an Arrhenius or WLF model is used. It is obviously better, where possible, to determine the constants C_1 and C_2 experimentally. In order to obtain an analytical expression that can be used to estimate the activation energy E_a from the WLF equation, Aklonis (Aklonis `72) placed the Arrhenius law written in the form shown in Eq. 2.25 back into the WLF Eq. 2.28 using a_T as the common term. This expression is used to determine the activation energy and will be very dependent on the actual glass transition temperature. If the universal constants are employed for C_1 and C_2 then the equation can be rewritten as 6.47 ($T_g{}^2$), which means that for a polymer with a α relaxation process at 353 K, an activation energy of 800 kJ/mol is obtained. The activation energy will obviously increase the higher the glass transition of the polymer i.e. will depend on the measurement frequency of the experiment.

$$E_a = 2.303 \frac{C_1 C_2 R T^2}{\left(C_2 + T - T_g\right)^2} = 2.303 \left(\frac{C_1}{C_2}\right) R T_g{}^2 \qquad\qquad Eq.\ 2.30$$

R = Universal gas constant .

Chapter Three

3 Epoxy Resins

3.1 Introduction and Background

Epoxy resins are used in a large number of fields, including surface coatings, in adhesives, in potting and encapsulation of electronic components, in tooling, for laminates in flooring, in rigid foams and in the manufacture of fibre reinforced composites for high end engineering applications and to a smaller extent as moulding compounds for compression or injection moulded components. The resins react by a rearrangement polymerisation without the elimination of small molecules such as water and as consequence exhibit low cure shrinkage. The curing or crosslinking reaction involves the formation of a three-dimensional network as a result of the reaction of an epoxy with an appropriate hardener. Although the detailed properties will depend greatly on the type of resin, the tightly crosslinked network provide the properties highly demanded from the advanced materials industry such as a very high glass transition temperature T_g, low shrinkage on cure, strong adhesion to many substrates, good chemical resistance and low volatility. Epoxies are characterised by the inclusion of an epoxy ring (also called oxirane, illustrated with a blue colour in Fig. 3.1) in the main chain molecule which can react with a curing agent. A wide range of epoxy resins are commercially available which differ in functionality (from two to four) and molecular weight. The commercial market for epoxy pre-polymers is dominated by the reaction products of bis-phenol A and epichloro-hydrin (DGEBA). Bis-phenol A is prepared by the reaction of acetone and phenol and is comparatively inexpensive and easy to manufacture whereas Epichlorohydrin is the more expensive component and is derived from polypropylene (Brydson `95).

Diglycidyl Ether of bisphenol A (DGEBA)
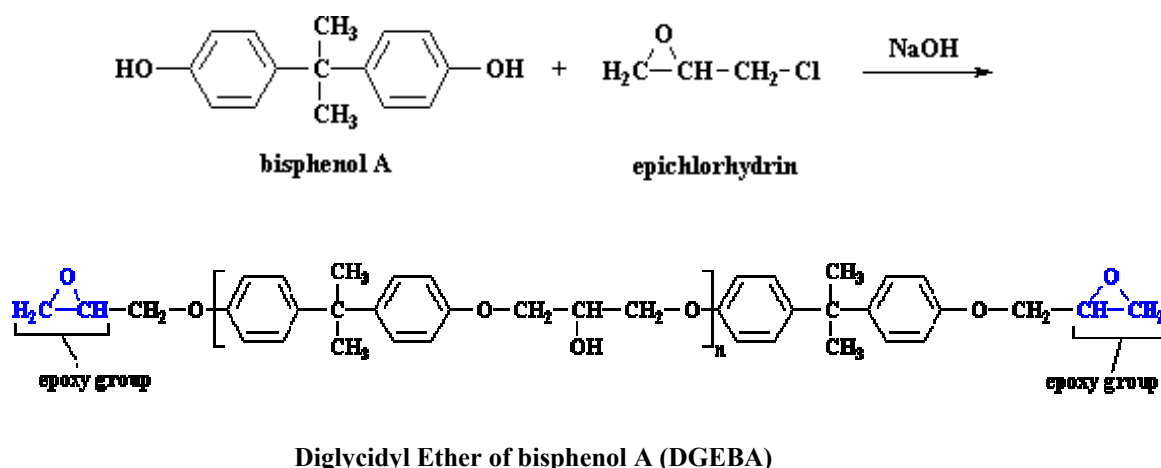
Fig. 3.1 *Production of DGEBA resin from Bisphenol A and Epichlorohydrin*

The general reaction scheme can be represented by the following reactions (Ellis `93) and is illustrated in Fig. 3.2. The amine curing agent has a molecular structure which typically consists of four hydrogen "arms and legs". Because there are at least four hydrogens on the curing agent they can react with four epoxy resin groups, resulting in large interlocking structures or crosslinks. These hydrogens react with the oxirane (epoxy group) ring unit on the ends of the epoxy resin. Due to the opening of the epoxy ring a new carbon-hydrogen bond is formed, this time using the hydrogen from the curing agent and freeing the epoxy group's hydrogen to unite with the group's oxygen to form an OH pendant. This hydroxyl group contributes to the epoxy's outstanding adhesion to many substrates. The aromatic ring unit, which the hydroxyls attach to, help provide the epoxies positive thermal and corrosion properties.

- **Primary amine addition**
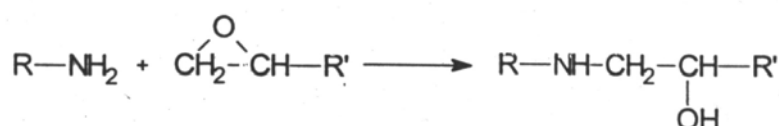
- **Secondary amine addition**
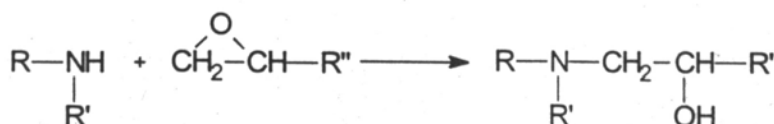
The hydroxyl groups formed by the amine/epoxy reaction can themselves act as catalysts accelerating the reaction at the early stages and showing the typical characteristics of an auto-catalysed reaction. The exact nature of the cure reaction depends on the specific reactants involved and on the presence of any catalysts. Cure reaction mainly involves homopolymerisation of the epoxy groups initiated by a curing agent and a polyaddition/copolymerisation with a multifunctional curing agent. Curing agents can be classified under two main categories:

- basic hardeners usually include Lewis bases or primary and secondary amines
- acid hardeners such as Lewis acids, anhydride acids and phenols

3.2 Major Transitions During Epoxy-Amine Cure

During the cross-linking reaction and depending on the cure temperature two macroscopic phenomena can occur: **gelation** and **vitrification** converting the fluid to a solid in the thermosetting process. Prior to cross-linking the resin can be represented by small polyfunctional units of low molecular weight or monomers. Each group of monomers connected directly or indirectly by closed bonds is called a macromolecule or cluster. The functionality *f* of a molecule represents the number of bonds each unit can form with other units of its kind. The cure of a bifunctional epoxy prepolymer and diamine hardener and network formation is illustrated in schematic form in Fig. 3.2.

A: Unreacted resin   **B: Partially cured**   **C: Gelation**
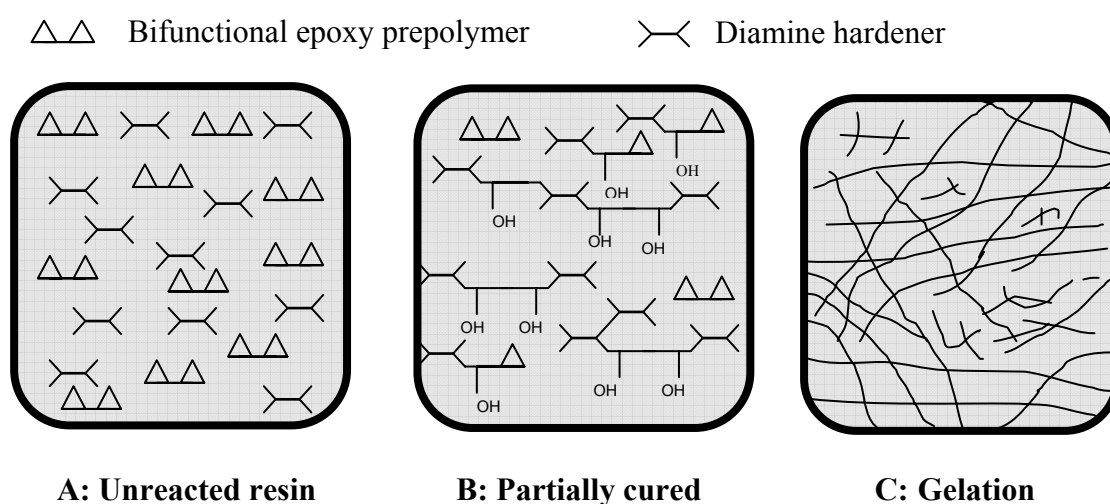
Fig. 3.2 *The cure of epoxy resin.* **Stage A**: *Uncured resin,* **Stage B**: *Partially cured resin (small branched molecules have formed),* **Stage C**: *Gelation (branched structures extend throughout the whole sample).*

As the cure reaction progresses the number of high molecular weight particles or clusters increases. Before the gel point has been reached the liquid polymer is referred to as 'sol' because it is still soluble in most appropriate solvents. As the reaction progresses the molecules crosslink into larger clusters by forming covalent bonds and at a critical extent of reaction referred to as <u>gelpoint</u> the largest macromolecule extends from one end of the sample to another. The point where the growth and branching of polymer chains, caused by intermolecular reactions causes a phase change from the liquid state to the rubbery state is called **gelation**. The solid polymer beyond the gelpoint is no longer soluble even in a good solvent. Macroscopically this point is accompanied by a dramatic increase in viscosity and the onset of elasticity. This transformation is a critical point in resin cure and occurs at a specific point of chemical conversion depending on the curing system and curing environment. The critical point of conversion is referred to as p_c and typically occurs between 50 and 60 % conversion for an epoxy resin. At conversions below p_c the molecules have a finite size whereas at higher conversions, some are infinite. Mathematical theory was first introduced (Flory, `53) to describe the phenomenon of random gelation, known as branching theory. This work was extended (Gordon `68) using the cascade theory. As the reaction proceeds beyond gelation the amount of gel increases at the expense of the sol. The cross-linking reaction leads to an increase in crosslink density and the reaction slows as the reactive species find it increasingly difficult to find a reactive partner due to limited segmental motion. Eventually the reaction becomes diffusion controlled and is quenched as the material vitrifies.

The different stages in isothermal cure are typically described using a Time-Temperature-Transformation TTT diagram (Gillham `88) in which the progression of the glass transition temperature over time is used to monitor cure. The TTT diagram provides a graphical aid for understanding the curing process and formation of predictive models as the structural development signified by the increase in T_g is closely related to the mechanical properties of the cured component. Fig. 3.3 (Wisanrakkit `90) shows a schematic diagram illustrating the main features. The diagram displays the time to reach various levels or events during isothermal cure. As a thermosetting material cures, its glass transition temperature T_g, increases from an initial value of T_{g0} due to increasing molecular weight, which occurs with a corresponding decrease in the fraction of free volume associated with chain ends (e.g. unreacted epoxy and primary amine groups). The diagram indicates the distinct regions encountered in the thermosetting process such as liquid, sol-glass, sol/gel-rubber, gel-rubber, sol/gel-glass, gel/glass and char. Three critical temperatures are shown T_{g0}, $_{gel}T_g$ and $T_{g\infty}$. T_{g0} is the glass transition temperature of the uncured monomer, $_{gel}T_g$ is the cure temperature at

which gelation and vitrification can occur simultaneously and $T_{g\infty}$ is the maximum glass transition temperature of the fully cured resin. Considering the usual curing process involving the transitions liquid-rubber-glass during isothermal cure then the cure temperature T_{cure} must be below $T_{g\infty}$ and above $_{gel}T_g$ for both gelation and vitrification to occur. The term cure temperature T_{cure} is used although it is accepted, as discussed by Yoon (Yoon `92), that the thermal transition of an epoxy depends on the internal temperature of the curing system and not on the applied cure or mould temperature. During cure as the cross-linking network develops the glass transition temperature T_g of the system increases and is indicative of this structural development (Babayevsky, `73). At gelation the formation of infinite molecules at a fixed conversion occurs at an intermediate T_g value between T_{g0} and $T_{g\infty}$ and is called $_{gel}T_g$. After gelation, T_g increases due to increasing crosslink density or number-average molecular weight of the sol/gel mixture and the decrease in chain ends. As T_g approaches the cure
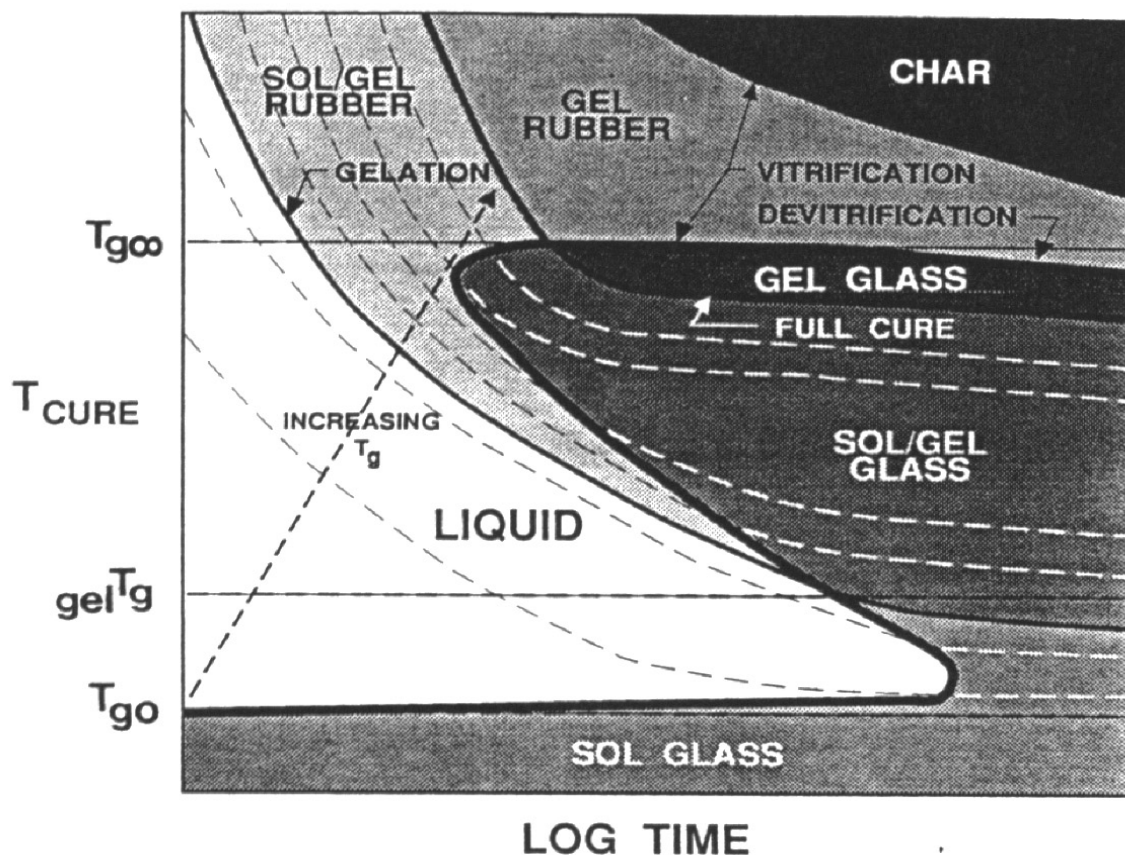
TTT CURE DIAGRAM

Fig. 3.3 *Isothermal cure diagram for a thermosetting resin (Wisanrakkit `90)*

temperature, the material enters the glass transition region and is defined to vitrify when T_g equals T_{cure}. The gradual cessation of the reaction marks the transition from rubber to glass. This transition is defined as **vitrification** and is considered the end of cure. If the cure temperature is above the T_g of the fully cured material, $T_{g\infty}$ by definition, the material cannot vitrify at T_{cure} and in this case the chemical kinetics will govern the progress of the reaction. If the temperature is held for long periods of time at $T_{g\infty}$ then devitrification which is caused by degradation may occur as well as char formation at even higher temperatures. One particular feature of the TTT diagram that should not be overlooked is the S-shaped curve form between the boundary lines T_{g0} and T_g showing that an increase in reaction rate will mean that the cure time for a particular event or transition will decrease decrease with increasing cure temperature. The time axis has a logarithmic scale so that for example a sol/gel glass state may only realistically be achieved over a period of days or weeks. In a typical commercial curing cycle the resin will pass from a liquid to a gel/rubber state and vitrify (otherwise it would deform on removal from a mould). Cure times vary very broadly from days to minutes depending on the manufacturing process for example hand lay-up or automated resin injection moulding.

3.3 Cure Modelling: Kinetics and Chemorheology

During the cure of a thermosetting resin a number of complex chemical and physical changes occur as the material turns from a viscous liquid to a highly crosslinked solid. These changes are reflected in the chemorheological characteristics of each individual resin system and determine the optimum set of process parameters for the production of a material. Adequate models combining cure kinetics and chemorheology are a primary component of thermosetting composites manufacturing simulations. Two main approaches to modelling can be distinguished:

1. Phenomenological or empirical modelling: tends to ignore the chemical reaction mechanisms and utilises approximate relationships which usually resemble chemical kinetic expressions. This is the more traditional method of searching for a rate law and its activation parameters which describes the overall reaction within a range of conversion as well as possible.

2.   Mechanistic modelling: Overall reaction is broken down by a combination of reaction steps with constant activation parameters. The single steps can be described by all known rate laws for homogenous and heterogeneous reactions. A reaction scheme representing the curing mechanism is selected which can be described by a mathematical reaction rate equation system. The fact that a multiple parameter estimation for a non-analytical expression of resin kinetics makes mechanistic models sometimes unattractive. However, new evaluation programs (Flammersheim `02) provide help in this area. The formal kinetic models as a rule do not correspond to real elementary reactions but provide very high fitting values i.e. are helpful in understanding real reaction behaviour.

The complexity as well as the importance of cure kinetics is reflected by innumerable publications and models which can be found relating to points 1 and 2. Despite the effort that has been expended on cure kinetics of epoxy, there is still no general model which can be applied to the cure of all epoxy resins. As I am interested in comparing various physiochemical analytical techniques, the suitability of applying phenomenological models for comparison purposes was looked at.

A wide variety of models are available to aid in analysis and prediction of the curing reaction. Choice of kinetic or chemorheological depends largely on area of interest and analytical technique. Every chemical reaction is associated with a certain heat of reaction. It therefore follows that the heat flow rate is proportional to the rate of reaction. Kinetic modelling is therefore typically based on calorimetric measurement techniques. Techniques sensitive to network formation or progress of modulus or viscosity naturally come under the title chemorheology. A linear relationship exists between conversion and T_g (related to structure development) for the kinetic part of the crosslinking reaction so that both kinetics and chemorheological models are known to be closely interlinked (Gillham `79). Although this relationship still exists it breaks down signified by non linearity in the latter part of cure at high conversion values (> 60%). At this point the reaction becomes diffusion controlled i.e. at temperatures $T_{cure} < T_g$. Traditionally many kinetic evaluation techniques were directed at finding a rate law and its parameters which describes the overall reaction within a conversion range. As discussed in Chapter 3.1 Epoxy cure may take place in a series of reaction steps e.g. catalysis and autocatalysis may even occur simultaneously and published models are therefore usually material specific and not universal. This point will be discussed in the following section starting with the basis equation for rate constant calculation and therefore kinetic analysis, known as the Arrhenius equation.

3.3.1 Application of the Arrhenius Equation

Chemical reactions are normally associated with a certain heat of reaction. It therefore follows that the heat flow rate is proportional to the progress of the reaction. This process is normally explained by the barrier theory and the activation energy. The basic assumptions are that for a reaction to occur, reactant species must come together and secondly must have sufficient energy to form a product (overcome an energy barrier). The Swedish chemist Arrhenius (1859 to 1927) postulated that the energetic term (E_a) correlates with the enthalpic activation barrier for the reaction and can be described by the following equations:

$$k = A_0 \times e^{\frac{-E_a}{R \times T}} \qquad \text{or logarithmic form} \qquad \ln \frac{k}{A_0} = -\frac{E_a}{R \cdot T} \qquad Eq.\ 3.1$$

A_0 = Pre-exponential term; k = rate of reaction

R = Gas constant; E_a = Activation Energy (J/mol)

The actual equation was formed from observations on the effect of temperature on reaction rate. It was found empirically that a plot of *log k* vs. *1/T* produced a linear relationship. Thus a plot of *ln k* vs. *(1/T)* will provide a line with a slope of – E_a/R and an intercept of *ln A*. The (extrapolated) cut with the *ln y*-axis provides directly the value of the pre-exponential factor *A*, and the slope of the straight line gives the activation energy E_a. (Standard: ASTM E698). One of the primary objectives of kinetic analysis is parameterizing the temperature dependence of the reaction rate. Although both Arrhenius parameters *A* and E_a are needed to describe the temperature dependence, the discussion of the reaction kinetics tends to focus on the activation energy. This is probably because the temperature sensitivity of the reaction rate is predominantly determined by E_a, whereas *A* plays the role of a scaling parameter, which determines the absolute value of the reaction rate.

3.3.2 Reaction Rate Laws in Kinetic Modelling

Every quantitative kinetic analysis starts with the determination of a continuous sequence of concentration of reactants versus time data. The goal of kinetics is to measure a concentration of a species at a particular time during the reaction so that a rate law may be

determined. When thermoanalytic techniques such as Differential Scanning Calorimetry DSC are used for the investigation of kinetic problems, the concentrations of the reactants which are often unknown are usually replaced by degrees of reaction α that are typically obtained from DSC measurements (Borchardt `57). In this case the measured heat of reaction is Q. For a curing reaction the degree of conversion α is calculated from the heat of reaction and is determined from the ratio of the partial area Q_t to the total area Q_∞ of an exothermal DSC peak and α ranges from 0 to 1.:

$$\alpha(t) = \frac{Q_t}{Q_\infty} \qquad \qquad Eq.\ 3.2$$

Three general methods (Höhne `03) can be described for the determination of kinetic parameters although numerous variations are available. The direct method following the procedure of Borchardt (Borchardt `57) is used here. A general reaction rate *k(T)* law may be written as follows:

$$\frac{d\alpha}{dt} = k(T) \cdot f(\alpha) \quad \text{where } f(\alpha) = (1-\alpha)^n \qquad Eq.\ 3.3$$

f(α) is assumed to be a function of conversion independent of temperature. The value *n* describes the order of a reaction with respect to a certain reactant. It is defined as the power to which the concentration (or conversion) term in the above rate equation is raised. If the correct reaction order is chosen then a linear plot of *(1-α) vs.* reaction time should result (Standard: DIN 53 529). At present different calorimeter manufacturers offer linear regression software so that multiple experiments at different heating rates can be quickly and efficiently analysed and values for *n, lnA* and E_A can be determined. For an epoxy amine system such as described in this work the reaction is quite complicated and cannot be described by just one rate constant. The cure process can be split into three regions: kinetic control with initial small activation energies which can be attributed to the initial *catalytic or autocatalytic reaction*. As the reaction advances, the autocatalysis reaction diminishes giving way to the non-catalytic epoxy amine addition reaction with a consequent increase in the activation energy of the reacting system and a transition to the *diffusion control* region with an accordingly strong decrease in reaction rate. For such multiple step reactions it is generally accepted that the Arrhenius equation, which describes a linear relationship between reaction rate and temperature, can only be used as a reaction rate law in a limited range. Even so, most authors

(Guibe `96; Karkanas `97) agree that this equation provides a good linear fit to experimental data up to about 60 to 65 % conversion. Some authors argue that because both catalysed and non-catalysed reactions (may have different activation energies) can occur simultaneously for epoxy amine reactions a true description of multiple step reactions is risky using Arrhenius approximations because they may actually hinder further advances towards understanding the true reaction mechanism. This statement should be approached with care as even with modern software the large number of free parameters used in kinetic modelling, mean that often only a very experienced user could come to any conclusion about the "real" reaction mechanism. The advantage of using more complex models which employ an overall rate law is that they allow for catalytic and autocatalytic reactions, and often provide a more accurate fit to experimental data. One such popular model employs the Sourour-Kamal (Sourour `71) equation:

$$\frac{d\alpha}{dt} = k_1 \cdot c \cdot (1-\alpha)^n + k_2 \cdot \alpha^m \cdot (1-\alpha)^n \qquad \textit{Eq. 3.4}$$

where c is the concentration of the catalyst, n and m are formal reaction orders, k_1 is the rate constant for the initial reaction including effects of catalysts and k_2 describes the autocatalysed reaction. The reaction orders n and m are mathematical fitting parameters and as such the physiochemical validity is questionable. For an epoxy amine crosslinking systems this equation only characterises the initial stages of the reaction. Deviations are observed in the later stages such that the reaction is decelerated or even quenched due to restrictions in chain mobility by the tightening molecular network. This process is referred to as vitrification and can also be described in terms of state as a rubber to glass transition T_g. In the vicinity of vitrification diffusion of the reactive species will become very slow and governs the curing reaction. The separate reaction mechanisms can then be divided into: pure chemical reaction and diffusion control. For both phenomenological and mechanistic models at high conversions, modification to Sourour-Kamal (Eq.3.4) kinetic model has to be introduced. Therefore to achieve a complete evaluation of reaction kinetics the above model must also take into account the more or less complete change from chemically to diffusion controlled reaction steps. The most frequently used integration formulation is given below (Rabinowitch `37).

$$\frac{1}{k_{overall}} = \frac{1}{k_{chem}} + \frac{1}{k_{diff}} \qquad \textit{Eq. 3.5}$$

As usual the term k_{chem} describes the pure chemical reaction (k_1, k_2) with no diffusion considerations. Several approaches to determine k_{diff} are discussed in the literature (Karkanas `97; Höhne `03). However, whilst the chemical rate constant follows an Arrhenius dependence this is not the case for the diffusion rate constant. Since diffusion is a measure of the structure development, it must follow the changes both in T_g and in cure temperature. (Karkanas `00). One of the more popular techniques to determine $k_{diff}$ uses a modified WLF equation (Enns `83) that is also described by Wise (Wise `97). The parameters $C_1$ and $C_2$ are presumed to be constants with respective values of 40 and 51.6 K (Ferry `80). k_d is the diffusion rate constant and $k_{d0} = k(T_g)$ is taken as the diffusion rate constant at T_g. T_{cure} is the cure temperature.

$$\log \frac{k_d(T)}{k_d(T_g)} = \frac{C_1(T_{cure} - T_g)}{C_2 + (T_{cure} - T_g)} \quad or \quad \ln k_d = \ln k_{d0} + \frac{2.303 C_1(T_{cure} - T_g)}{C_2 + (T_{cure} + T_g)} \qquad Eq.\ 3.6$$

$$where\ k_{d0} = A_d \exp\left(-\frac{E_d}{RT_{cure}}\right)$$

In particular Karkanas (Karkanas `00) provides a convincing argument based on experimental data from several epoxy resins that C_1 and C_2 do not remain constant during cure, further complicating evaluation procedures. When diffusion becomes significant the rate constants (k_1 and k_2) in Eq. 3.4 should be replaced by apparent rate constants, which are a combination of the diffusion rate constant and the chemical reaction constants shown in Eq. 3.5 and estimated using Eq. 3.6. Taking these factors into consideration the Sourour-Kamal equation (Eq. 3.4) can now be modified to include diffusion control (Karkanas `96).

As shown the equations and models typically employed to describe the reaction kinetics of a curing epoxy can become quite complex. Taking all factors into consideration Skordos (Skordos `00) stated that his colleague (Karkanas `97), derived non-linear equations with 7 to 11 free parameters to fit experimental data obtained from four different epoxy systems. The fits achieved using these models are excellent, but it is relatively easy to loose the overview. Such models have been shown to function quite well for a specific resin system however any alteration of the resin system will require the reiteration of the laborious model parameter estimation procedure. In such cases the models become more mathematically based and have limited validity in rigorous chemistry terms. This is the main argument for using a mechanistic model whereby a reaction scheme representing the curing

mechanism is selected which can be described by a mathematical reaction rate equation system. The disadvantage is that mechanistic results are very dependent on adequacy (in particular in terms of quantity) of experimental data. This traditional form of searching for rate laws and activation parameters for the overall reaction is as shown complicated and time consuming and therefore evaluation programs independent on which modelling system is used are very useful.

3.3.3 Network formation and Glass Transition

Up to this point the objective was to find a relatively simple a rate law that is best suited to describe the chemical reaction and that could be employed to model the measured ultrasound results used in this work. All models presented rely almost exclusively on data obtained from DSC experiments. Rheological models describing the development of the modulus or viscosity throughout cure are much rarer. This is most likely due to the fact that most rheological instruments are limited in their measurement range and a model is only as good as the experimental data available. Therefore models only exist for prediction of viscosity behaviour up to about gelation point (50 to 60% conversion). The most common equation used to model viscosity or rheological measurements in this range is an adapted WLF equation (Williams `55), adapted to describe the variation of viscosity of thermoplastics with temperature (Ferry `80). It should be noted that in the original WLF formulation the temperature is replaced by cure temperature T_{cure}. The equation implies that if we know the viscosity η at some temperature η_T then we can estimate the viscosity at T_g where C_1 and C_2 are normally taken as constant with respective values of 17.44 and 51.6 K.

$$\ln \frac{\eta_T}{\eta_g} = -\frac{C_1(T_c - T_g)}{C_2 + (T_c - T_g)} \qquad \qquad Eq.\ 3.7$$

Unlike thermoplastics, thermosets undergo a polymerisation reaction so that a change of structure occurs and C_1 and C_2 will become as material dependent parameters (Mijovic `89). The rate of network formation is a function of kinetics which in turn is a function of temperature and time. Hence to correctly employ Eq. 3.7 one requires (a) the increase in glass transition as a function of network formation i.e. degree of cure and (b) variation of C_1 and C_2 as a function of cure temperature from viscosity experiments. Karkanas provides

(Karkanas `00) provides a detailed explanation on the calculation of $C_1$ and $C_2$ using linear regression mathematics. Taking these factors into consideration the authors (Mijovic `89 and Karkanas `00) were able to provide excellent models for viscosity advancement for a range of epoxy resins. Of course the modelled data, is just as good as the experimental results available, which means only the early stages of cure (about 50 to 60% conversion) were considered, so that such models are not suitable for predicted diffusion behaviour i.e. have not been employed to model vitrification.

Therefore a different model or more importantly experimental analysis technique is required to describe the relationship between glass transition and conversion or extent of reaction. It is well known that in the case of epoxy/amine reactive mixtures the relationship between T_g and conversion is independent of cure temperature. The most comprehensive expression that correlates segmental motion and chemical conversion with T_g is the following expression (Adabbo `82 and DiBenedetto `87):

$$T_g = T_{g0} + \frac{(T_{g\infty} - T_{g0})\lambda\alpha}{1 - (1-\lambda)\alpha} \qquad \text{where } \frac{F_x}{F_m} = \lambda \qquad \qquad Eq.\ 3.8$$

where α is the conversion at the glass transition; glass transition temperatures of the uncross-linked T_{g0}, partial- T_g and fully cross-linked $T_{g\infty}$ polymer and F_x/F_m is the ratio of segmental mobility's for the polymer at T_{g0} and $T_{g\infty}$.. Theoretically the adjustable parameter λ is equated to the ratio of the respective heat capacities c_p for the initial mixture c_{p0} and the fully cured network $c_{p\infty}$ (Pascault `90; Georjon`93).

$$\frac{c_{p\infty}}{c_{p0}} = \lambda \qquad \qquad Eq.\ 3.9$$

This is an important statement as quite often segmental motion activity can only be estimated whereas heat capacities can be measured using modern calorimetric techniques. It has been suggested (Karkanas `00) that a single λ value is able to describe all characteristic cure behaviour for a specific resin. For each new thermosetting polymer analysed it will have to be determined experimentally. The results from the above authors show a significant amount of scatter when the experimental results, degree of conversion α versus T_g are fitted with the experimental model obtained from the Eqs. 3.8 and Eq. 3.9. The authors attribute this to the lower sensitivity of conversion in the later stages of cure.

4 Analysis Techniques for Cured and Reactive Epoxy

4.1 Ultrasound Measurement Systems

4.1.1 Ultrasonic Measurement Assembly and Working Principles

The sensors employed are untypical in that they can withstand consistent dynamic heating and cooling periods in the temperature range from 25 to 200 °C. The ultrasound sensors Type K4 were developed at the Krautkrämer GmbH (now AGFA) in corporation with BAM (Döring `00). They have a middle frequency of 3.5 MHz, which refers to the natural mechanical frequency of oscillation of the piezoelectric plate. This ceramic resonator is normally damped by a thin layer of a polymeric based backing material on the cable side that plays a major role in forming a short distinguishable pulse. A basic schematic diagram is shown in Fig. 4.1. Total sensor length without plug is 31 mm with a head diameter of 8 mm.

A steel delay line at the front of the sensor provides protection in industrial environments and separates the excitation pulse from the response. The second set of sensors employed have an operating frequency range between 200 too 700 kHz. The sensors are prototypes developed by the company Imasonic, France as part of an EU project (Mc Hugh `03). The sensors were originally designed for high
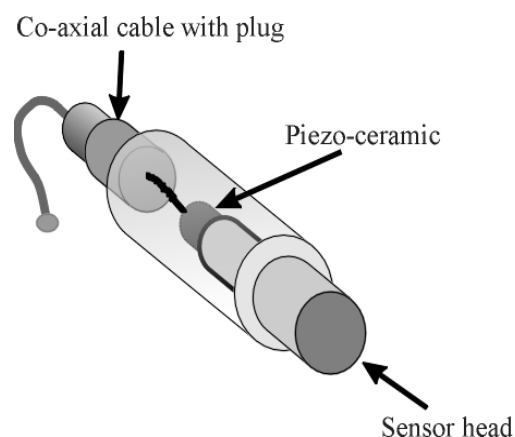
Fig. 4.1 *Schematic diagram of an ultrasound sensor illustrating working principle*

temperature and pressure testing of polymers used in ultrasound applications in oil boreholes at depths up to 10 km (180 °C and 1400 bars). The sensors are constructed from several individual array elements wired in parallel so that the functionality is similar to a monocomponent sensor such as already described. The sensors have no delay line just a thin polymer shielding layer to protect active components. Due to intellectual property rights further disclosure of technical details is not permitted. All sensors are connected using high temperature Lemo connectors and coaxial cables with a high temperature resistant Teflon shield. The flow chart in Fig. 4.2 illustrates the operation principles of the measurement assembly. All equipment works according to through transmission principles with one sensor functioning as sender and one as receiver. The sensors are controlled by a Type 5800 impulse generator (300 V electrical excitation pulse) and amplifier from the company Panametrics. This excitation pulse causes the piezoceramic material to oscillate sending a sound wave though the sample material. Pulse form and frequency range are dependent on sensor type. The mechanical wave generated travelling at sound velocity passes through the material and is converted back into an electrical signal by the receiver. This analogue electrical signal is amplified and converted into digital format by the Analogue-Digital (A/D) card in a digital oscilloscope type Yogogawa DL7100. The signal Amplitude scan (A-scan) is displayed on
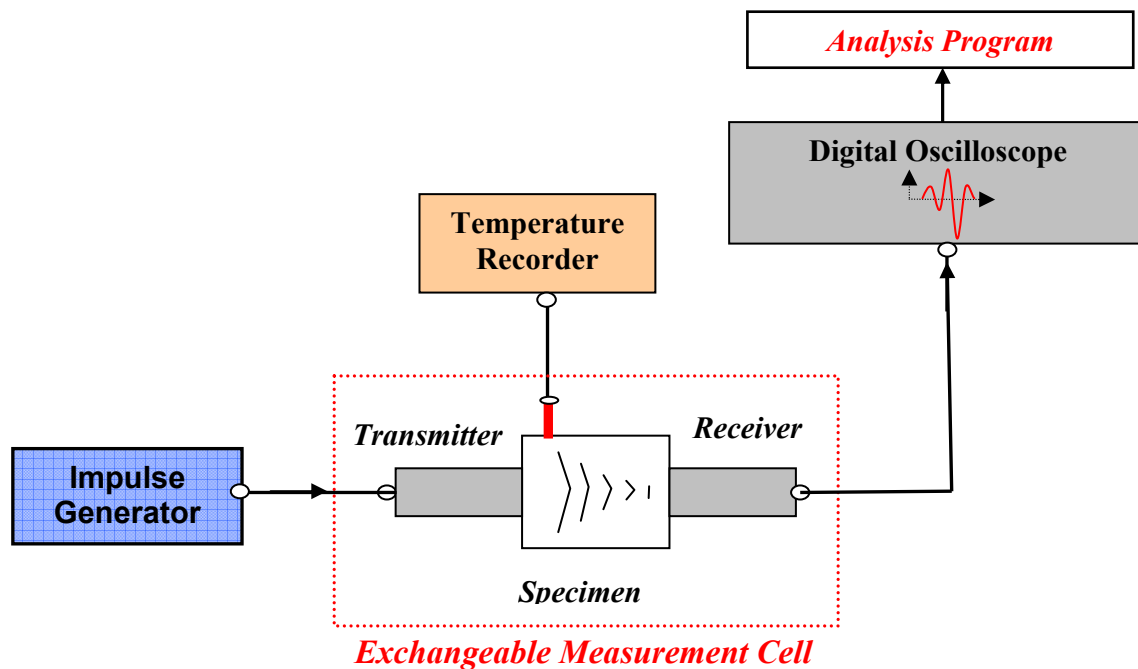
**Fig. 4.2** *Block diagram of ultrasonic measurement assembly*

oscilloscope, recorded and has a similar form to amplitude scans shown Figure 4.8. Recorded A-scans for each sample thickness are saved to hard disk in ASCII (**A**merican **S**tandard **C**ode for **I**nformation **I**nterchange) format. In transmission mode the received signal with the shortest transmission time will have travelled the shortest distance i.e. through the material. The technique has the added advantage that interference caused by surface waves, reflections at material boundaries and electrical noise (because two separate electrical lines are used) will not be as strong as for a reflection technique.

4.1.2 Design and Function: Testing Equipment and Ultrasound Sensors

4.1.2.1 Thermal Analysis at 2 to 7 MHz on a fully Cured Epoxy

Fig. 4.3 illustrates a measurement cell designed for testing solid polymers. The cell contains 4 sensors i.e. two measurement lines in through transmission. Two solid polymer samples with different thicknesses are measured simultaneously using this technique. The measurement cell was originally designed for use in high pressure autoclaves and therefore has a threaded (not visible) steel adapter. Both samples were clamped using personal judgement (hand tight) without applying any excessive pressure. The main criterion was that no deformation of samples occurred. Both top and bottom sensor rows can be adjusted individually and the clamp adjusts the bottom cylindrical back plate (on the adapter side). The opposite aluminium cylindrical plate on the side of the clamp is stationary. This means the assembly can be adjusted quite finely to obtain optimal contact with the samples while at the same time ensuring samples of varying thicknesses can be safely clamped in position. For heating or cooling experiments the whole cell is placed in a silicon oil bath. The clamped samples are heated to approximately 180 °C over a 2 hour period and held at this temperature for 30 minutes before the experiment is started. This is to ensure that the samples are fully cured. As it is difficult to control the temperature in a dynamic heating run, the oil-bath containing cell and samples is heated to 200 °C and cools slowly in air, to room temperature. Metal components are constructed from aluminium. Although one measurement can take up to 8 hours before the oil-bath reaches room temperature, this technique has the advantage that samples with different thicknesses should have equivalent homogeneous temperatures. Temperature was monitored using a Type K thermocouple wire placed in the vicinity of the epoxy samples Another thermocouple wire is placed in the oil-bath itself to monitor

differences. The thermocouple is connected to a WE 4000 measuring station from Yogogawa which is connected to the computer by an RS232 interface. Samples are prepared by pouring the epoxy mixture at room temperature into a 12 mm diameter cylindrical silicon mould. The prepared samples are then sanded down to thicknesses of approx. 4 mm and 8 mm. Sample thickness is checked before and after each measurement to account for sample deformation or shrinkage. The advantages of employing a two sample technique are explained in Chapter 4.2. Sample thicknesses were specifically chosen to minimise geometry effects as explained in Chapter 2.2.3. For example, sample thickness is always several times the wavelength of the sound wave.
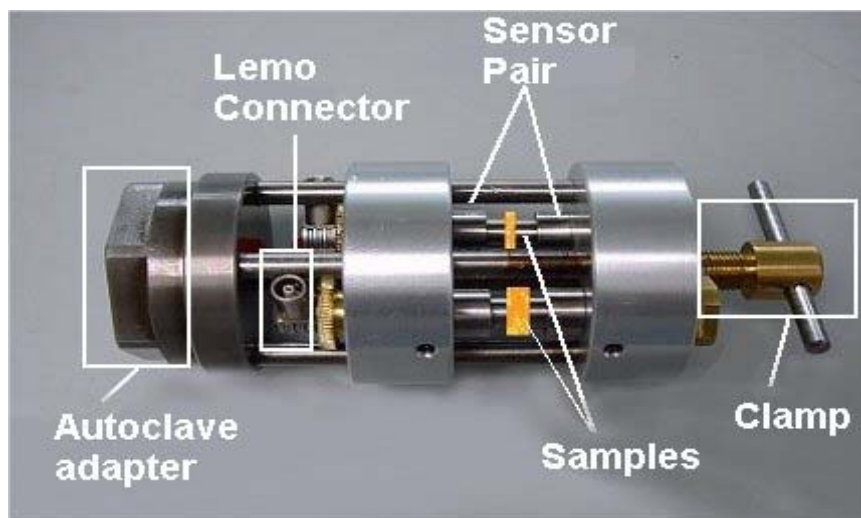
Fig. 4.3. *Measurement cell containing two measurement lines operating in through transmission. Connecting wires are not shown. Samples are clamped between the sensors.*

4.1.2.2 Thermal Analysis at 200 – 700 kHz on a fully Cured Epoxy

The second measurement cell is based on the same operating principles already described. A new cell was required because of the new sensor design and in particular the large head diameter. Some essential differences in design needed to be considered. The sensors are covered by a thin copper foil with a red colour as shown in Fig. 4.4. They are not as robust as the commercial Krautkrämer sensors discussed above. A clamping or holding force can only be applied from behind, not from the side. Sensor diameter is 14 mm with no delay line. The sensors are prototypes and only one sensor set was available. This means that per material

tested (two thicknesses required), two individual experiments are required. Cylindrical samples with a diameter of 32 mm and respective thicknesses of 10 and 16 mm were prepared in a purpose build silicon mould. In order to speed up the heating and cooling processes the whole assembly was constructed to fit in a glass beaker, which can be placed on a hot plate. A magnetic stirrer ensures a good temperature distribution. In the measurement assembly illustrated the bottom sensor is fixed. The top sensor can be moved with the top plate and clamped into position by tightening the screws connecting the top plate to the cylindrical bars. It is important that a similar clamping force is applied to all samples to ensure constant boundary conditions. For this reason a temperature stable spring (on the right hand side of Fig. 4.4) was placed in a special mount allowing a maximum sensor displacement of 0.5 mm. A thermocouple Type K wire was also placed in the vicinity of the sample. Sample preparation and measurement scheme is the same as described in Chapter 4.1.2.1**.**
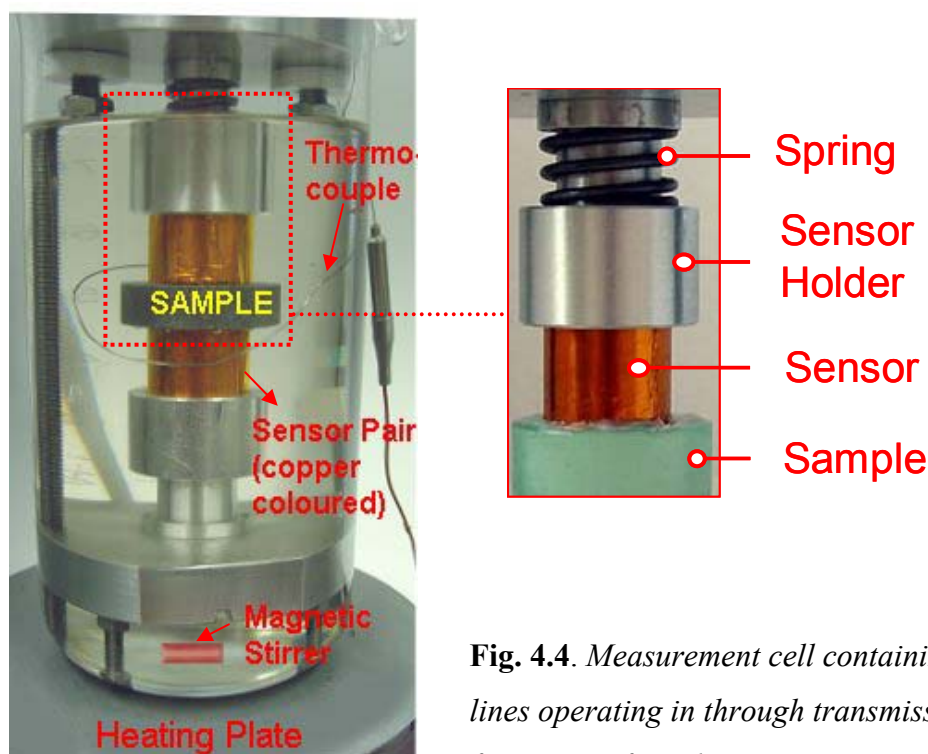
Fig. 4.4. *Measurement cell containing 2 measurement lines operating in through transmission at a middle frequency of 450 kHz.*

4.1.2.3 Cure Monitoring on Reactive Epoxy at 2 to 7 MHz

The technical design for the construction of the brass epoxy measuring cell has been described at an earlier date (Mc Hugh `03). The cell consists of two halves, each containing an ultrasonic sensor and illustrated in Figs. 4.4 and 4.5. Figure 4.4 illustrates an opened

measurement cell. It is possible to open and close the measuring cell by lifting the upper mould half with an insulated handle which facilitates the fast removal of samples for DSC analysis. On the left hand side of the photo is the top half consisting of an outer cylinder and a threaded internal cylindrical core with a steel sensor located in the middle. When the cell is closed the distance between the two sensors can be set from zero to 9 mm by turning the inside core cylinder. It is engraved with a metric measurement scale with one full turn representing 1 mm thickness change and operates similar to a micrometer screw. This inside cylinder is dipped into the epoxy resin sample so that the distance between sensors is equal to the sample thickness. The front surface of this inner core is half the internal diameter of the cavity ring and is rounded presenting a smaller surface area for the cured epoxy to adhere to.

The bottom half of the opened measuring cell is shown on the right hand side of Fig. 4.4. It consists of a single cylinder with a steel sensor located in the middle. A ring can be screwed onto this cylinder and when fully tightened functions as the mould cavity. The liquid epoxy sample is poured into this cavity. A small channel is cut into this the ring to enable a thermocouple wire shown in Fig. 4.4 to pass through into the cavity. This K-Type thermocouple is embedded in the resin to guarantee excellent temperature monitoring of the sample. Temperature is recorded using the WE 4000 measuring station. At the end of each experiment the wire is encapsulated by the epoxy and is therefore simply cut and reused by re-soldering or reuniting the split ends. The surface of the cavity is flat and highly polished so that the cured epoxy part can easily be removed by opening the cell and unscrewing the cavity ring together with the sample. The moulded epoxy part is pushed out by hand and the ring re-used. Before the measuring cell is used the inner surfaces are sprayed with a Teflon based release agent. The measuring cell is thoroughly cleaned before each new measurement series or after every 5 to 6 removed samples. All parts of the cell that are in contact with the epoxy resin are rounded or chamfered so that no sharp or angular surfaces are left. This eases opening and if required cleaning of the cell. The head of the ultrasonic sensors are plane parallel to the mould surface.

As shown in Fig. 4.5 the temperature of the upper and lower cell halves is monitored by two Pt-100 type (platinum resistance temperature detectors RTD's. The Pt-100 RTD's provide accurate data required to control the lower and upper cell temperatures using two heating rings as shown. Both upper and lower mould halves can be controlled and adjusted individually by a Hasco temperature controller. All measurements using this equipment take place at constant temperature as the temperature controller is not suitable for dynamic heating experiments.
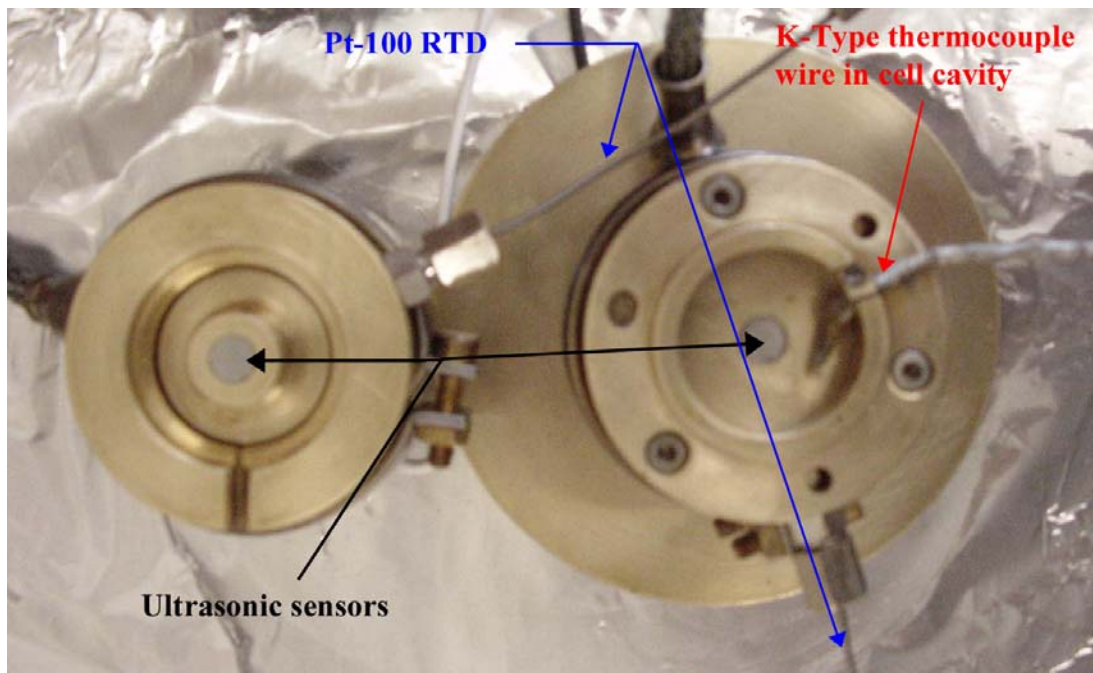
Fig. 4.5. *Photo of the opened measuring cell for reactive thermosetting resins*
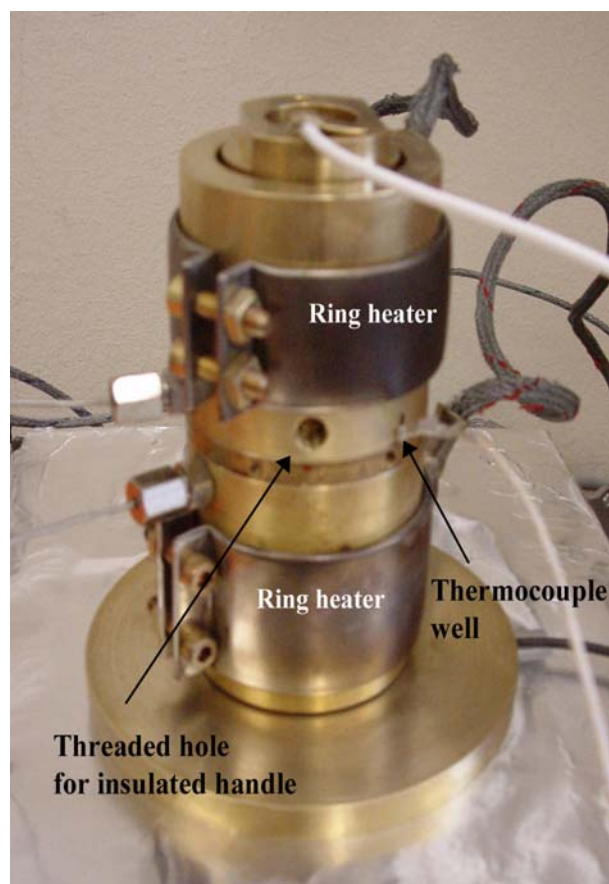
Fig. 4.6. *Photo of the closed measuring cell for reactive thermosetting resins*

4.2 Ultrasound Generation and Detection

The amplitude of a sound wave passing through different media will decrease continuously with distance as it loses mechanical energy. In the discussion on wave theory and interrelation to mechanical modulus, it was shown that sound velocity in the medium is related to the elastic constants whereas attenuation depends primarily on the inelastic or viscous properties. Two principle forms of acoustic losses are of particular relevance to this study:

1. Scattering processes or reflections on material boundaries causes a decrease in wave amplitude. Such losses are a result of different material impedance values as the wave propagates through one medium to another (see Eqs. 4.3 and 4.4 on following page). Particularly during dynamic temperature runs (from 20 to 200 °C) it is expected that the impedance difference between, for example, the surface of a steel sensor and a polymer will not remain constant. The polymer will exhibit a much larger change in sound velocity than a metal in this temperature range. .

2. Absorption of wave energy mainly caused by internal friction or relaxation effects, and hysteresis (frequency dependence of wave propagation in polymers). Essentially this refers to dissipative dispersion or any mechanism leading to the conversion of acoustic energy to thermal energy that results in a loss of wave amplitude (increase in attenuation).

Great care has been taken in preparing the samples so that no inhomengenities or voids occur and therefore related scattering effects can be neglected. The measured acoustic attenuation will be influenced strongly by a combination of both the above effects. To understand which mechanism actually leads to a reduction in signal amplitude, it was necessary to find a means to quantify or separate each effect. This may be achieved experimentally. The attenuation α in the polymer sample is calculated from the ratio of the ultrasonic wave amplitude entering the sample A_i and exiting the sample A_e taking into consideration sample thickness d (Eqs. 4.1 and 4.2). A schematic illustration of measurement setup is also shown in Fig. 4.7.

$$A_i = A_e \cdot e^{-\alpha d} \qquad\qquad\qquad Eq.\ 4.1$$

$$\alpha = \frac{1}{d} \ln \frac{A_e}{A_i} \qquad\qquad\qquad Eq.\ 4.2$$

The measured amplitude value A_e will be influenced by several factors including frequency, thickness of sample and boundary losses already discussed. In order to determine the actual material attenuation, other sources of acoustic losses need to be accounted for. One of the main sources causing a loss in amplitude occurs at the boundary. Each material has its own characteristic sound velocity c and density ρ, which are related by the acoustic impedance Z. The reflection factor R at the boundary of two materials with respective impedances Z_1 and Z_2 can be calculated as follows:

$$Z = \rho c \qquad\qquad \text{Eq. 4. 3}$$

$$R = \frac{Z_2 - Z_1}{Z_1 + Z_2} \qquad\qquad \text{Eq. 4. 4}$$

The problem with reflectivity on material boundaries is aggravated by the fact that the temperature during experiments on the cured epoxy is not constant. This means accurate evaluation of attenuation is difficult using one sample because material dependent impedance values and reflectivity e.g. between steel sensor and epoxy boundaries will very probably vary disproportionately over the temperature range employed. If two identical samples with different thicknesses are used the reflectivity factor R may be considered identical (Fig. 4.7) and the attenuation may be calculated directly from the amplitude ratio of the samples. The attenuation α is calculated from the measured signal amplitude A_1 and A_2 after transmission through the respective samples with thickness d_1 and d_2. Attenuation α in damped oscillations measures the rate at which the amplitude decays and is described by an exponential function $e^{-\alpha d}$ as shown in Eq. 4.1. In the following Eq. 4.2 is adapted to the two sample measuring technique as follows and presented in Neper and dB units.

$$\alpha = \ln\frac{A_2}{A_1} \ \frac{1}{d_2 - d_1} \ \text{[Np/mm]} \qquad\qquad \text{Eq. 4.5}$$

$$\alpha = 20\log\frac{A_2}{A_1} \ \frac{1}{d_2 - d_1} \ \text{[dB/mm]} \qquad\qquad \text{Eq. 4.6}$$

Also sound velocity c is calculated using the two sample technique by measuring the sample transmission times τ_1 and τ_2 for different thicknesses d_1 and d_2 as shown in Eq.4.7.

$$c = \frac{d \ (thickness)}{\tau \ (Transmission \ Time)} \quad \text{or} \quad c = \frac{d_2 - d_1}{\tau_2 - \tau_1} \qquad\qquad \text{Eq. 4.7}$$

Apart from material impedance values another important factor (*see point 2 above*) which needs to be considered is frequency dependence of both sound velocity and attenuation. The ultrasound transducers used in this work are broadband i.e. they operate at a range of frequencies. Typically a sensor will be classified by its middle frequency, the frequency with the highest amplitude in the magnitude frequency spectrum. As a result of bandwidth the ultrasound mechanical wave propagating through the material will also consist of a number of frequency components. Dispersive materials such as polymers have the potential to damp an acoustic wave whereby each frequency component may be attenuated to a different extent. For example the high frequency components are often more suppressed than the low frequency. Dispersion effects such as frequency dependence of sound velocity (Chapter 2.2.4) will depend on material state and it is likely for polymer materials that dispersion does not remain constant over a temperature range. Absolute values for the attenuation coefficient (α) are also frequency dependent and for polymers typically increase linearly with frequency. This effect is referred to as hysteresis and according to an experimental work Hartman (Hartmann `72) is not related to relaxations or transitions in polymers. It has been well documented for Polymethylmethacrylate and Polyethylene measured at room temperature that attenuation behaviour exhibits a linear relationship to increase in frequency (Hartman `72).
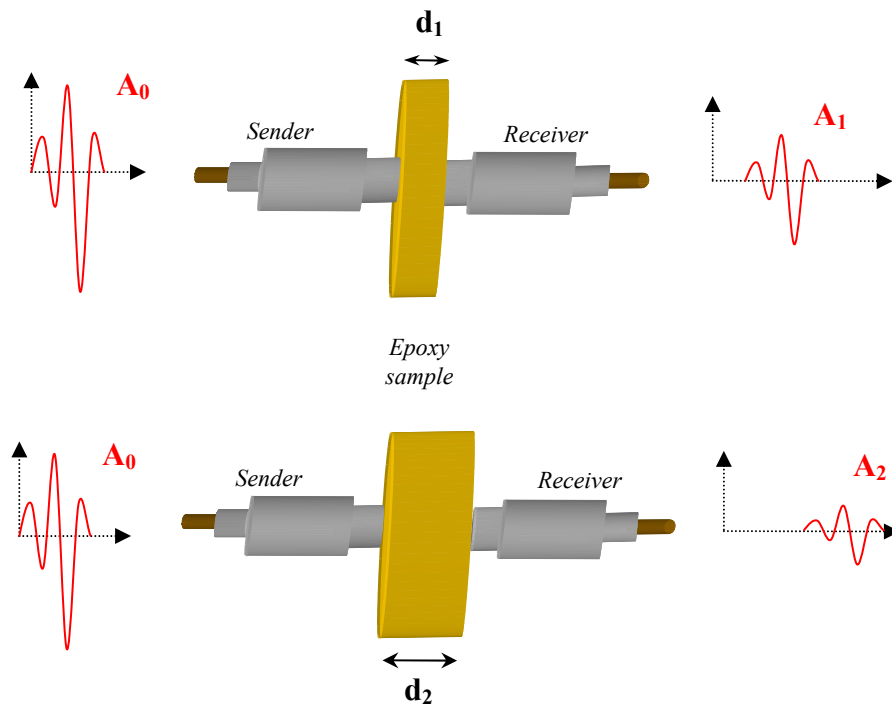
Fig. 4.7: *Schematic diagram of sound velocity and attenuation measurement using two different sample thicknesses*

Therefore to obtain accurate values for the polymers elastic modulus (estimated from sound velocity and attenuation), phase and group velocities of waves in dispersive media as well as frequency dependent attenuation need be determined. This is achieved using spectral analysis of the broadband pulses. At each temperature an oscillogram or amplitude scan (A-scan) is recorded and analysed. For this specific application using a two component technique no evaluation software was available facilitating the evaluation of attenuation and sound velocity as a function of frequency. For this reason a program was written by J. Mc Hugh and J. Bartusch at BAM using the Labview® computer language from National Instruments. In the following paragraphs the basic background and evaluation principles used for this analysis software are described starting with a basic description of Fast Fourier Transformation FFT analysis.

4.2.1 Spectral Analysis using Fast Fourier Transformation FFT Software

The advantage of using the Labview® program language is that several Digital Signal Processing DSP functions such as the FFT analysis are available in the program library and can be adapted to specific problems. The following passages provide a step by step breakdown on how the phase velocity and attenuation are evaluated using this software. The hardware setup for recording the A-scans has been discussed in Chapter 4.1.1. To demonstrate how the program functions a real evaluation example is provided for measurements using the two sample set-up shown in Fig. 4.3. Two fully cured epoxy samples 10 and 16 mm thick are placed in the experimental assembly illustrated. The assembly is placed in an oil bath which is used as a heating medium. The sensors operate in the kHz range and have a middle frequency of 450 kHz. An A-scan is recorded at specific temperatures using a digital oscilloscope described in section 4.1 and loaded into the Labview program. The ASCII files loaded contain the recorded amplitude (curve form) information with 1002 sample points containing amplitude values. Time information is obtained from the oscilloscope measured window settings, in this example the A-scan is measured in the 0 to 20 µs time window. As different time and amplification settings may be employed, these settings are also written into the source file name – white box above the A-Scan in Figure 4.8 e.g. *20dB_25°C_10mm.* Window settings and amplification are then typed into settings boxes clearly marked with yellow and black colours above the A-Scan.

Fig. 4.8. *Recorded A-Scans for 10 and 16 mm epoxy samples. Oscilloscope settings were 20 μs time window and amplification 20 dB for both samples.*

FFT analysis of the above signal provides frequency information in the time range (+/- 1/t), in other words a two sided spectrum in complex form (real and imaginary parts). A two sided spectrum is normally considered symmetrical and only the positive half of the spectrum is displayed, the negative side is considered redundant. The FFT spectrum provides 2 main kinds of information; phase and magnitude. The magnitude for the power spectrum is normally calculated and defined as the mean squared amplitude (energy content) at a specific frequency (in dB or Np). It contains no phase information (see Eq. 4.6). In order to obtain phase information the complex array is converted into its real and imaginary parts. This can be achieved using the rectangular to polar conversion function (Labview® program library) that converts the complex array into its magnitude M and phase θ spectrum equated in the form shown below in Eq.4.8 and 4.9. Actual amplitude and the phase spectrum for the A-scan signals in Fig. 4.8 are illustrated in Fig.4.9. N is the number of points in the acquired time domain signal.

Amplitude spectrum in quantity peak

$$= \frac{Magnitude[FFT(A)]}{N} = \frac{\sqrt{[Re[FFT(A)]]^2 + [Im[FFT(A)]]^2}}{N} \qquad Eq.\ 4.8$$

Phase spectrum in radians =

$$Phase[FFT(A)] = arctan\left(\frac{Im[FFT(A)]}{Re[FFT(A)]}\right) \qquad Eq.\ 4.9$$

The equations describe the basic signal analysis computations employed to obtain the phase and amplitude spectrum. The actual equations are based on Fourier mathematics and are quite complex but a rather good explanation of FFT analysis in combination with signal processing applications can be found in the literature (Karrenberg `01, Schnorrenberg, `89). It is worth noting that the arctan function in Eq. 4.9 returns values of phase between -π and π, which if graphically illustrated form a zigzag muster. A positive to negative phase change occurs with a direct 90 degree phase shift, meaning that the -π and +π phase can be easily summated (function also available in the Labview® program library). After summation takes place, phase information is presented as a linear function of frequency as shown in Fig. 4.9 on the right hand side. In principle this is not complicated, however as is often the case the complexity often lies in the details. In the following a brief overview of some of the main problems encountered and solutions are discussed. The explanations are intentionally basic and brief:
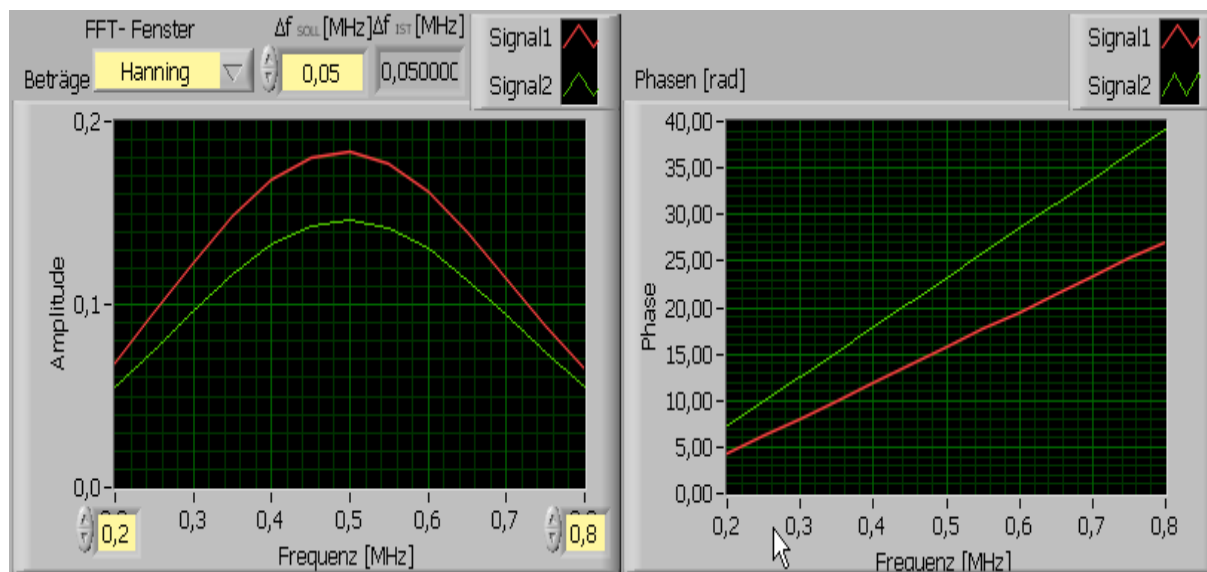
Fig. 4.9 *Magnitude (left) and Phase (right) spectrum windows for 10 (red) and 16 mm (green) epoxy samples*

- *The FFT analysis provides frequency information about phase and amplitude over an almost unlimited frequency spectrum. However only 1002 sample points are available and therefore resolution will suffer, if as in the case here only a tiny part of the spectrum (200 to 800 kHz) is analysed.*

If only the spectrum, as in this example, between 2 and 7 MHz is considered the number of sample points and therefore resolution is reduced considerably. The resolution (distance between points) in the frequency spectrum is given by $\Delta f = 1/(N \cdot \Delta t)$, where Δt is the sampling period, Δf frequency period and N is the number of points in the acquired time domain signal. The sampling frequency will determine the frequency bandwidth of the spectrum and for a given sampling frequency, the number of points acquired in the recorded time domain signal determines the resolution frequency. Simply, if one wishes to increase frequency resolution, increase the number of points acquired at a given sampling frequency. As the A-scan (time domain) is recorded and not analysed in real time, it can be loaded into the program and easily padded with extra points through interpolation. In this case the amplitude before the green line is set to exactly zero and padded by 10000 zero amplitude sample points having the effect of spectrum smoothing and increasing the frequency resolution.

- *The green and red cursor line can be shifted with the mouse so that only the signal of interest is analysed (as shown in Fig. 4.8). For signal analysis of the frequency spectrum a Hanning window was used. Why?*

Under normal signal acquisition conditions it is difficult to obtain a nicely scaled, single sided spectrum. This has largely to do with the fact that the FFT algorithm assumes that signals contained in the time domain are periodic at intervals that are a multiple of the original signal. If the time domain has a non-integral number of cycles, this assumption is violated and spectral leakage occurs. Another way of looking at this case is that the non-integral cycle of the frequency component does not correspond exactly to one of the spectrum frequency lines. This may eventually lead to a smearing of the spectrum known as spectral leakage eventually leading to some amplitude error in the frequency peak. This is a common problem in Digital Signal Processing DSP and several window functions are available for analysis, which help avoid such discontinuities. The windowing of input data is mathematically equivalent to convolving the original spectrum with the spectrum of the window function. All window functions are a compromise between resolution and amplitude. Using a no-window function is in fact a rectangular window (convolution of a sine function spectrum). To guarantee continuity in results only a Hanning- that is sometimes referred to as Hann- window is used. A

Hanning window has the advantage that it softens the sharp edges of the rectangular window and enables selective analysis and separation of the signals at the edges of the spectrum leading to less smearing.

4.2.2 Evaluation of Phase Velocity and Attenuation

To obtain accurate sound velocity values, phase information as shown in Fig. 4.9 is required. The phase velocity is calculated according to Eq. 4.10 that is well known from the literature (Sachse `78; O'Donnell `81). The general equation employed by the authors is only modified to integrate the terms for the two sample testing setup employed in this work. By subtracting the measured phase angles ϕ for the 16 and 10 mm samples already illustrated in Fig. 4.9, the phase difference can be calculated over the relevant frequency range. The difference in sample thickness is known so that the phase velocity may be calculated at specific frequencies f as shown in Eq. 4.10 and in Fig. 4.10.

$$\textit{Phase Velocity } v(f) = \frac{2\pi f L}{\left(\phi_{s1} - \phi_{s2}\right)}$$ *Eq. 4.10*

ϕ_{s1} *Phase angle for sample thickness d_1*
ϕ_{s2} *Phase angle for sample thickness d_2*
L = Thickness difference $[d_2 - d_1]$

Determination of attenuation values as a function of frequency is obtained by placing the respective frequency dependent sample amplitudes A_1 and A_2 from the magnitude spectrum shown on the left hand side of Fig. 4.9 into the attenuation equation described in Eq. 4.5. The evaluation window is shown in Fig. 4.10 on the next page. On moving the yellow and red cursor lines along the frequency axis, the attenuation and phase data will be displayed in the white boxes under the diagram. This information may be recorded manually or saved to an Excel (*.xls data) spreadsheet.
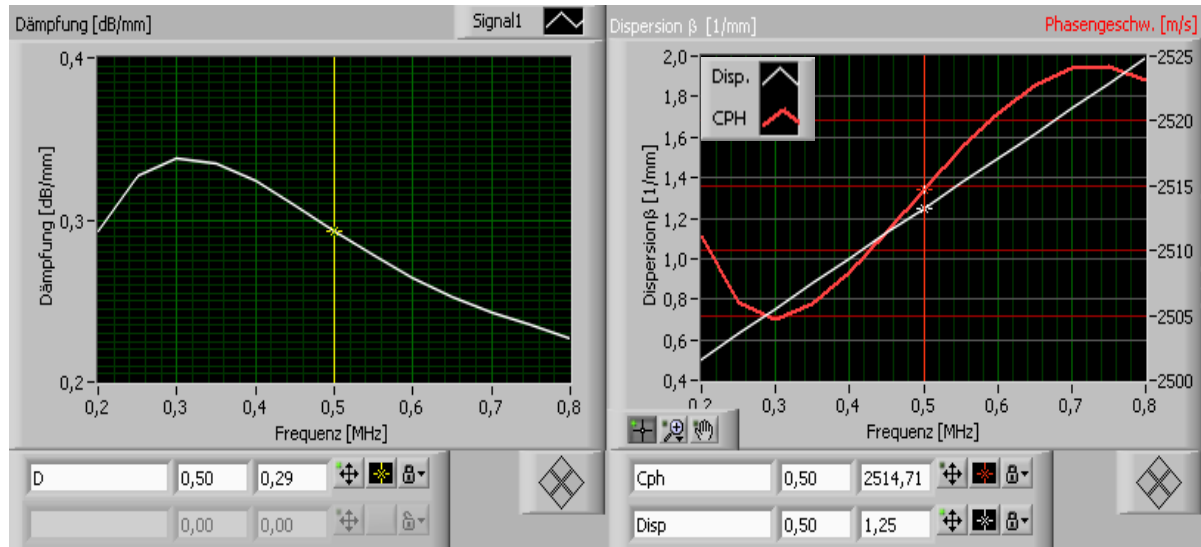
. **Fig. 4.10** *Illustration of attenuation and phase velocity as a function of frequency for a fully cured epoxy measured at 25 °C*

4.2.3 System Qualification:

To check the accuracy of this evaluation technique in combination with the measurement setup already described, phase velocity and attenuation measurements were performed on a standard calibration block illustrated in Fig. 4.11 (International Institute of Welding: IIW Type US-1) containing steel and polymer Polymethylmethacrylate materials. IIW type blocks are used to calibrate instruments for both angle beam and normal incident inspections. Measurements took place using the above FFT software and Time of Flight TOF techniques in both reflection and transmission modes. For both techniques an average sound velocity of 5920 m/s was measured for 22 mm steel with a deviation of ± 10 m/s or approx. 0.3 %. For
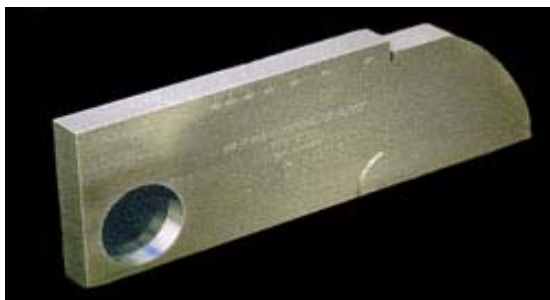
Fig. 4.11 IIW Type US-1 calibration block

these reference experiments a thin layer of silicon oil was used as coupling medium. The quoted deviation could easily be a result of manual error and the results are very satisfactory. Additionally when two identical material samples with different thicknesses are employed it is relatively simple to confirm the accuracy of sound velocity measurements using a TOF measurement with Eq. 4.7. The results should compare well with FFT analysis techniques taking into consideration frequency effects.

4.3 Conventional Analysis Techniques (Polymer Characterisation)

4.3.1 Dynamic Mechanical Analysis, DMA

Dynamic mechanical analysis techniques measure the response (deformation) of a material to periodic forces by applying mainly sinusoidal excitation and response techniques. DMA analysis took place using two different instruments a Myrenne Torsional Pendulum ATM3 and a Netzsch DMA 242C. Using the torsional pendulum the specimen is set in motion by a once off torsional force and undergoes damped free sinusoidal oscillations with a displacement not greater than 3 degrees. If the mechanical properties of the specimen change, the instrument mechanically places different weights on the inertia disk to guarantee a frequency of 1 ± 0.1 Hz. It is possible using Thermal Mechanical Analysis also incorporated in the Myrenne Torsional Pendulum instrument to measure the change in length of a rectangular sample with the standard dimensions of 60*5*1 mm. Such measurements are, in principle, also possible with the Netzsch instrument. However, changes in length using torsional measurements are more accurate than using a three point bending testing setup.

Most work has been carried out on the DMA 242 C instrument because the ATM3 can only be employed in a very limited frequency range. Both instruments operate in the temperature range -150 to 600 °C. To achieve defined heating and cooling rates and for measurements at low temperatures either nitrogen gas or liquid can be blown into a furnace chamber containing the sample holder. The DMA 242 C is based on forced vibration i.e. deformation is measured at a specific measurement frequency. To facilitate measurements on a variety of different sample geometries, both on soft elastomers and on high elasticity composite materials one requires a wide range of different loads with the appropriate sample holder systems. For this work a dual cantilever sample holder as shown in Fig. 4.12 on the next page is chosen because it is well suited to thermoset materials. Using this configuration both ends of the sample are clamped firmly and the load is applied by the inner clamp located in the sample middle. This inner clamp is vibrated by means of an electromagnetic driving shaft which provides a sinusoidal dynamic force at a specific frequency. This shaft can be driven at frequencies between 0.01 to 100 Hz which provides the frequency range of measurement. The applied force or stress σ is proportional to the a.c. current fed to the drive shaft and is applied sinusoidally. The sample displacement is detected using a Linear Variable Differential Transformer LVDT positional sensor.

$$E* = \frac{l^3}{4(bh^3)}\left(\frac{F*}{a*}\right)$$
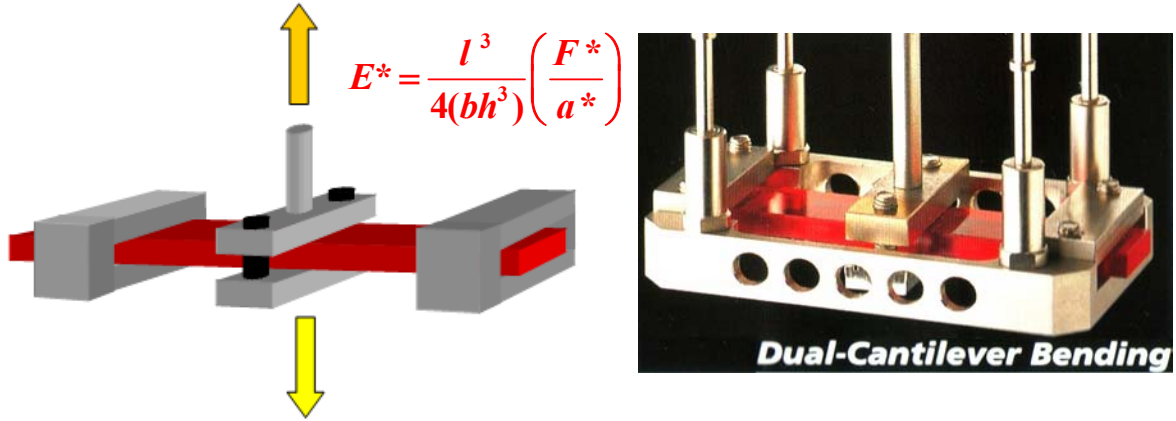
Fig. 4.12. *Dual Cantilever Sample (in red) Holder for Netszsch DMA 242 C instrument: Geometry Factor GF for dual cantilever setup is shown in red*

Strain ε is calculated from the displacement. For an elastic solid the in-phase sinusoidal stress and strain is written as:

$$\text{Stress}: \ \sigma = \sigma_0 \sin \omega t \qquad \text{Strain}: \ \varepsilon = \varepsilon_0 \sin \omega t \qquad \textit{Eq. 4.11}$$

For viscoelastic solids, the stress and strain are not in phase, the strain lagging behind the stress by the angle δ. The stress can be considered to consist of two components, one in phase with the strain ($\sigma' = \sigma_0 \cos \delta$) and one out of phase ($\sigma'' = \sigma_0 \sin \delta$). When these are divided by the strain, one can separate the modulus into an in-phase (real) and out of phase (imaginary) component. These relationships are:

$$E' = \frac{\sigma'}{\varepsilon_0} = E* \cos \delta \qquad \qquad \textit{Eq. 4.12}$$

$$E'' = \frac{\sigma''}{\varepsilon_0} = E* \sin \delta \qquad \qquad \textit{Eq. 4.13}$$

$$|E*| = \frac{\sigma_0}{\varepsilon_0} = \sqrt{E'^2 + E''^2} \qquad \qquad \textit{Eq. 4.14}$$

In terms of complex notation the complex dynamic modulus (Eq. 4.14) can be written as:

$$E* = E' + iE'' \qquad \qquad \textit{Eq. 4.15}$$

The real part of the modulus E′ is sometimes referred to as the storage modulus because it is related to the storage of energy as potential energy and its release in periodic deformation. The imaginary parts of the modulus E′′ is called the loss modulus and is associated with the dissipation of energy as heat when the materials are deformed.

The phase lag between the stress and strain is used to determine the loss tangent *tan(δ), ω* is the angular frequency normally expressed in radian. The loss tangent describes internal friction and damping and is the ratio of energy dissipated per cycle to the maximum potential energy stored per cycle.

$$\tan(\delta) = \frac{E''}{E'}$$

Eq. 4.16

Before the complex tensile modulus E* may be calculated, the sample geometry and type of loading have to be taken into consideration. Each sample holder has a Geometry Factor GF that has to be included in the calculation of the various mechanical moduli. The GF equation for the dual cantilever setup is included in Fig. 4.12, where *l* is sample length, *b* is sample width, *h* is sample height, *a** is the complex mechanical displacement and *F* is the complex dynamic force (N).

4.3.2 Rheometric Analysis

The experiments were performed on a Haake RS150 rheometer. The rheometer uses 20 mm diameter disposable aluminium plates saving considerable experiment preparation times as otherwise samples would have to be burned of in a furnace after each measurement. Measurement principles are very similar to DMA. By applying a sinusoidally varying stress to a sample, a response strain (and vice versa for applied strain) will be induced. This describes the two possible modes of measurement: In the controlled deformation (CD) mode an angle of deformation or displacement is given and the shear stress response is measured. In the controlled stress (CS) mode a defined stress is applied to the material and the deformation is measured. Both modes of measurement should lead to equivalent results. Prior to the full experiments, frequency and deformation sweeps were made to ascertain if they remain within the linear viscoelastic region for the epoxy resin. This is the recommended procedure explained in most handbooks. All measurements using the Haake rheometer were performed in the CD mode. This mode has the advantage that it can automatically adjust the measurement parameters within a set range depending on the material state. For example, a large deformation angle is chosen at the beginning of the measurement e.g. 0.7 degrees for measurements in the liquid state. As the modulus of the resin increases during cure, a smaller angle of deformation is chosen automatically by the rheometer so that less torque on the rotor

is required to deform the sample. Shear stress is directly related to the torque measured by a geometry factor which takes into consideration the 20 mm plates used (Eq. 4.17). In each case the stress required to achieve a specified deformation is measured. The instrument sets the angle of deformation automatically and can normally measure a larger range in modulus than would be achieved in the CS mode. Shear modulus values up to 10^5 Pa can realistically be measured. According to instrument specifications the rotation angle of the rotor can be measured to an accuracy of 1 millionth of a degree. The lower measuring limits in terms of shear modulus are between about 1 and 10 Pa for the 20 mm plates used are. This lower limit of accuracy is caused by the plate geometry. For example the shear stress is calculated from the product of the rotor torque M_t and plate geometry factor *A* as shown in Eq. 4.14.

$$\tau = M_t A \qquad \left[A = \frac{2}{\pi r^3} \right] \qquad \textit{Eq. 4.17}$$

$\tau = \textit{Shear Stress}$

$M_t = \textit{Torque}$

$A = \textit{Stress Factor (636 KPa/Nm for the 20 mm plates)}$

The shear modulus is calculated from the shear stress and the phase angle at a specified strain rate as is the case in CD mode (see Eq. 4.19). For liquids or in this case an epoxy resin before gelation, the material has a low viscosity of about 0.05 Pas at 140 °C. For contrast, water has a viscosity of about 0.1 mPas at 20 °C (Schramm `95). For the epoxy resin in this example a low rotor torque of about 5 μNm is required which roughly corresponds to a shear stress of 1 Pa. Below this value the instrument cannot measure accurately. The natural conclusion would be to use larger plates, however a compromise has to be made. For example, the stress factor will be lower in the case of 40 mm plates (80 kPa/Nm) and therefore the instrument can measure low viscosity liquids more accurately than the 20 mm plates (at the same torque). The disadvantage is that with such large plates it is not possible to measure high modulus values beyond gelation. Therefore the 20 mm plates provide an optimal compromise for the measurement range required (shear modulus between 10 and 10^5 Pa). The Haake rheometer is named RS 150 as

Angle of rotation < 1°

Resin

Fixed Plate
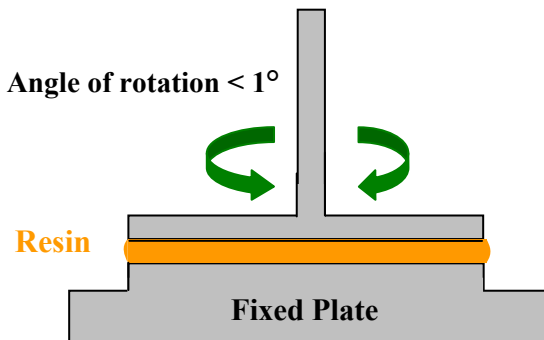
Fig. 4.13 Oscillating Plate Rheometer (1 Hz)

150 mNm is the maximum torque at which the instrument can measure. The *20 mm* measurement plate diameter will not influence the determination of the gel point which typically occurs at a viscosity of 10 kPas and is well within instrument measurement tolerances. All experiments were conducted under isothermal conditions in the temperature range between 60 and 100 °C. Before each measurement the parallel plate system was fully closed and preheated to the isothermal temperature required. The instrument is then opened and a few drops of resin are placed between the gap (see Fig. 4.12) and the measurement starts when a gap of 0.5 mm is reached. Temperature is monitored by a thermocouple located directly under the surface of the lower plate on which the resin is placed. Both the upper and lower plates are electrically heated and an insulating ring is placed around the plates to minimise heat loss. In the case of a pure solid the strain is directly related to the stress. The strain response is said to be 'In Phase' and the phase angle $\delta = 0°$. For a Newtonian liquid the strain follows the stress at $\delta = 90°$. In reality for an epoxy resin during cure the phase angle is not constant and is between $0 < \delta < 90°$. In the controlled deformation mode, the deformation or strain is described by the maximum amplitude or displacement γ_0 and the angular velocity ω.

$$\gamma = \gamma_0 \cdot \sin(\omega \cdot t) \qquad \qquad Eq.\ 4.18$$

The resulting shear stress is characterised by the amplitude of the stress and the phase angle δ.

$$\tau = \tau_0 \cdot \sin(\omega \cdot t + \delta) \qquad \qquad Eq.\ 4.19$$

The complex modulus G * and its parts G′ and G′′ are calculated as follows:

$$G* = \frac{\tau_0}{\gamma_0} \qquad \qquad Eq.\ 4.20$$

$$G* = G' + iG'' = \frac{\tau_0}{\gamma_0} \qquad \qquad Eq.\ 4.21$$

$$G' = G* \cdot \cos \delta = \frac{\tau_0}{\gamma_0} \cos \delta \qquad \qquad Eq.\ 4.22$$

$$G'' = G* \cdot \sin \delta = \frac{\tau_0}{\gamma_0} \cdot \sin \delta \qquad \qquad Eq.\ 4.23$$

For oscillatory shear measurements, the complex modulus and its parts are related to the measured shear stress (Eqs. 4.18 to 4.23). The empirical Cox-Merz rule (Cox `58) states that

the shear viscosity η should be the same function of shear rate $\dot{\gamma}$ as complex viscosity $\eta*$ is of frequency ω where:

$$|\eta*| = \frac{1}{\omega}\sqrt{G'^2 + G''^2}$$ *Eq. 4.24*

$$\eta' = \frac{G''}{\omega} \text{ and } \eta'' = \frac{G'}{\omega}$$ *Eq. 4.25*

The real or dynamic component η´ is often described as being related to the steady state or shear viscosity and that it measures the rate of energy dissipation whereas the parameter η´´ is related to the elastic or stored energy of the resin as described in Eq. 4.25. This is sometimes confusing as one could easily assume that the steady state viscosity (typically measured in rotation η) is equal to the dynamic viscosity η´. The measured viscosity for a steady shear flow at low strain rates or velocity gradients is actually equal to the complex viscosity $|\eta*|$ (as illustrated in Eq. 4.24) under the condition that small deformation angles or amplitudes are employed for such experiments (Cox `58). This rule applies for liquids and not for relaxations in polymers or viscoelastic materials i.e. ωτ<<1 (see Chapter 2.3.1). The deformation range in which this rule may be applied is usually determined by varying the deformation amplitude as function of measurement frequency. In the linear range this rule is generally accepted as being valid in most scientific literature (Schramm `95).

4.3.3 Differential Scanning Calorimetry (DSC)

All experiments were conducted on a Netzsch DSC 204 F1 Phoenix instrument and take place in the presence of nitrogen to avoid oxidation of the samples. The construction is based on the heat flux principle. The instrument (Fig. 4.14) holds two identical pans: a sample pan with about 10 mg of resin and a generally empty reference or neutral pan. The pans and lids are composed of aluminium and are not airtight as it may lead to unwanted volume changes between sample and reference. Heat flux is based on the transfer of heat to the sample and reference being closely controlled while the instrument monitors the temperature difference between the two pans. Experiments are performed both at constant temperature and also by changing the temperature at various constant heating rates, called temperature scanning. As long as the sample and the reference pan respond to the temperature program in the same way, the heat flux remains nearly constant as does the temperature difference between the two

sensor plates located beneath the pans. If the sample absorbs heat because of melting or glass transition, a difference in the heat flux occurs and an endothermal effect is detected in the DSC curve. If crystallisation or curing takes place, energy is released by the sample and an exothermal effect is observed. Prior to each set of experiments the instrument background was collected by running the same experiment with the empty cell instead of a cell filled with resin. This calibration is necessary to determine the heat flow from the measured temperature difference. An example showing the curing reaction of an epoxy resin for a typical heating run conducted at 10 K/min is illustrated in Fig 4.15. Integration of the total area under the thermogram provides the heat released during the reaction, ΔH_T, assuming that the reaction has proceeded to 100 % cure. Determination of T_g as a function of conversion takes place in three steps. Firstly, by a dynamic heating run to a pre-specified temperature e.g. 140 °C and as soon as the temperature is reached the sample is quenched rapidly at 20 K/min until -50 °C is reached. During the subsequent re-scan at 10 K/min the T_g is determined as the midpoint of the endothermic step observed.

This heating run continues until the sample is fully cured and the thermogram will exhibit an exothermal peak that is a fraction of the total heat of reaction released ΔH_T. The respective degree of conversion can be calculated from the residual heat of reaction ΔH_{res} after partial
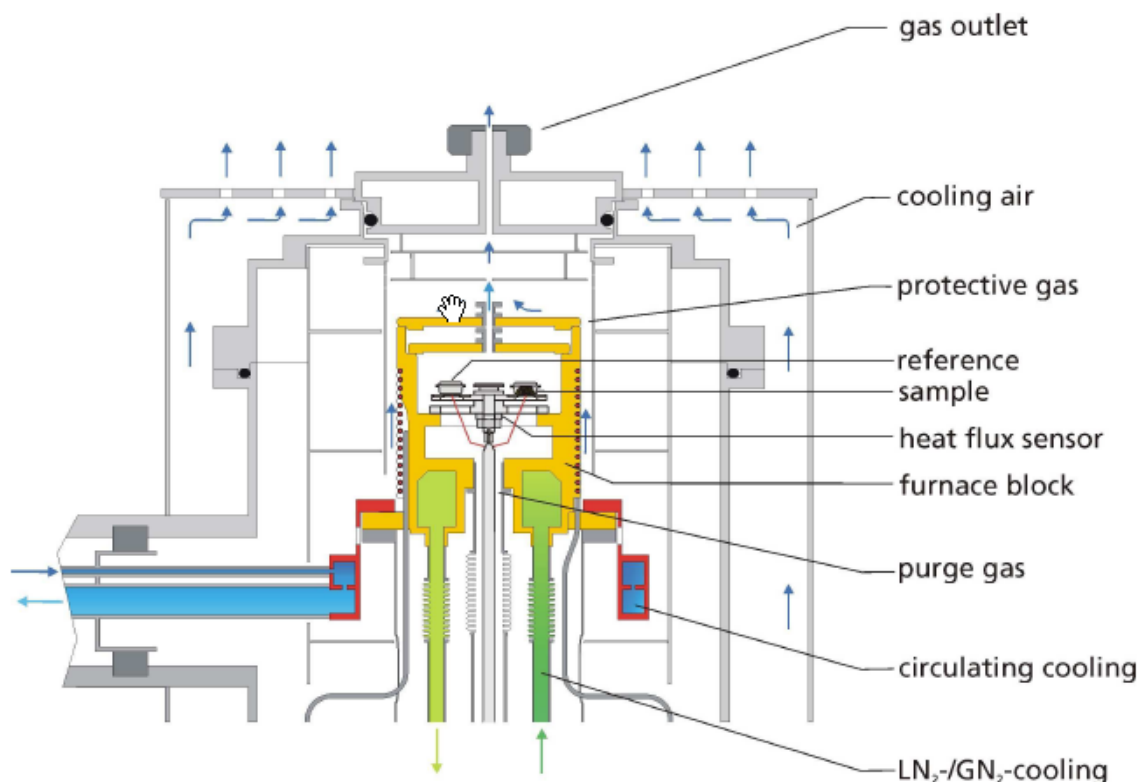
Fig. 4.14 *Schematic of a heat flux DSC (DSC 204 F1 Phoenix – Netzsch Instruments)*

cure (during the rescan) as shown in Eq. 4.26:

$$\alpha = \frac{\Delta H_T - \Delta H_{res}}{\Delta H_T}$$ *Eq. 4.26*

For isothermal experiments the furnace is preheated and the sample pan is inserted requiring about 1 to 2 minutes for thermal equilibrium. The samples were cured until the heat of reaction ΔH is zero i.e. the reaction comes to an end at a specific temperature. The measurement of the heat released during the reaction is used for the determination of cure kinetics. The degree of cure at any time during the isothermal reaction can be obtained from:

$$\alpha = \frac{\int_0^t \frac{dH}{dt} dt}{\Delta H_T}$$ *Eq. 4.27*

The numerator is the heat released until the time t and is equivalent to partial area under the exothermal peak at time *t*.
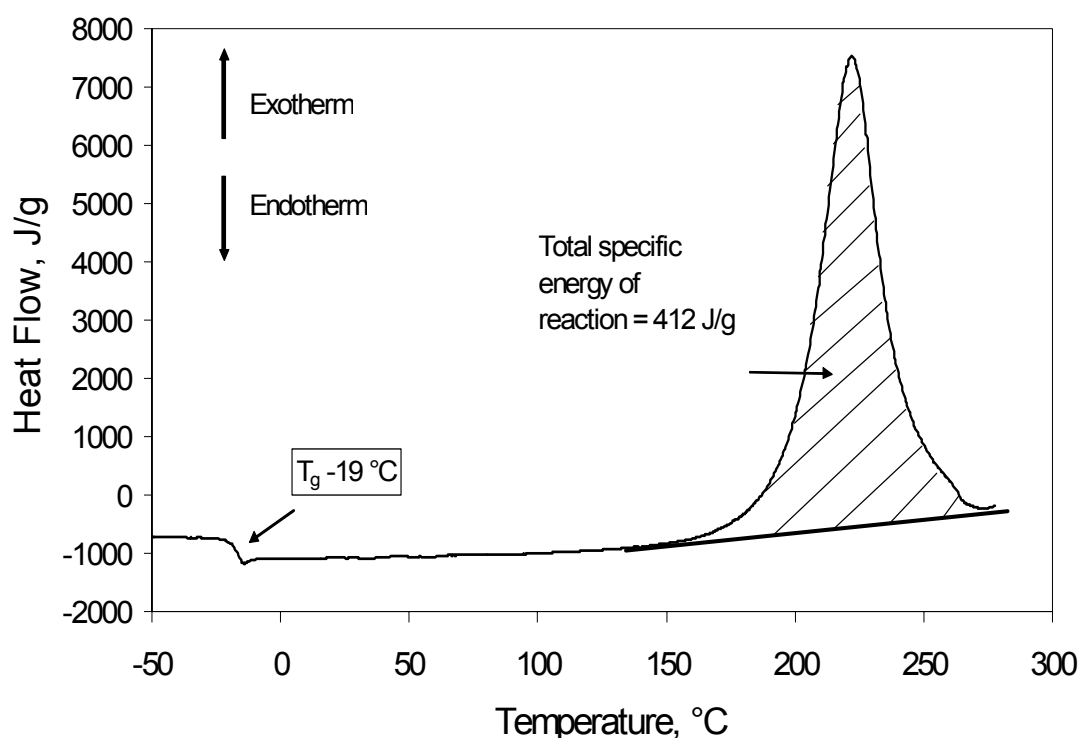
Fig. 4.15 *DSC thermogram of an epoxy prepolymer (RTM6). Dynamic run at 10 K/min heating rate employed to determine T_g and total heat of reaction (Mc Hugh`02)*

4.4 Epoxy-Amine System

Only one epoxy resin system is employed throughout this thesis. It is a commercial epoxy laminating epoxy resin with the trade name L335 from the company Martin G. Scheuffler (now part of the Hexion Group). The resin system is approved by the German Federal Aviation Authority and it is mainly employed in the production of light airplanes, gliders and boots. It is also employed as a laminating resin in combination with either glass or carbon fibre. It has a pot life at room temperature that depending on mixing ratio ranges between 10 mins and 6 to 7 h. It is most commonly used in combination with an amine based hardener systems referred to as H335 or H340. The resin system employed here is a combination of L385:H340 in the mixing ratio of 100:38 parts per weight. At room temperature cure times of between 24 and 30 h requiring about 4 h to gel (defined as time to reach a viscosity of 5000 mPas) are recommended. The viscosity value of 5000 mPas is an arbitrary value normally provided on manufacturer's data sheets. For viscosity values higher than 5000 mPas it becomes increasingly difficult to achieve mould filling and fibre impregnation. The amine hardener referred to by the number H340 has a light blue colour. Both components L335:H340 are mixed until a homogene blue colour is obtained for the mixture. All mixing takes place at room temperature independent of the experimental routine or heating regime following. The cured epoxy has a light blue transparent colour and according to its data sheet has a glass transition temperature of approx. 75 °C for the fully cured resin system. No information is provided on how this value is obtained and it is presumed that it is determined by the peak maximum in the loss modulus for DMA techniques at low frequency, which is common for material data sheets. The epoxy system has a density of 1.18 to 1.2 g/cm³. Viscosity of the epoxy is listed on the data sheet as between 2300 to 2900 mPas and the hardener has a viscosity of 170 to 190 mPas both measured individually at room temperature.

Chapter Five

---

5 Experimental Results

Remarks on Layout of Experimental Results

Experimental results are split into <u>three sections</u>: <u>Chapter 5.1</u> is concerned with principle questions relating to the suitability of acoustic measurements for accurate analysis of dynamic mechanical thermal properties of a non-reactive fully cured epoxy*. Factors such as interpretation of longitudinal L´ and shear G´ storage moduli as determined from wave propagation experiments as well as the influence of measurement frequency are considered and the results are compared with conventional DMA. A detailed breakdown of objectives is provided on the next page.

In <u>Chapter 5.2</u> starting on page 87 the two sample technique already presented is adapted for cure monitoring experiments. The crosslinking reaction for epoxy polymers is exothermic and the thicker the sample the more heat will be given off. If a two sample technique with varying sample thickness were used it would be difficult to maintain or guarantee constant temperatures for both samples. However, constant temperatures are essential for comparison of all cure monitoring experiments using different analysis techniques. In Chapter 5.2 the adaptation as well as accuracy, limitations and advantages of a new single sample technique are discussed using experimental results.

In <u>Chapter 5.3</u> the sensitivity of a single sample technique to variations in the viscoelastic properties resulting from the curing reaction of an epoxy is evaluated. The measured ultrasound parameters are compared with conventional analysis techniques typically used to characterise chemorheological cure properties i.e. changes in viscoelastic properties as a result of the curing reaction. More detailed explanations and breakdown of objectives and procedures are provided in Chapter 5.3.1 and starting on page 88.

* Only one epoxy is used for all experiments (see Chapter 4.4)

5.1 Investigations on a Cured Epoxy

A breakdown of the objectives for experiments on cured epoxy is provided in the following. As it is difficult to maintain an overview, the results are divided under three sub-headings. All experiments take place in the dynamic temperature range between 20 and 200 °C.

1. The mechanical behaviour of an epoxy is analysed using conventional DMA in the frequency range 0.1 to 50 Hz. From the results the parameters for the Williams Landel Ferry WLF relation can be determined using Time Temperature Superposition principles and employed to predict the influence of measurement frequency on experimental results up to MHz range. This information provides a means of predicting and interpreting results at ultrasound measurement frequencies.

2. Interpretation of the measured ultrasound parameters sound velocity and attenuation as a function of temperature are considered. This takes into account the influence of dispersion and attenuation on measured results. Secondly, the measured ultrasound parameters are converted into longitudinal storage L' modulus and $\tan(\delta)$. Reduced equations (Eqs. 2.9 to 2.16) are validated by showing that the term $\alpha\lambda/2\pi \ll 1$ and may be used to evaluate L' and G'. Using a two sample technique quantitative values for attenuation can be determined and the influence of high attenuation α values at T_g on the accuracy of the calculated modulus L' and $\tan(\delta)$ can be discussed. Lastly the influence of measurement frequency is discussed and the α relaxation is shown to obey a WLF-temperature dependence.

3. The longitudinal L' and shear G' storage moduli are measured using wave propagation techniques as a function of temperature. By measuring any two storage moduli, it is possible to evaluate any other modulus term or Poisson's ratio μ_p' (see Chapter 2.2.3). Because shear waves do not propagate in soft polymers it was only possible to estimate G' in the soft polymer by extrapolating μ_p' to known values for rubbers. In this manner, the respective bulk K' and tensile E' storage moduli could be determined over a large temperature range and for an α relaxation process. This provides the opportunity to study the interrelationship of the various moduli and to investigate the sensitivity or limitations of longitudinal modulus L', in contrast to for example other more commonly used moduli such as G' or E'.

5.1.1 DMA in the Frequency Range between 0.1 to 50 Hz

Fig. 5.1 illustrates the tensile storage E´ modulus and tan(δ) as a function of temperature at specific frequencies between 0.1 and 50 Hz. Measurements were performed using the DMA 242 C instrument (Chapter 4.3) and a dual cantilever setup. Straight lines and symbols are employed only to differentiate between the curves and should not be mistaken for measurement points. All curves are smoothed automatically with Netzsch instrument software and the data is saved as ASCII file. From the elastic modulus values, three distinct regions can be identified in the 25 to 200 °C temperature range. At low temperatures, the polymer is stiff or frozen with an accordingly high modulus and low tan(δ). As the temperature increases, the polymer softens and in the third region (>100°C) the material behaves like a soft rubber and has a low modulus. This transition from a hard stiff polymer to a rubber-like polymer and the associated loss peak is referred to as glass transition T_g or α relaxation depending on relevance (see Chapter 2.3.1). In analogy with this process a drop in modulus occurs and the loss factor tan(δ) forms a peak. For reference purposes this transition region is typically described by one specific temperature referred to as T_g and taken as the peak maximum temperature of tan(δ). A shift in the tan(δ) maximum from 82°C at 0.1 Hz to 98°C at 50 Hz is observed, which is an apparent shift of 16 K over 2.5 decades in frequency or approx. 6.5 K per decade change in frequency. This is close to a general rule of thumb stating that the α relaxation will be observed at 7 K higher temperatures for every decade increase in frequency (Sperling `92; Cowie `91). As discussed in Chapter 2.3.2 this rule assumes a linear relationship between frequency and the reciprocal of temperature, commonly illustrated by an Arrhenius plot. Although some exceptions exist, an Arrhenius plot of α relaxation temperature values versus frequency will typically form a curve (Aklonis `72). In such cases the Williams Landel Ferry (WLF) equation (Eq. 2.28) is more suitable to describe frequency behaviour. Values for WLF parameters may be obtained using Time Temperature Superposition (TTS) principles. Rather than presenting temperature dependent measurements at specific frequencies, the same mechanical modulus or loss factor may be plotted as a function of frequency at constant temperature. A master curve may be formed by shifting these partial isothermal temperature curves to form a smooth composite curve (Fig. 5.2). On constructing this master curve the time-dependent modulus obtained at 80 °C was used as reference (full circles), while all other curves were horizontally displaced along the logarithmic frequency axis by a shift factor denoted as a_T.
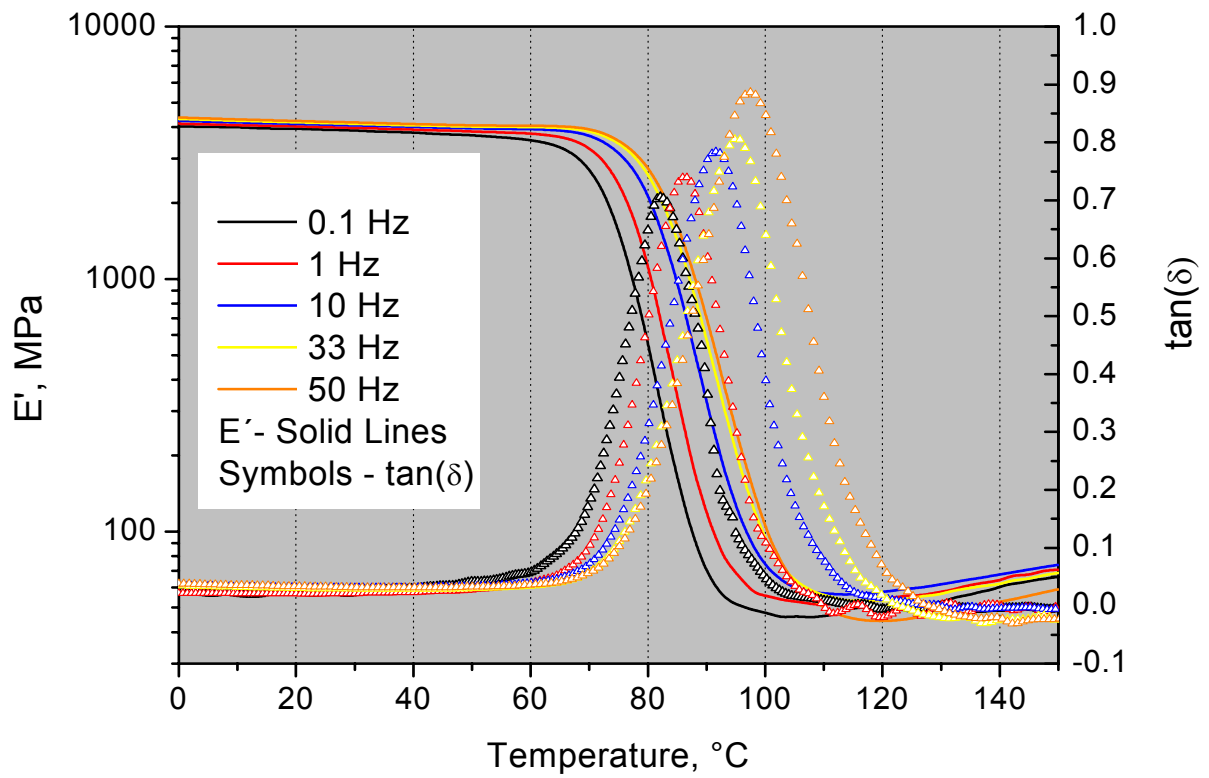
Fig. 5.1 *Tensile storage modulus E′ as a function of temperature at various frequencies*
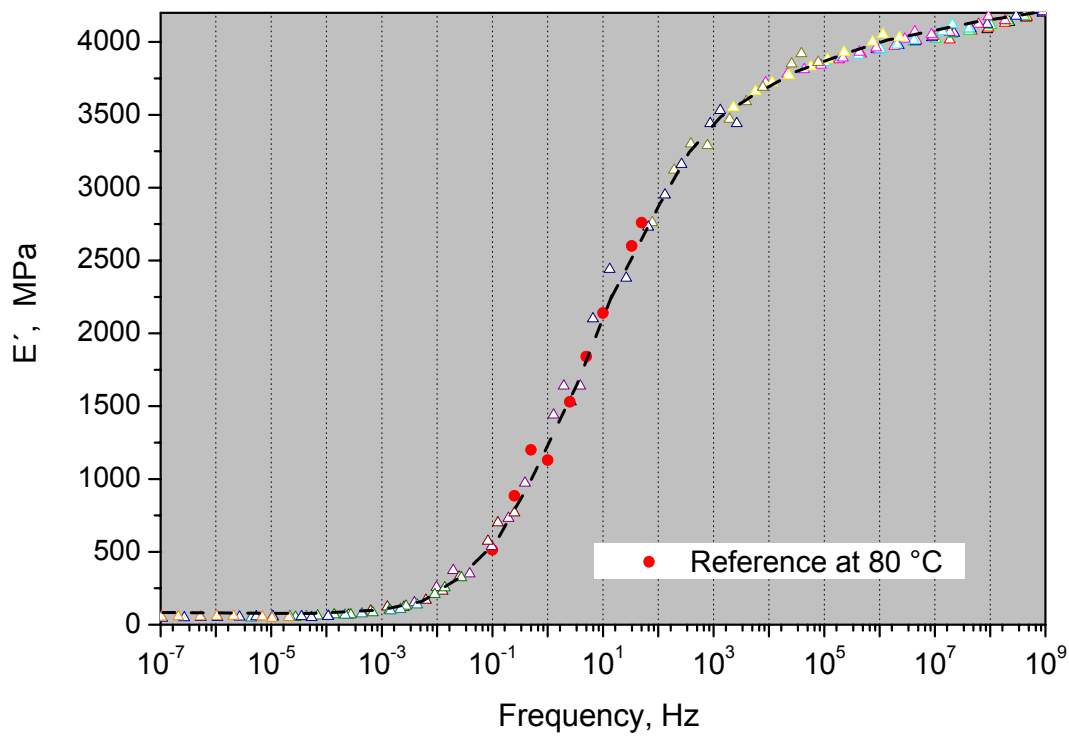
Fig. 5.2 *Plot of E′ at different constant temperatures (taken from Fig. 5.1) as a function of frequency. Open triangular symbols shifted by the factor $\pm a_T$ to form a composite modulus E′ curve about a reference temperature taken as 80 °C (solid circles)*

The master curve in Fig. 5.2 shows the frequency dependence of the tensile storage modulus E′ at 80 °C. Another reference temperature could have been chosen as long as it is in the vicinity of T_g, for example between 80 and 90 °C and the same master curve will result. The master curve has a very similar form to the temperature profile illustrating an inverse relationship between time and temperature i.e. increasing the temperature of a sample is equivalent to decreasing the measurement frequency. Fig. 5.2 illustrates that if DMA experiments would be performed in the high ultrasound frequency range (10^5 to 10^6 Hz) then the modulus E′ of this epoxy will have a value in the GPa range that is indicative of a stiff solid. On the other hand Figs. 5.1 and 5.2 show that at low frequencies (e.g. 1 Hz) the polymer will exhibit strong signs of softening indicating a transition at 80 °C. Various material states are caused by thermally activated movements of segments of macromolecules and have corresponding activation energies and relaxation times. Segment relaxation times τ at two different temperatures (T_1 and T_g) are typically governed by the Arrhenius relationship adapted from Eq. 2.25 and illustrated below.

$$a_T = \frac{\tau_2}{\tau_1} = \exp\frac{E_a}{R}\left(\frac{1}{T_1} - \frac{1}{T_g}\right) \qquad \text{see Eq. 2.26}$$

The reference temperature is taken as the α relaxation or T_g and defined by a peak in tan(δ) at 86 °C at 1 Hz (Fig. 5.1). A plot of shift factor a_T versus the reciprocal of temperature is shown in Fig. 5.3. Two distinct regions of behaviour are noted in the plot. At low temperatures in the range -20 to 65 °C, the data fits linear Arrhenius behaviour whereas at higher temperatures in the range 70 to 130 °C the data is better fitted using the Williams Landel Ferry WLF equation. Similar behaviour with two distinct behavioural regions has been observed by several authors for a range of thermoplastic materials (Higgenbottom `01; Gao `96). The activation energy E_a of the lower temperature region was calculated as 95 kJ/mol using the slope of the best line fit (linear regression) and placing it into Eq. 2.26. The excellent fit (red line) as well as the determined activation energy is indicative of a thermally activated process as expected for independent local motion of side groups. Similar values ranging from 29 to 84 kJ/mol have been published elsewhere (Higgenbottom `01). It is very likely that this behaviour is caused by a secondary named β relaxation that is attributed to local motions of side chains. The β relaxation peak for diamine cured epoxy polymers is typically observed at -60 °C taken as the tan(δ) maximum at 1 Hz and according to Ochi (Ochi `92) it results from the combined contributions of hydroxyether groups and the network structure. The β relaxation peak is not

illustrated in Fig. 5.1 as it is outside of the experimental measuring range. In the case of anhydride cured epoxy, a β relaxation is expected at -70 °C (tan(δ) maximum at 1 Hz) and can be more clearly assigned to the motion of diester segments introduced in the network by the acid anhydride curing agent (Masaki `84; Nguyen `95). Nguyen (Nguyen `95) calculated activation energy values for the β relaxation of 49.1 kJ/mol. Such secondary relaxations are manifestations of segmental motion within a polymer in the frozen or glassy state. They arise from localised motions either in the main chain or side groups. Secondary relaxations are typically described using the Arrhenius equation whereas the WLF or Vogel-Fulcher-Tammann VFT equations that are mathematically equivalent (Schönhals `02) and are typically used to model primary or α relaxations. Primary relaxation behaviour is indicated by the curved portion of the shift plot (blue points) in Fig. 5.3 and can be best fitted using the WLF equation (Eq. 2.29). As discussed in Chapter 2.3.2 the universal constants C_1 and C_2 used in this equation typically have respective values of 17.44 and 51.6 K. However, it is more likely that C_1 and C_2 are not universal (Strobl `96) but are material dependent parameters varying in the range in the range C_1 = 14 to 18 and C_2 = 30 to 70 K under the prerequisite that the reference temperature T_{ref} = T_g. For this reason it was decided to calculate C_1 and C_2 values from experimental data.

$$\log a_T = \frac{-C_1(T - T_{ref})}{C_2 + T - T_{ref}}$$

see Eq. 2.29

T_{ref} in Eq. 2.29 is taken as T_g = 86 °C i.e. from the tan(δ) peak maximum at 1 Hz. Values for C_1 and C_2 were obtained from DMA data (as described in Chapter 2.2.3) and have respective values of 17.3 and 56 K. These values are very close to the universal constants quoted in several textbooks (Aklonis `72; Sperling `92). To check the accuracy of results the experimental data was fitted by calculating a_T in 5 K temperature steps using the WLF equation and the data plotted in Fig. 5.3 and illustrated by a blue line. The values for the constants used, provide an excellent fit with experimental data. Using Eq. 2.30 the activation energy may be calculated from the WLF constants. An activation energy E_a of 760 kJ/mol was calculated for the α relaxation.

$$E_a = 2.303 \left(\frac{C_1}{C_2} \right) R T_g^{\,2}$$

see Eq. 2.30

This activation energy may appear high but correlates well with values determined by Li (Li `00) using DMA experiments on an epoxy polymer. As Eq. 2.29 clearly signifies, absolute values for the activation energy will only depend on the T_g of the polymer employed, as universal values are employed for C_1 and C_2 (i.e. are constant). High activation energies have also been determined by other authors (Ferry `80; Sperling `92) and Ferry concludes that the temperature dependence of relaxation processes are independent of chemical structure, otherwise the WLF could not be employed for organic liquids. Although the physical importance of E_a values obtained using Eq. 2.29 is minor, the values are helpful in comparing results from literature. The main objective of employing the WLF equation in this work was to assert the influence of measurement frequency on determining the α relaxation temperature. This is performed by placing the peak maximum values at 1 Hz either for the loss modulus E´´ taking $T_{ref} = T_g = 78 \,°C$ (see Fig. 2.2) or for tan(δ) taking $T_{ref} = T_g = 86 \,°C$ into Eq. 2.28. The results are shown in Fig. 5.4 with circular and triangular symbols representing the respective peak maximum temperatures for tan(δ) and E´´ over a range of
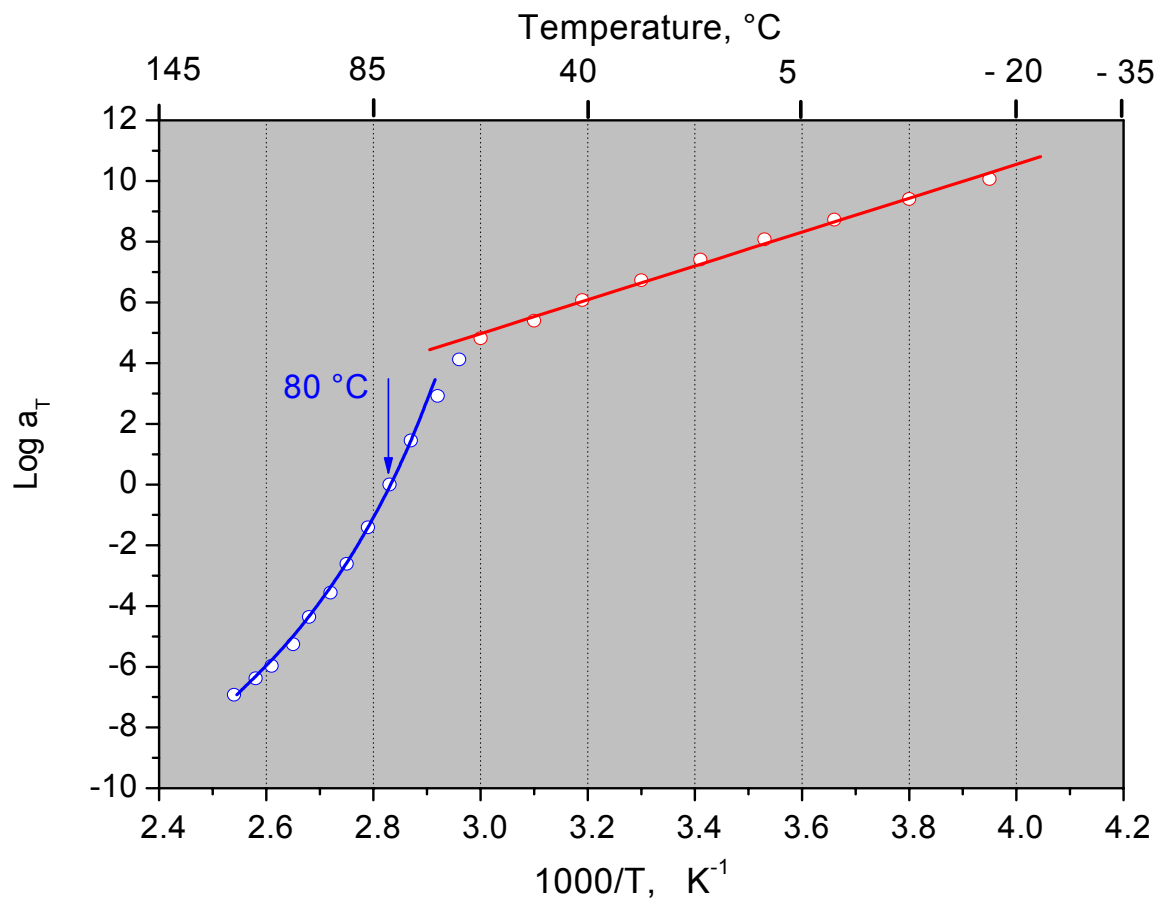
Fig. 5.3. *Shift factor a_T versus reciprocal of temperature. Features Arrhenius process (linear fit – red line) and the glass transition modelled using the WLF equation (curve fit - blue line)*

frequencies. The WLF plot formed enables α relaxation temperature to be predicted over a large frequency scale. The experimental data for tan(δ) deviates slightly from the red line fit. This is because the determined "C" constants employed for WLF equation are obtained from the composite E´ master curve (in Fig. 5.2) and not directly from tan(δ). On the other hand, E´´ provides a direct correlation with E´. The temperature to the half step height in E´ is equal to the peak maximum in E´´ (Chapter 2.3.1). It will therefore make no difference if the TTS diagram is formed by using E´´ or E´ data. However, it is easier to form a composite master curve from E´ data than for example E´´ or tan(δ) because peak heights and widths will also vary with frequency which means calculation of the shift factor is more difficult. For this reason tan(δ) will deviate slightly from the WLF fit curve whereas E´´ provides a good fit because of its close relation to E´. From the fit curves it is expected that the α relaxation should be observed at roughly 115 °C for DMA experiments at 1 MHz.
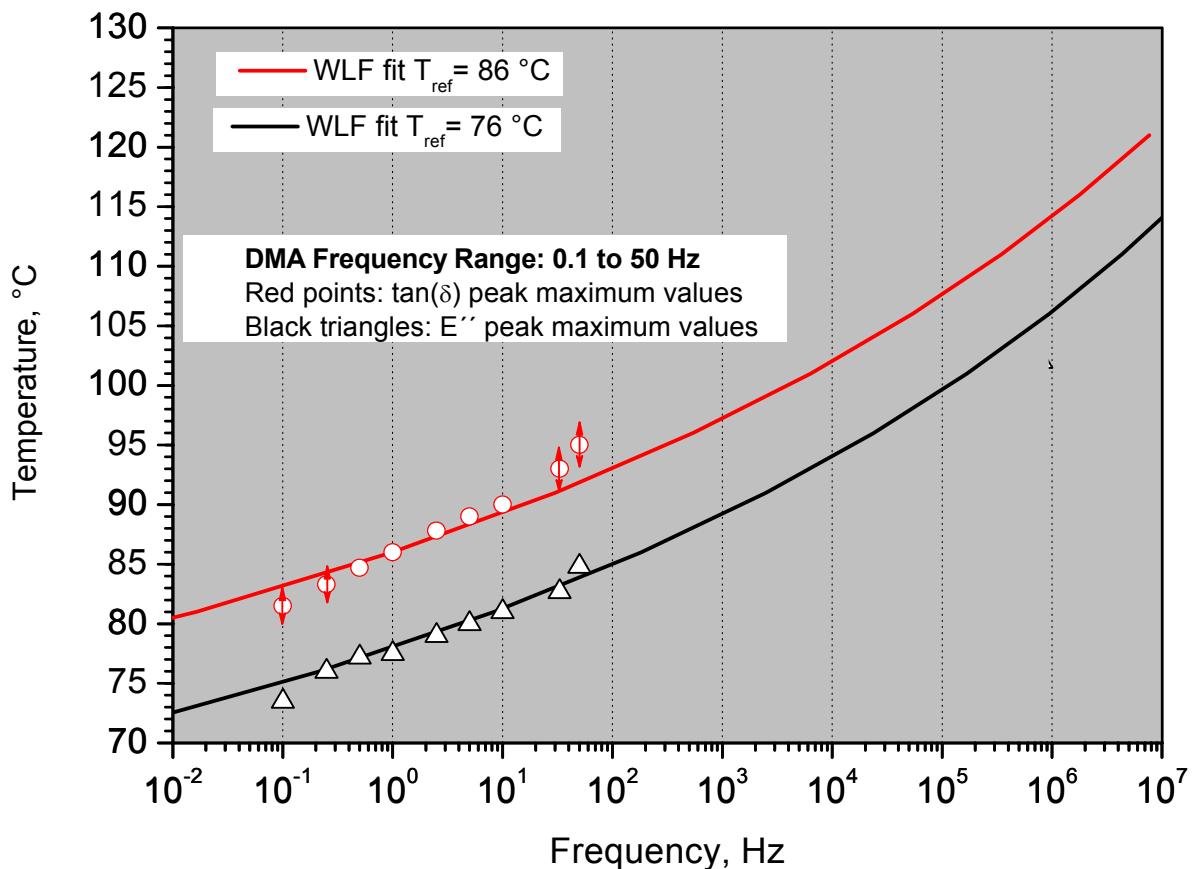
Fig. 5.4. *Temperature plot of peak maxima for tan(δ) and E´´ versus frequency for a cured epoxy. Tolerances are illustrated using symbol size unless otherwise indicated (arrows indicate wider tolerances due to peak broadening). Red and black fit lines are calculated from WLF equation.*

5.1.2 Ultrasound Measurements: (300 kHz to 6 MHz)

Ultrasound phase velocity and attenuation were evaluated as a function of frequency in the temperature range from 25 to 200 °C and the results are illustrated in Fig. 5.5. In the frequency range shown, sound velocity and attenuation maintain a similar profile to DMA parameters E´ and tan(δ) (compare Figs. 5.1 and 5.5). The sound velocity values of approx. 2500 m/s at room temperature and 1400 m/s at temperatures above 160 °C are representative of the respective hard and rubber-like material states. The attenuation profiles go through a maximum at all measurement frequencies. Similar to conventional DMA the temperature at which a peak maximum is observed will dependent on the measurement frequency and ranges from 109 to 125 °C between 400 kHz and 5 MHz. The results provide reasonable agreement with the prediction from the WLF equation that a tan(δ) maximum associated with the α relaxation should be observed at temperatures around 115 °C (see Fig. 5.4).
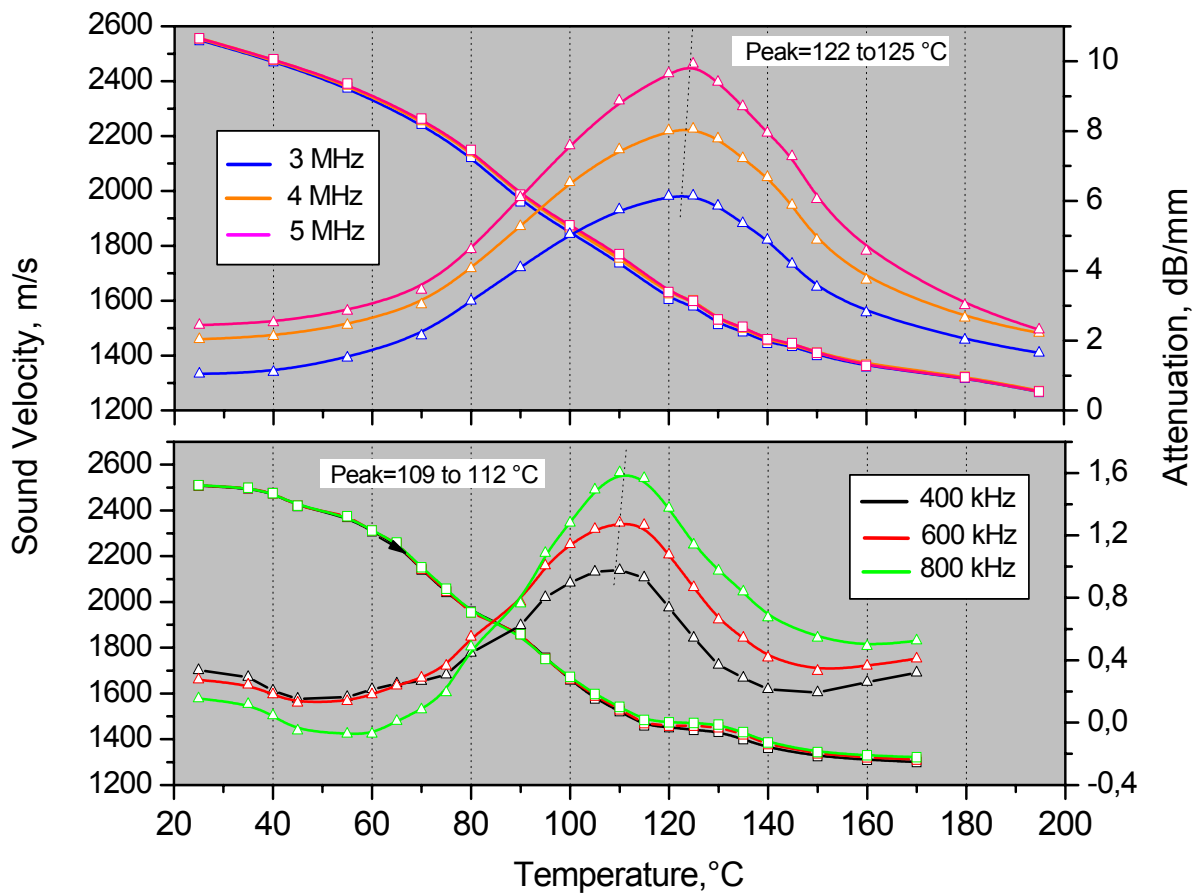
Fig. 5.5 *Sound Velocity (square symbols) and attenuation (triangular symbols) measured on a fully cured epoxy at specific frequencies as a function of temperature*

Combining this information with the interpretation of the temperature profile of the corresponding sound velocity data it is supposed that the attenuation peak and large change in sound velocity occurring in the 90 to 130 °C range are caused by a the α relaxation. This is easily confirmed by calculating the parameters $\tan(\delta)$ and L′ and placing the information into the WLF equation as will be demonstrated later in this chapter. At present it is worth discussing some other interesting effects, in particular regarding the attenuation profile and measured values obtained. Firstly, the intensity of the attenuation peak is frequency dependent, clearly increasing with increasing frequency. This behaviour is well known and is also observed in conventional DMA when the behaviour of the loss modulus E″ and not $\tan(\delta)$ is considered. For the α relaxation process, the peak intensity of the loss factor is directly related to the co-ordinated chain molecular friction, which dissipates mechanical energy as heat (Ding `06). Therefore at higher frequencies energy dissipation is larger and accordingly the intensity of attenuation. However, an effect that is not well understood is the frequency dependence of attenuation intensity at lower temperatures or well above or below the primary α relaxation process. For example, if attenuation is plotted as a function of frequency at 40 °C a linear dependence is observed as illustrated in Fig. 5.6. According to the literature this attenuation behaviour is typical for polymers either with amorphous or crystalline structures (McIntire `91; Hartmann `72). Hartman (Hartman `72, `94) compared some of the more common acoustic models with experimental results (on PMMA and PE thermoplastic polymers) but came to no satisfactory conclusion that would provide a physical explanation for this behaviour. He also concluded, from experimental data, that this effect is not caused by relaxation behaviour or as Ferry (Ferry `80) suggested by a broad distribution of relaxation times. It is most likely caused by anelastic behaviour i.e. time dependence of the stress strain response of polymers outside regions of molecular relaxation. If the stress strain curve for a single cycle of vibrations is in the form of a hysteresis loop, then the area enclosed under the loop will represent the mechanical energy that has been lost as heat (Kolsky `63). It is known that hysteresis losses due to absorption $\alpha_h$ in polymers should follow a linear frequency dependence, where $C_h$ is a constant and the notation *h* refers to hysteresis (McIntire `91):

$$\alpha_h = C_h f$$

As the wavelength is inversely proportional to frequency at constant sound velocity then hysteresis absorption is one for which: $\alpha\lambda = const$. The effect of this type of hysteresis is that the energy loss per cycle will be constant so that the actual intensity of $\alpha\lambda$ will be

independent of frequency (Gemant `40). This is illustrated in Fig. 5.6 whereby wavelength absorption αλ is plotted versus frequency, see red line. Allowing for small deviations the results fall on a similar line. The slight deviations in αλ from linearity are caused by measurement inaccuracy as values for both attenuation and wavelength are independently measured and are both dependent on frequency. Wavelength is calculated from the sound velocity and frequency at 40 °C taken from Fig. 5.5. As shown in Eq.2.15 the above statement (intensity of αλ independent of frequency) will also be valid for tan(δ). tan(δ) is qualitatively defined in several books (Ferry `80; Sperling `92) and is proportional to ratio of the energy dissipated to potential energy stored per cycle in a sinusoidal deformation i.e. absolute values will be largely independent of measurement frequency (not considering relaxation behaviour).

$$\tan \delta = \frac{\alpha\lambda}{\pi} \qquad\qquad \text{see Eq. 2.15}$$

Therefore to differentiate between different absorption effects it is often desirable to express ultrasound attenuation results in the form αλ or tan(δ). For the same reasons when conventional DMA is considered then at temperatures well above or below the α relaxation the intensity of tan(δ) should remain constant as confirmed in Fig.5.1 (e.g. at 40 °C).
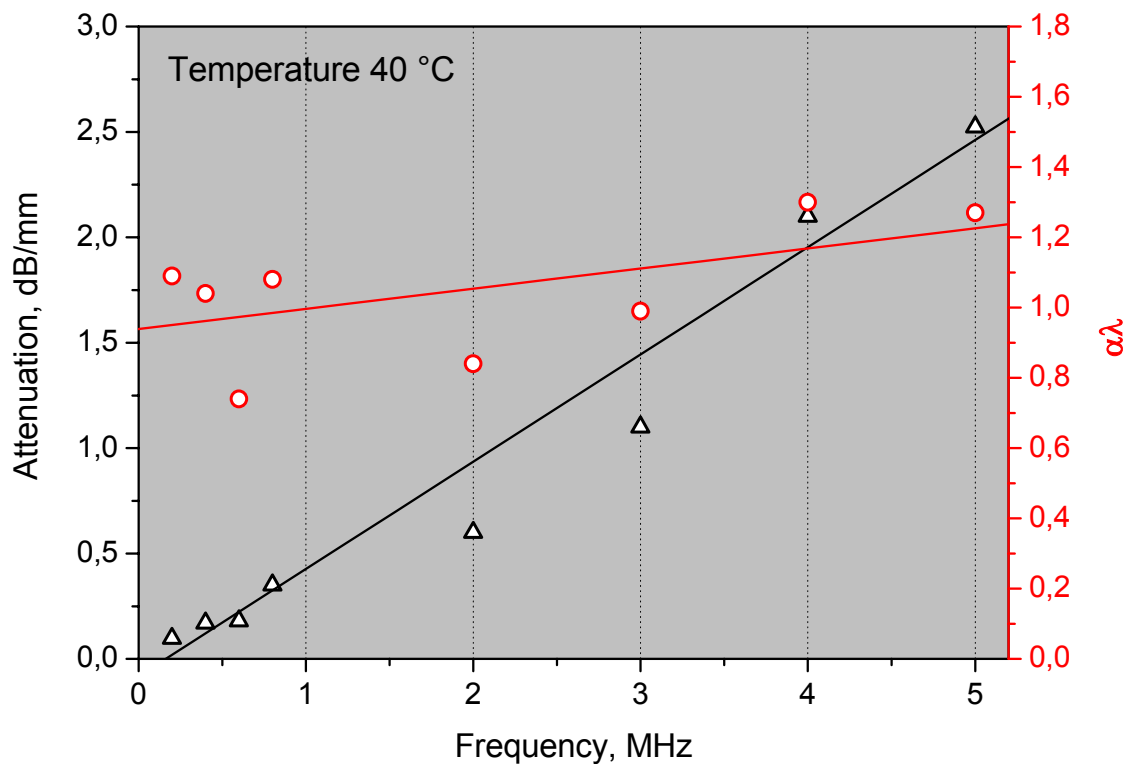
Fig. 5.6. *Attenuation and αλ as function of frequency at 40 °C (from data in Fig. 5.5): lines represent linear fits using regression analysis*

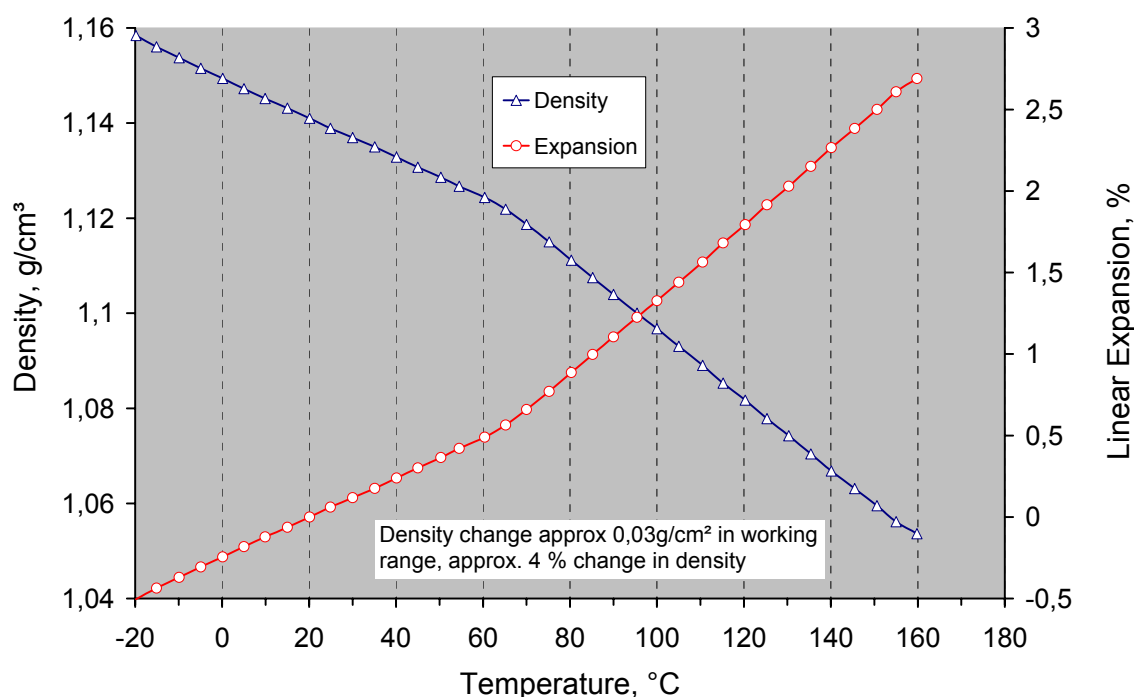## 5.1.3 Comparison of Ultrasound Results with Conventional DMA

To compare ultrasound with the results from conventional DMA, sound velocity and attenuation need to be converted into corresponding modulus terms L′ and L′′ and tan(δ). As shown in Eqs. 2.9 to 2.12 the calculation of tan(δ) and the longitudinal moduli *L′* and *L′′* can be greatly simplified if the term αλ/ω shown in Eq. 2.13 has a value much less than unity. As accurate values for both α and λ as functions of frequency are available from the experiments, it can be demonstrated that αλ/ω<<1 is valid even for peak maximum values occurring at α relaxation. Maximum attenuation values (Fig. 5.5) are taken as 8 dB/mm at 4 MHz and a correlating wavelength λ of 0.54 mm (2160 m/s). The attenuation term α employed in the wave equation to derive the complex modulus in Chapter 2.2.3 is measured in *Neper* whereas results presented in this work use decibel *dB* units, which are more common for acoustic applications. To convert from *dB* to *Neper* a multiplication factor of 8.686 is employed (see Eq. 2.13).

$$\frac{\alpha c}{\omega} = \frac{\alpha \lambda}{2\pi} = \frac{8 \bullet 0.54}{2\pi \bullet 8.686} = 0.08 << 1$$

With this knowledge the following reduced equations are valid for longitudinal modulus L′ and loss L′′ taking αλ/ω <<1 .

$$L' = \rho c^2 \quad \text{and} \quad L'' = \rho c^3 \alpha \Big/ \omega \qquad \qquad \textit{see Eqs. 2.9 to 2.12}$$

Before L′ and L′′ can be calculated the change in density ρ as a function of temperature is required. Firstly ρ is measured at room temperature using Archimedes principles according to DIN 53479. Using Thermal Mechanical Analysis TMA (Chapter 4.3) the change in sample length for a rectangular sample can be measured experimentally over the temperature range from -20 to 160 °C and the results are shown in Fig. 5.7. When the change of length is known then the resulting change in volume *V* for a sample of known geometry can be calculated. Mass *m* is taken as constant and the density change over the temperature range can be easily calculated from using *m/ΔV*. Density only changes by about 4 % in the relevant temperature range from 20 to 160 °C. All necessary parameters have been determined making it possible to determine L′; L′′ and tan(δ) as function of temperature.

Density change approx 0,03g/cm² in working range, approx. 4 % change in density

Fig. 5.7 Linear expansion and density of a rectangular epoxy sample

.

The results for both E´ and L´ and tan(δ) are illustrated in Fig. 5.8 on the next page enabling a direct comparison of the ultrasound results in the top two diagrams and conventional DMA in the bottom diagram. All results show an excellent correlation with each diagram displaying softening (decrease in modulus) and tan(δ) peak associated with the α relaxation. It should be noted, as stated at the start of this chapter, that the data points displayed for conventional DMA (bottom diagram Fig 5.8) are obtained from a spline fit of experimental data i.e. smoothed representation of experimental data. This is not the case with acoustic data as each point represents exactly the experimental data. Taking this explanation into consideration the results leave little doubt about the suitability of ultrasound as DMA technique. By comparing longitudinal modulus with sound velocity data in Fig. 5.5, one quickly notices that little difference exists between the graphical illustrations of these variables. This result is too be expected because as shown in Fig. 5.7, the change in density will only play a minor role in the variation of longitudinal modulus as a function of temperature (see Eq. 2.2) Therefore to a reasonable approximation sound velocity can be taken as proportional to square root of longitudinal modulus ($c \propto \sqrt{L'}$). Because longitudinal modulus is a rather unfamiliar term, sound velocity will therefore be employed for the rest of this thesis to describe changes in the mechanical modulus of this epoxy.

As shown in Figure 5.8, although tan(δ) profiles are very similar for measurement techniques, the intensity of peak maximum values are not. For acoustic measurements tan(δ) has a maximum value of about 0.14 whereas for tensile measurements at low frequencies values almost six times higher of about 0.8 are reached. tan(δ) values for acoustic wave measurements correlate well with published values (Murayami`78) for a dynamic plate modulus L´ using a conventional DMA technique for a range of polymers at 11 Hz. The author quotes almost exactly the same maximum intensity values for tan(δ) of 0.12 at T_g as obtained for acoustic measurements. This indicates that the values are most likely related to the type of applied loading or deformation rather than measurement technique. Lower values for measured tan(δ) are observed for wave propagation than for conventional DMA. This may
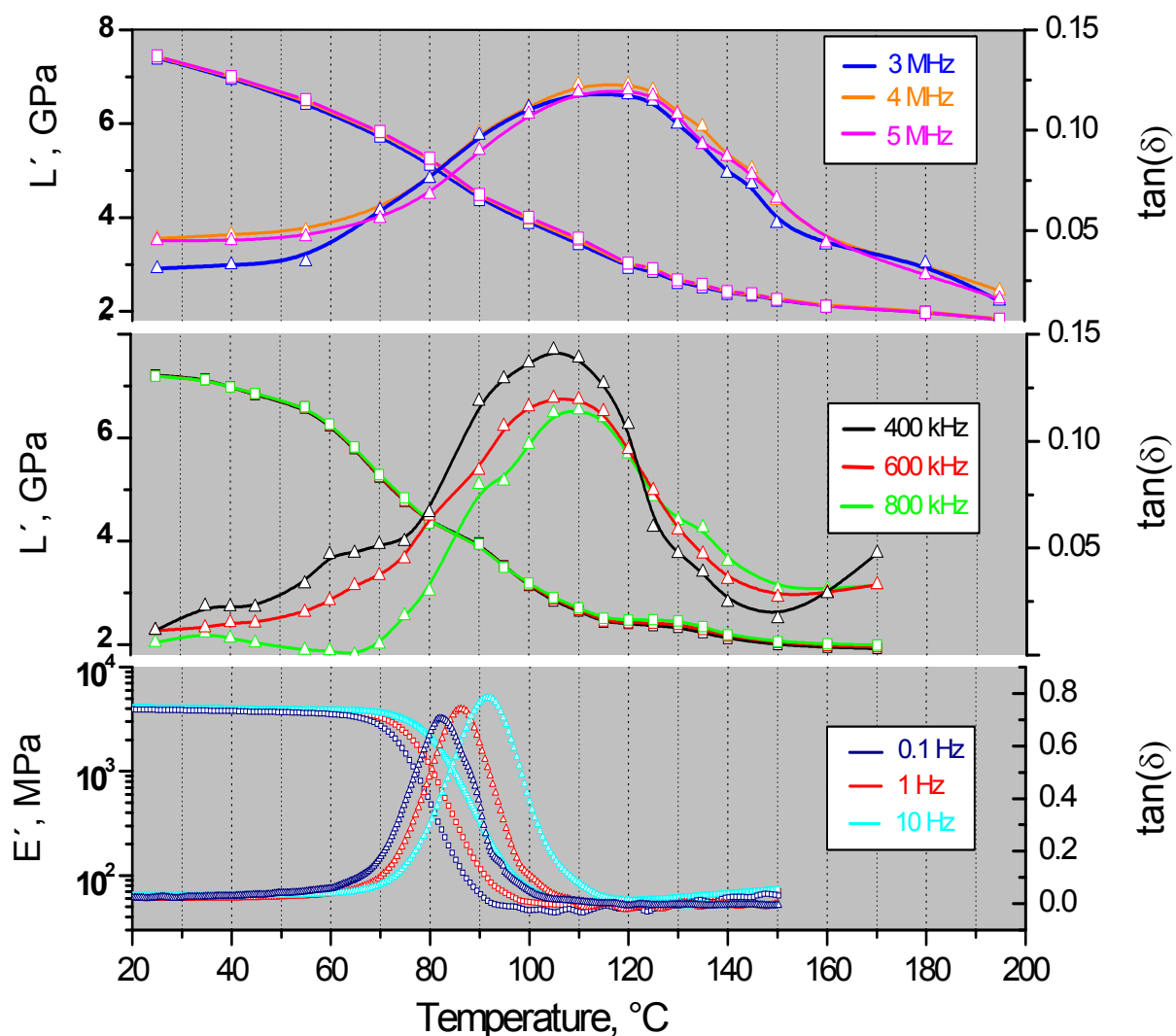
Fig. 5.8 . *Storage modulus as square symbols and tan(δ) as triangular symbols versus temperature for a range of frequencies using both conventional DMA (bottom diagram) and acoustic analysis techniques (top two diagrams)*

 may be explained by a remark from Ferry (Ferry `80) that compressional deformation will not be expected to involve changes in long range molecular configurations or contour shape and therefore differences in material states (liquids, rubbers, solids) will not be as striking in compression as in tensile loading. Therefore both L′ and tan(δ) determined from longitudinal wave propagation will not exhibit such a large change in magnitude as for example E′ (shown on a logarithmic scale) or tan(δ) determined from tensile loading experiments. A shift in tan(δ) maximum from lower to higher temperatures as the frequency increases is observed. Peak maximums are observed in the frequency ranges 0.1 to 33 Hz at 82 to 92 °C; in the 400 to 800 kHz range at 108 to 112 °C and in the 3 to 6 MHz range at 115 to 118 °C. Using these values for all techniques the data can be integrated illustrated together with the WLF fit (taken from Fig. 5.4) and are shown in Fig. 5.9. The data and the WLF fit provide satisfactory agreement. The reasons for deviations from the fit line at temperatures between 80 and 95 °C have been discussed already for Fig. 5.4. At higher frequencies especially at 400 to 800 KHz deviations may be caused by the influence of divergence of primary and secondary relaxations
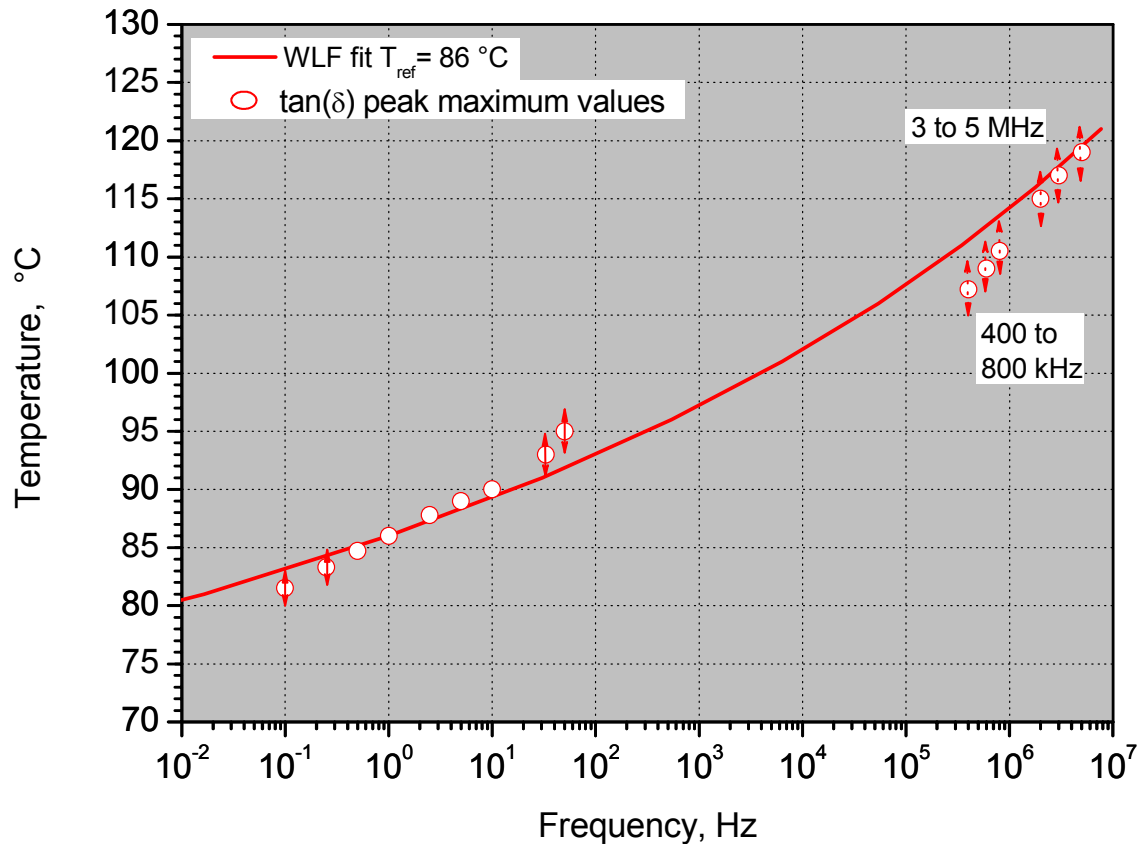

Fig. 5.9. *α relaxation temperatures obtained from tan(δ) maximum. Tolerances are illustrated by symbol size unless otherwise indicated (arrows used for wider tolerances resulting from broadening of tan(δ) peak). Red line is WLF fit.*

at higher frequencies. As shown in Fig. 5.4 a secondary relaxation will exhibit a linear frequency dependence and the primary relaxation is best described by WLF behaviour. An example is provided in literature for an epoxy (Nguygen `95) whereby both relaxation regions diverge at ultrasound frequencies. The author could not identify a ß relaxation using ultrasound and states that its effect is expected to be small.

At present, only tan(δ) values have been considered to describe loss or damping properties. The ultrasound loss modulus L´´ could also be used but as shown in Fig. 5.10 the frequency resolution is worse for L´´ than for tan(δ). In this illustration the symbols represent measured data points and the lines represent general trends (not fits) which best describe the measured data profile. Due to the large scatter of results it becomes more difficult to differentiate between peak maximum values for L´´ values even in the quite large frequency range shown. This is mainly caused by the large influence of sound velocity to the third power in Eq. 2.12 used for the evaluation of L´´. As a consequence even small errors in sound velocity will lead to large changes in L´´ often leading to quite large deviations of data points from the general trend lines. Therefore tan(δ) would seem to be a more suitable parameter than L´´ for describing damping losses in polymers.
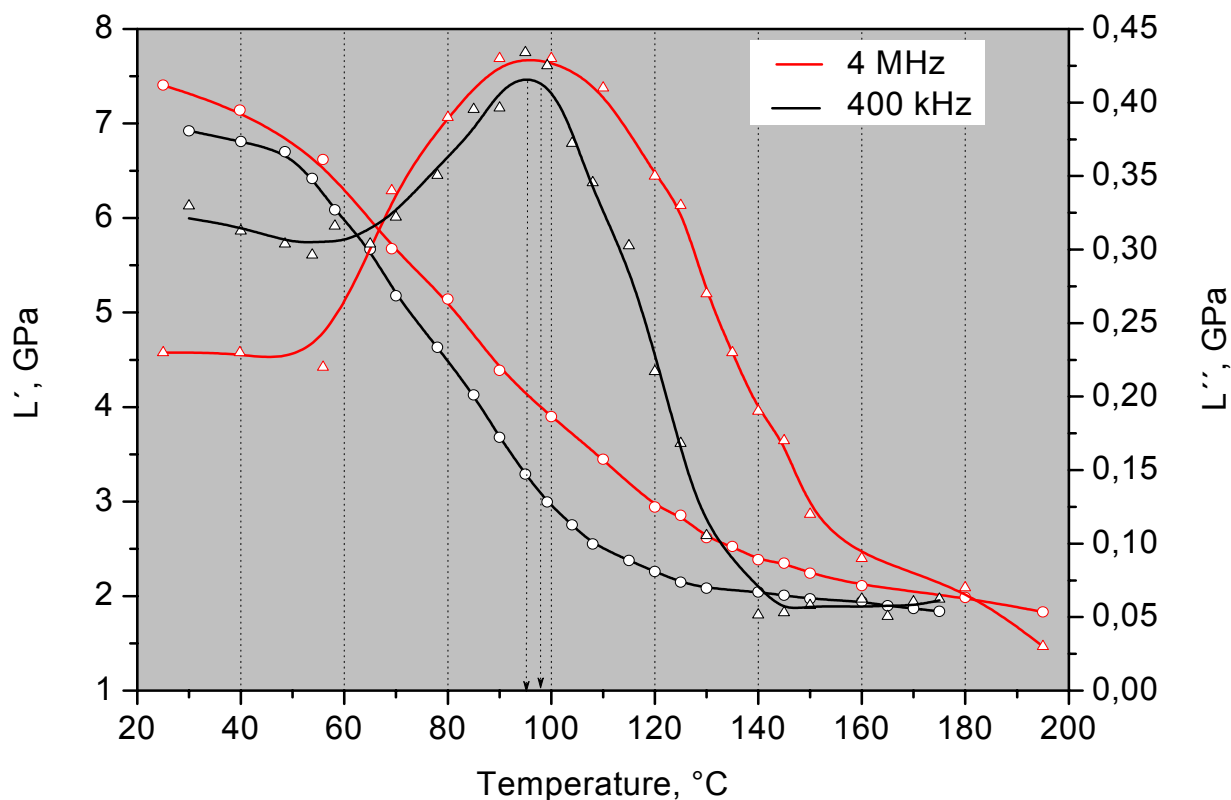
Fig. 5.10 *Storage L´ (circles) and loss L´´ (triangles) modulus as a function of temperature at specific frequencies*

5.1.4 Interrelation of Complex Moduli and Poisson's Ratio

The objective of this experiment was to study the sensitivity of longitudinal wave modulus to changes in viscoelastic properties as a function of temperature, by comparing the results with other more commonly used modulus forms. In the wave theory discussion in Chapter 2.2.3 several different relationships were presented with regard to the interrelation of mechanical modulus. As stated, if values are provided from any two modulus types (e.g. G′ and E′) then it is possible to define any other dynamic modulus or Poisson's ratio. Ultrasound measurements presented here are almost exclusively longitudinal wave propagation which naturally provides a longitudinal modulus. For studies of the dynamic mechanical properties and especially relaxation studies over large frequency ranges it would be preferable to employ the more common tensile modulus. Wave propagation techniques can be employed to measure a tensile and shear modulus but practical measurements on viscoelastic polymers are difficult mainly due to limitation in sample geometries (Nolle `58). For example tensile modulus measurements require long thin samples and corresponding sensors, a combination that is normally impractical over a large temperature range. On the other hand, longitudinal modulus can be estimated in all material states as long as some simple geometrical rules are upheld (Chapter 2.2.3, page 19). To calculate values for the various dynamic moduli or Poisson's ratio one requires in addition to longitudinal storage modulus at least one other storage modulus (e.g. shear) measured under the same conditions. To solve this problem, transversal wave sensors with the same geometry as the longitudinal sensors (Chapter 4.1.2.1) were employed to determine the shear storage modulus. The active piezoelectric ceramic element is basically a piece of polarized material with electrodes attached to two of its opposite faces. This active element may be cut in various ways to produce different wave modes (Krautkrämer `86). The new transversal sensors have the same middle frequency of 3.5 MHz and identical housing to the longitudinal sensors, which means that they may also be employed in the measuring cell illustrated previously (Fig. 4.3). The shear storage modulus G′ is calculated from shear wave velocity c_T and density ρ ($G' = \rho c_T^2$). As discussed in Chapter 2.2.1 transversal waves do not propagate in liquids or gel-like materials, meaning that the evaluation of shear velocity was not possible at temperatures higher 90 C because the material is too soft. Shear and longitudinal storage modulus are calculated from experimental values and as shown in Fig. 5.11 are both illustrated with different colours by using full lines and circular data points. The tensile storage modulus E′, Bulk storage modulus K′ and

Poisson's ratio μ_p' may be calculated from L′ and G′ as follows. Further details are provided in Chapter 2.2.3.

Longitudinal Modulus: $L' = K' + \dfrac{4}{3}G'$

Youngs Modulus: $E' = \dfrac{3L' - 4G'}{\dfrac{L'}{G'} - 1}$

Poisson ratio: $\mu_p{}' = \dfrac{E'}{2G'} - 1$

Refer to Equations 2.15 to 2.20

The real terms E′, K′ and μ_p' may all be evaluated from experimentally determined values for G′ and L′. As shown in Fig. 5.11 strong lines with no symbols are used to illustrate parameters evaluated from G′ and L′. At low temperatures the shear wave velocity is approximately 1140 m/s with a corresponding modulus of G′ = 1500 GPa.
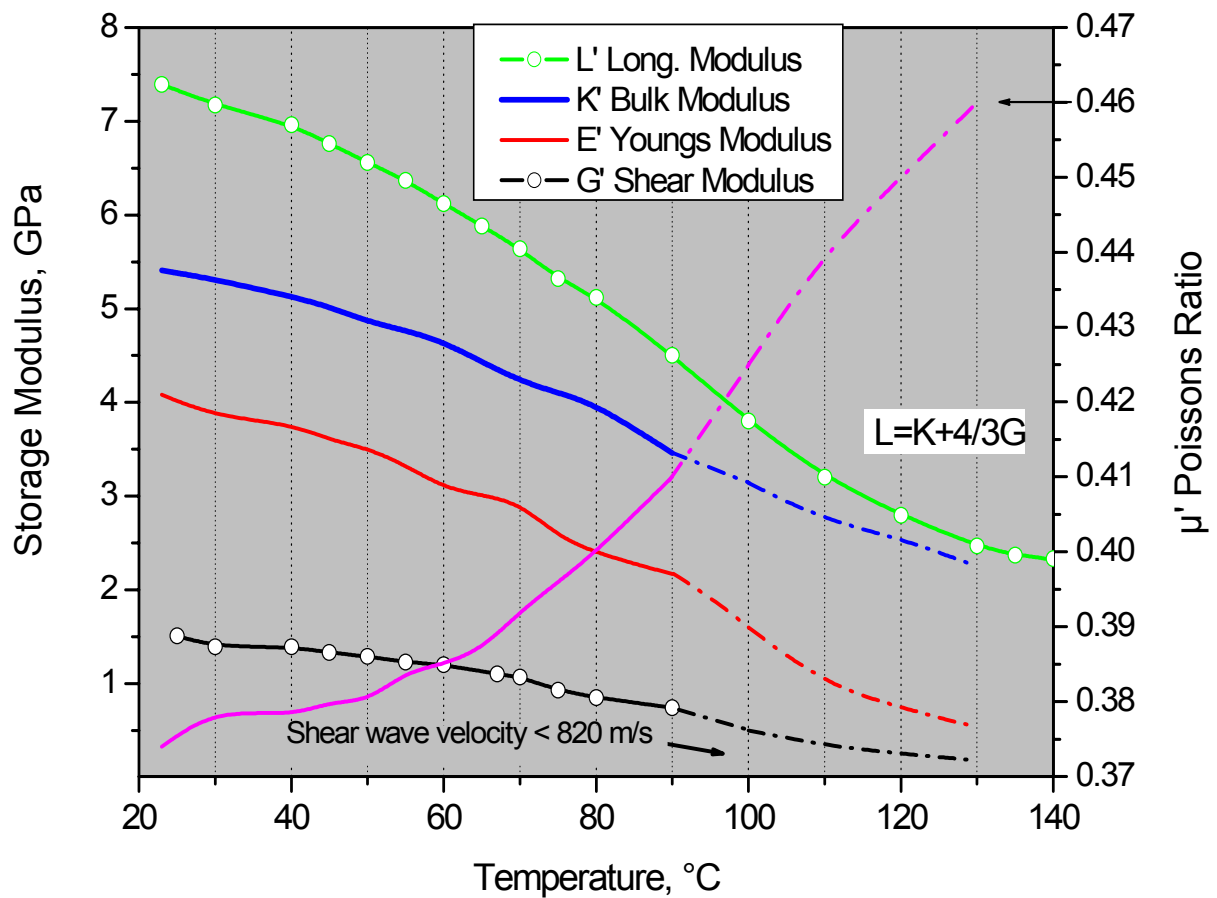
Fig. 5.11: *Modulus and Poisson's ratio plot as a function of temperature. Symbols represent measured data points. Full lines are calculated from measured data and dotted lines are calculated from longitudinal modulus and Poisson's ratio extrapolated from 90 to 130 °C.*

Shear waves propagate roughly 45 % slower than longitudinal waves and therefore the shear storage modulus calculated using $G' = \rho c_T{}^2$ is much lower than its longitudinal modulus counterpart. Both measured moduli decrease with increasing temperature and in the vicinity of the glass rubber transition at temperatures higher than 80 °C the signal to noise ratio becomes so small that it is no longer possible to evaluate shear wave velocity with certainty. The minimum velocity measured was approx. 820 m/s at 80 °C which would seem to represent a critical lower level measurement limit for shear wave propagation (Döring `02). From the determined values G′ and L′ it is possible to estimate the Poisson's ratio using the above equations. The calculated value of approx. 0.37 at 40 °C is typical for glassy polymers, for example synthetic glass sapphire has a Poisson's ratio of approx. 0.31. As already explained at T > 90 °C it was impossible to evaluate shear data and therefore from experimental data alone it would not be possible to calculate μ_p'. However from standard material values it is known that for incompressible elastic solid the theoretical Poisson's ratio is about 0.5. For example natural rubber is quoted (Sperling `92) as having a Poisson's ratio of 0.49 and according to Alig (Alig ´02) an epoxy material in the rubber state at temperatures above T_g has a value of 0.46. Considering this background, a value of 0.46 would seem to provide a reasonable estimate for polymers in a rubberlike state and therefore the Poisson's ratio curve was extrapolated to a value of 0.46 at 130 °C. This temperature was chosen because, as demonstrated in this chapter, this epoxy is definitely in the rubber state even for experiments at MHz frequencies. Therefore the μ_p' data measured up to 90 °C could be extrapolated up to 130 °C. This extended curve is illustrated in the form of a dotted pink line. As the longitudinal modulus is known throughout the whole temperature range (green line with circular symbols), it is now possible using the data from the extrapolated Poisson's ratio to continue calculation of E′, K′ and also G′. At temperature above 90 °C these values are also graphically illustrated using dashed lines. From the graphic illustration following conclusions can be made:

- All modulus forms have similar profiles and each show a clear decrease with temperature that is associated with the α relaxation.

- The magnitude values for the various storage moduli can be ordered in following sequence, with L′ having the highest magnitude L′>K′>E′>G′. This behaviour is expected as most materials resist a change in volume as determined by the bulk modulus K′ more than they would resist a change in shape, as determined by the shear modulus G′. This result is easily visualised when one considers the load required

achieving compressional deformation in a polymer in comparison to forces required to achieve a similar deformation using tensile or torsional loading techniques.

- A linear axis was chosen to best illustrate the results and one could quickly form an incorrect opinion that the longitudinal modulus L´ is more sensitive than the shear modulus G´ to changes in the viscoelastic properties due to what would seem to be a larger change in modulus. This would also contradict the last statement (above). In actual fact the opposite is true as G´ tends towards values in the hundred Pascal range. This means changes in G´ could actually cover several orders of magnitude and will therefore be more sensitive than a longitudinal or bulk compression modulus to modulus variation independent of cause.

- At high temperatures higher than 90 °C the shear modulus G´ will tend towards very low values because a viscous material cannot sustain shear wave propagation. Eq. 2.20 states $L´ = K´ + 4/3G´$ and shows that when G´ is low then the longitudinal storage modulus L´ is nearly equal to the bulk storage modulus K´. This can be observed in Fig. 5.11 at about 120 °C.

5.2 Adaptation of Measuring Set-up for Cure Monitoring

In the previous section a two sample measuring set-up was employed to characterise a cured epoxy. This was necessary because dynamic heating of both the epoxy sample and sensors leads to a disproportionate change in impedance values between material boundaries (see Eq. 4.4) making it difficult to accurately estimate the attenuation in the sample itself. Ideally this technique should also work for curing epoxy systems, however the reaction is exothermic and as a result the thicker the sample the more difficult it becomes to maintain or guarantee constant sample temperatures (McHugh `03). On the other hand very thin samples e.g. 1 mm may lead to errors in calculation of attenuation or sound velocity. A thickness error of just 0.1 mm would consequently lead to deviations in sound velocity (Eq. 4.7) of about 10 %. Most authors in the past were mainly interested in obtaining quantitative values for sound velocity whereas attenuation was only of secondary interest and therefore relative values or simply, the change in attenuation over the curing reaction were normally deemed sufficient for evaluation purposes. In such cases a measuring set-up using a single sample and a reference sensor to sensor signal is employed (Döring `01) to obtain this information. In this situation one of the two measured sample signals described under measurement principles (Fig 4.7, Chapter 4.2) is replaced by a constant reference value at thickness null. To obtain this reference signal the mould (Figs. 4.5 and 4.6) is fully closed so that the ultrasound sensors are in direct contact and a thin layer of silicon oil of negligible thickness is used as couple medium. The sound velocity and a relative attenuation are calculated as usual by comparing these two signals (one constant and one variable) over the curing reaction.

In the cure monitoring experiments discussed in the following chapter a quantitative value for attenuation is desired as it would facilitate a direct comparison with the DMA results already presented. As all experiments take place at constant temperatures it is possible to estimate if this new measurement setup will lead to significant errors in calculating quantitative values for attenuation or if a correction factor is required. For this reason A-scan signals were analysed at the start and end of cure. An evaluation example is provided below in Fig. 5.12. The results show the A-scan signals obtained from the reference signal and a 3 mm epoxy sample at the beginning of cure at 60 °C whereby the epoxy has a low viscosity. Impulse amplification was 40 dB for both reference and sample signal. The signals are converted into their magnitude spectrum using the FFT analysis technique. Both signals are similar in form and an attenuation loss in the 3 mm sample of 0.25 dB/mm was calculated at 3.5 MHz using Eq. 4.6. This attenuation value is quite low considering that the sound wave

has passed through 3 mm epoxy so that boundary effects resulting in a loss of signal amplitude by reflection do not seem to play a significant role. Similarly using the same technique and sample, the attenuation values at the end of cure at 60 °C were calculated as 2.4 dB/mm at 3.5 MHz. This value was compared to attenuation values obtained for the cured epoxy measured using a two sample technique with different thicknesses also at 60 °C. An attenuation value of 2.7 dB/mm was measured at 60 °C and 4 MHz for a fully cured epoxy as shown in Fig. 5.5. This is a difference in absolute values of 0.3 dB/mm depending on measurement set-up employed. As will be shown later (Figs. 5.14 and 5.15) attenuation values in the frequency range used vary by between 0.3 to 10 dB/mm leading to an error in determining quantitative values of attenuation using this technique of about 3 to 4 % throughout cure. The results to be presented are mainly concerned with maximum or peak attenuation values measured so that small errors in quantitative values of attenuation such as discussed above are quite acceptable and therefore no correction factor was used. Secondly this experiment proves that it is possible with calibration to determine absolute values for attenuation using just one sample.
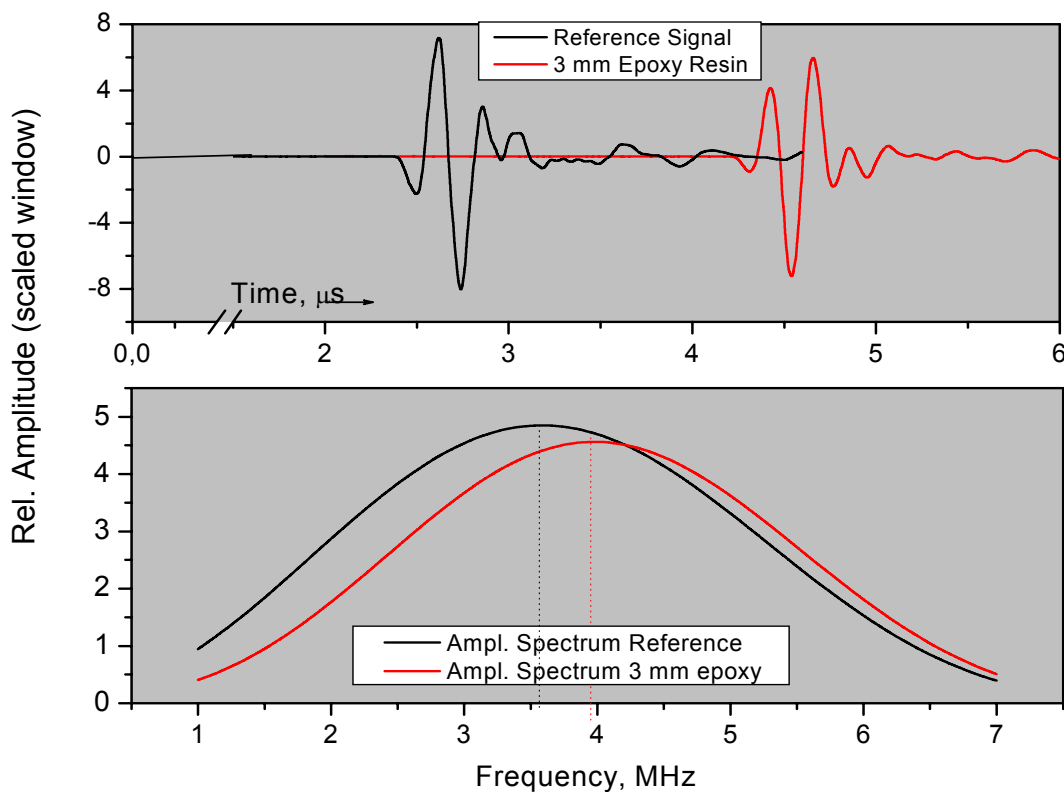
Fig. 5.12: *A scans recorded at 40 dB amplification for a reference (sensor-sensor) and a 3 mm epoxy resin in the liquid state. Mould temperature is constant at 60 °C.*

5.3 Characterisation of Cure Behaviour

5.3.1 Introduction and Background

As discussed in the literature review in Chapter 2.1.3 acoustic parameters seem to be sensitive to changes in the mechanical properties resulting from the growing network structure. However, in the past the majority of research has relied largely on empirical comparisons from a variety of analysis techniques that were based largely on differing physical measurement principles e.g. dielectric analysis and NMR. This makes it very difficult to form conclusions on how sensitive the acoustic technique is to chemorheological changes occurring during cure and in particular transformations such as gelation and vitrification. The objective of the following chapter is to investigate the sensitivity of ultrasound sound velocity and $\tan(\delta)$ to changes in the viscoelastic properties of a curing epoxy polymer. To achieve this goal the results from ultrasound are compared to other more common techniques used to characterise the curing reaction and changes in the viscoelastic properties of a curing epoxy. Following a description of these changes, the main topics of this section can be divided under following central themes:

- Evaluation of isothermal cure experiments from each individual analysis technique e.g. Ultrasound, DSC and Rheometric techniques.
- General comparison of techniques and application of an Arrhenius based relationship that provides an opportunity to quantitatively compare the sensitivity of analysis techniques based on different measuring principles, but which should all be sensitive to the curing reaction.
- Discussion on the sensitivity of ultrasound to overall reaction and the transformations: gelation and vitrification

# 5.3.2 Interpretation of Isothermal Cure Profiles

5.3.2.1 Signal Analysis

Two signal analysis techniques are available that can be employed for the evaluation of sound velocity and attenuation. The first is based on manual analysis of recorded A-scans using the FFT analysis and was described in Chapter 4.2.1. The second technique uses the automatic software "US-Plus system" developed at the BAM (Döring `02) and currently in use for commercial applications in the field of cure monitoring. The main difference between the two analysis techniques is that one is based on spectral analysis i.e. sound velocity and attenuation data are evaluated as a function of frequency and the other is based on direct analysis of ultrasound parameters from transmission times and signal amplitude over the whole frequency bandwidth. To differentiate between the techniques, the second technique that is mainly based on Peak Analysis will be referred to with the abbreviation PA. For the PA technique, amplitude values are taken as the peak amplitude values for the first positive peak observed in the sample and reference A-scans. Similarly transmission time is calculated by subtracting the time taken to reach the first positive maximum in the sample A-scan from the time to first positive maximum in the A-scan of the reference signal. This procedure is standard evaluation practice in conventional acoustics. The main advantage of employing PA is that measurement and evaluation takes place automatically in real-time by analysing peak amplitudes and transmission times from the A-scans using specially developed software (Döring `01). Once the sample amplitudes and transmission times have been recorded (using FFT spectral analysis and PA techniques) then the same equations can be employed to calculate attenuation and sound velocity (Eqs. 4.6 and 4.7). To illustrate the difference between the two techniques, both were employed to analyse data obtained during epoxy cure at 60 °C (see Figs. 5.13 and 5.14). As shown both evaluation techniques deliver similar sound velocity and tan(δ) profiles over time and this general cure profile will be discussed before commenting on specific differences between results. The sound velocity curves have a sigmoidal form and can be split into *three distinct regions* (independent of evaluation method) according to sound velocity magnitude.

Region 1: This region describes the low sound velocity values at the beginning of cure i.e. in the range between 1450 to 1530 m/s depending on the measuring frequency. Filling and closing the mould takes about 20 s and the epoxy assumes the environment temperature

immediately on filling due to the small amount of resin employed (less than 3 g). On filling a large reduction in viscosity is observed correlating well with sound velocity values for low viscosity liquids e.g. fresh water has a sound velocity of 1435 m/s (Krautkrämer `86).

Region 2: Designates the strong increase in sound velocity occurring after approximately 50 mins. This signifies an increase in viscosity or modulus associated with the development of a crosslinked network as a result of the curing reaction. The epoxy resin starts life as a low molecular weight liquid and as the reaction progresses begins to gel and eventually at high conversion levels it vitrifies under the precondition that the mould temperature T_{cure} is less than the maximum glass transition temperature $T_{g\infty}$ (see Time Temperature Transformation TTT diagram in Chapter 3.3).

Region 3: In this region the sound velocity curve slowly reaches saturation forming a plateau after approx. 350 mins whereby a maximum value of 2350 m/s at 6 MHz is achieved. This behaviour indicates that the crosslinking reaction becomes diffusion controlled resulting in a freezing of the network structure, whereby stable values for sound velocity are achieved. The sound velocity values obtained are typical for a polymer with medium stiffness values e.g. High Density Polyethylene HDPE at room temperature (McIntire `91).
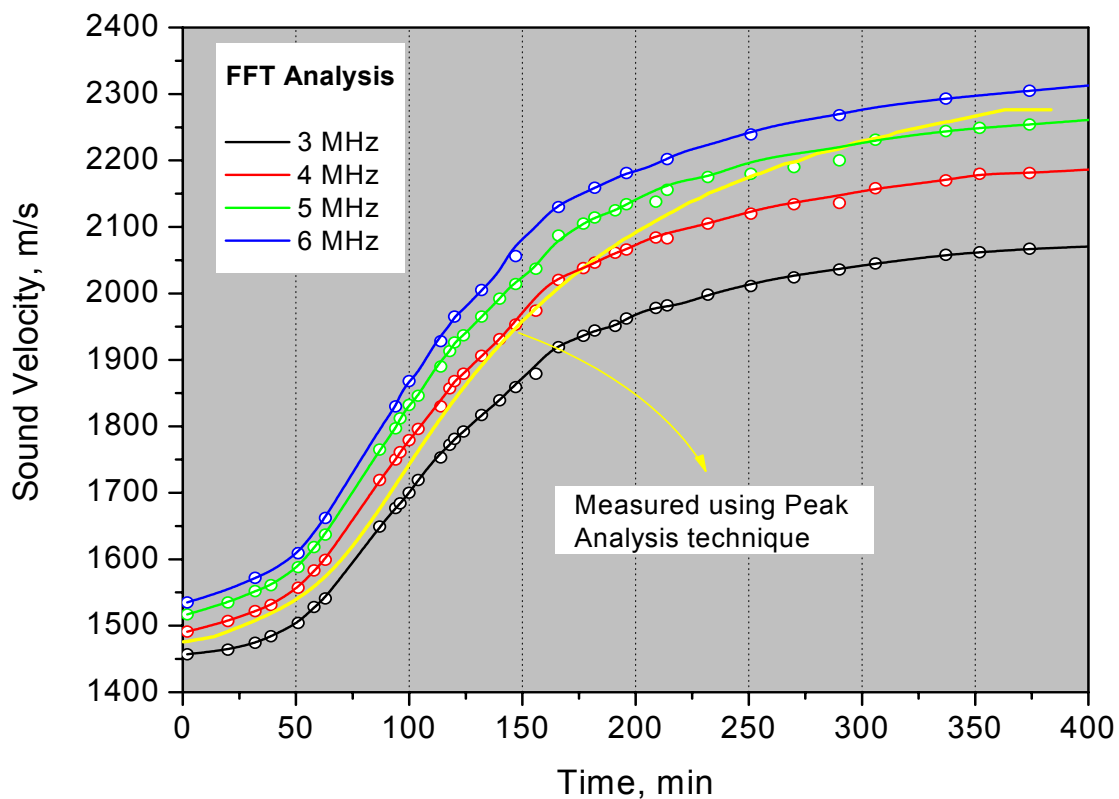
Fig. 5.13 *Sound velocity versus time plot for cure at 60 °C. Comparison between FFT analysis at 3 to 6 MHz and Peak Analysis PA techniques.*

tan(δ): As shown in Fig. 5.14 a maximum in tan(δ) is observed after 95 mins cure. This time correlates with *region 2* describing an intermediate state between liquid and glass and already described using sound velocity behaviour. No clear relationship between peak position (in minutes) and frequency could be identified. As described in the last section an ultrasound tan(δ) peak with an average intensity of 0.12 in the 100 kHz to 6 MHz frequency range will be observed for the α relaxation referred to also as the glass transition T_g as shown in Fig. 5.8. Both terms are clearly defined in Chapter 2.3.1. During isothermal cure the tan(δ) peak observed has an average magnitude of 0.115 at 4 MHz. It is well known that T_g will have much higher tan(δ) values than other polymer relaxations e.g. secondary relaxations. By taking both the sound velocity profile and the intensity of tan(δ) into consideration, there is no doubt that the observed peak describes the rubber to glass transition more commonly referred to as vitrification for reactive polymers.
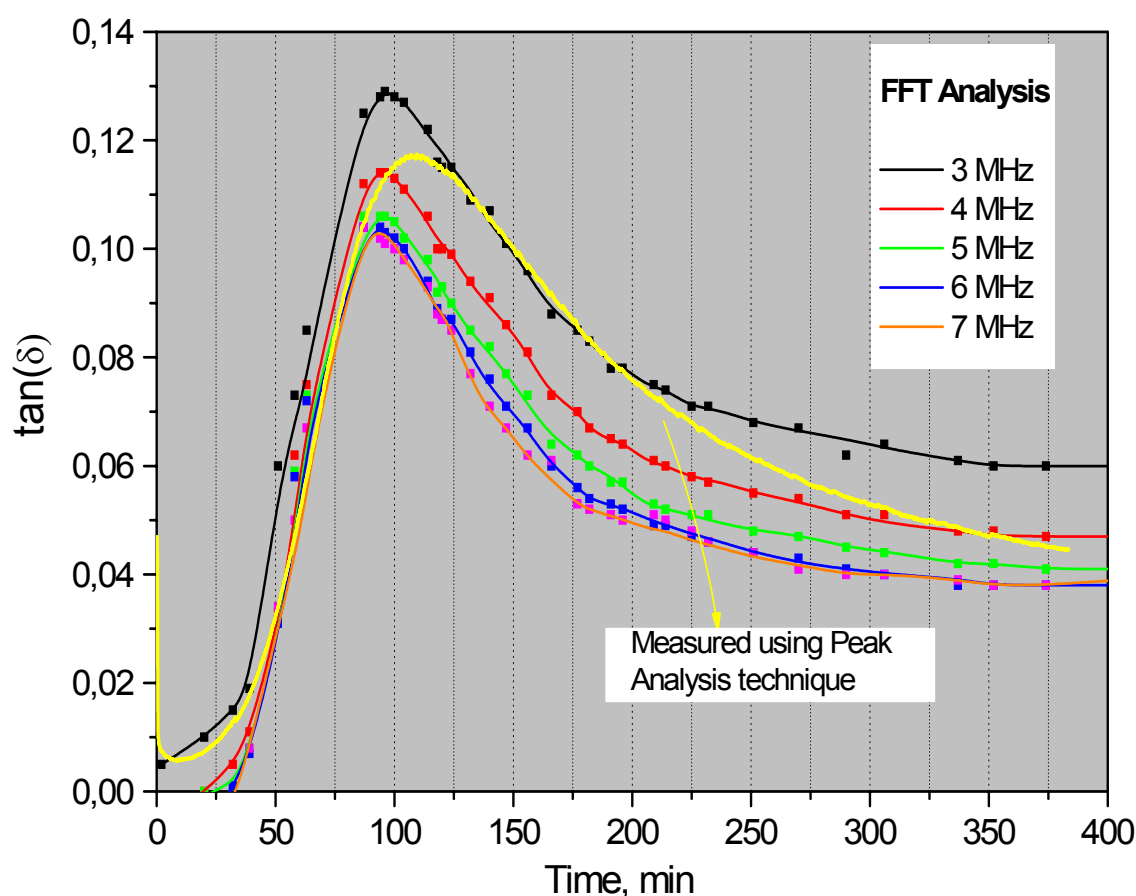

Fig. 5.14 *tan(δ) versus cure time at 60 °C. illustrated: FFT analysis between 3 and 6 MHz and Peak Analysis PA at approx. 4 MHz middle frequency*

Comments on Analysis Techniques: In Figs. 5.13 and 5.14 the colour yellow signifies measurements using the PA technique. One major disadvantage of this technique is that frequency specific information may be lost. However as the sensors operate in a limited frequency bandwidth of approx. 5 MHz as shown in Fig. 5.12, large errors resulting from assuming a middle frequency are not to be expected. To calculate $\tan(\delta) = \alpha\lambda/\pi$ using this technique values for both attenuation α and wavelength λ are required. Wavelength is calculated from sound velocity c and the frequency f is taken as constant at 4 MHz, associated with the sensor middle frequency (see Fig. 5.12). The middle frequency is an average value and will typically drift during cure by about $\pm\,0.5$ MHz, depending on extent of cure. This explains slight deviations of the yellow $\tan(\delta)$ curve from the frequency dependent measurements using FFT analysis at 4 MHz. Frequency dependence of sound velocity or dispersion is well known in polymer materials (see Chapter 2.2.4). If during cure a constant or middle frequency is assumed as is the case using the PA technique then dispersion effects will be neglected leading to a deviation of yellow sound velocity line from values measured at a specific frequencies e.g. red line at 4 MHz both illustrated in Fig. 5.13. To summarise; results will vary slightly depending on analysis technique employed but the same crucial information will remain, for example cure times required until sound velocity increases or reaches saturation and also a maximum in $\tan(\delta)$ is observed after similar cure times. The main advantage of using PA over FFT analysis is that ultrasound parameters can be evaluated automatically in real time, saving considerable evaluation time, especially where large amounts of data need to be evaluated.

5.3.2.2 Characterisation of Cure Behaviour at Constant Temperatures

Ultrasound measurements were performed at temperatures between 40 and 100 °C using the PA evaluation technique. To help compare the results with other characterisation methods, characteristic cure times common to the isothermal cure profiles were identified as shown in Fig. 5.15 at 60 °C. t_{onset} describes the cure time at which a strong increase in sound velocity is observed. t_{Offset} is the turnover time employed to define the cure time required until the sound velocity curve begins to saturate, after which only a very gradual increase in sound velocity is identified. Both turning points are defined by the crossing of two tangents drawn in the area of interest as shown in Fig. 5.15. t_{Offset} times are difficult to determine with high accuracy because their positions will vary depending on how the tangents are placed and should only

be used as orientation values. Further characteristic cure times are taken as the time required until a maximum in either tan(δ) [$t_{\tan\delta}$] or attenuation [t_{Att}] is reached. The results for cure temperatures between 40 and 80 °C are presented in Fig. 5.16 and Fig. 5.18. Sound velocity profiles at higher temperatures are not illustrated as the curves are similar in form to those already shown and would require a separate diagram. However t_{onset} and t_{Offset} are documented for all temperatures in Table 5.1 at the end of this chapter. As the sound velocity profiles at different temperature follow almost the exact sigmoidal form discussed in detail for Figs 5.13 and 5.14 in the last subsection, only general cure behaviour and anomalies are discussed in the following. For roughly every 10 K increase in cure temperature (Fig. 5.16), the time taken to reach t_{onset} almost halves indicating that the reaction rate doubles. Sound velocity values at the start and end of cure also decrease with increasing cure temperature. This information relates *only* to the magnitude of sound velocity at a) cure begin i.e. before t_{onset} is reached and b) towards the end of cure after t_{Offset} and for all cure temperatures is illustrated in Fig. 5.17.
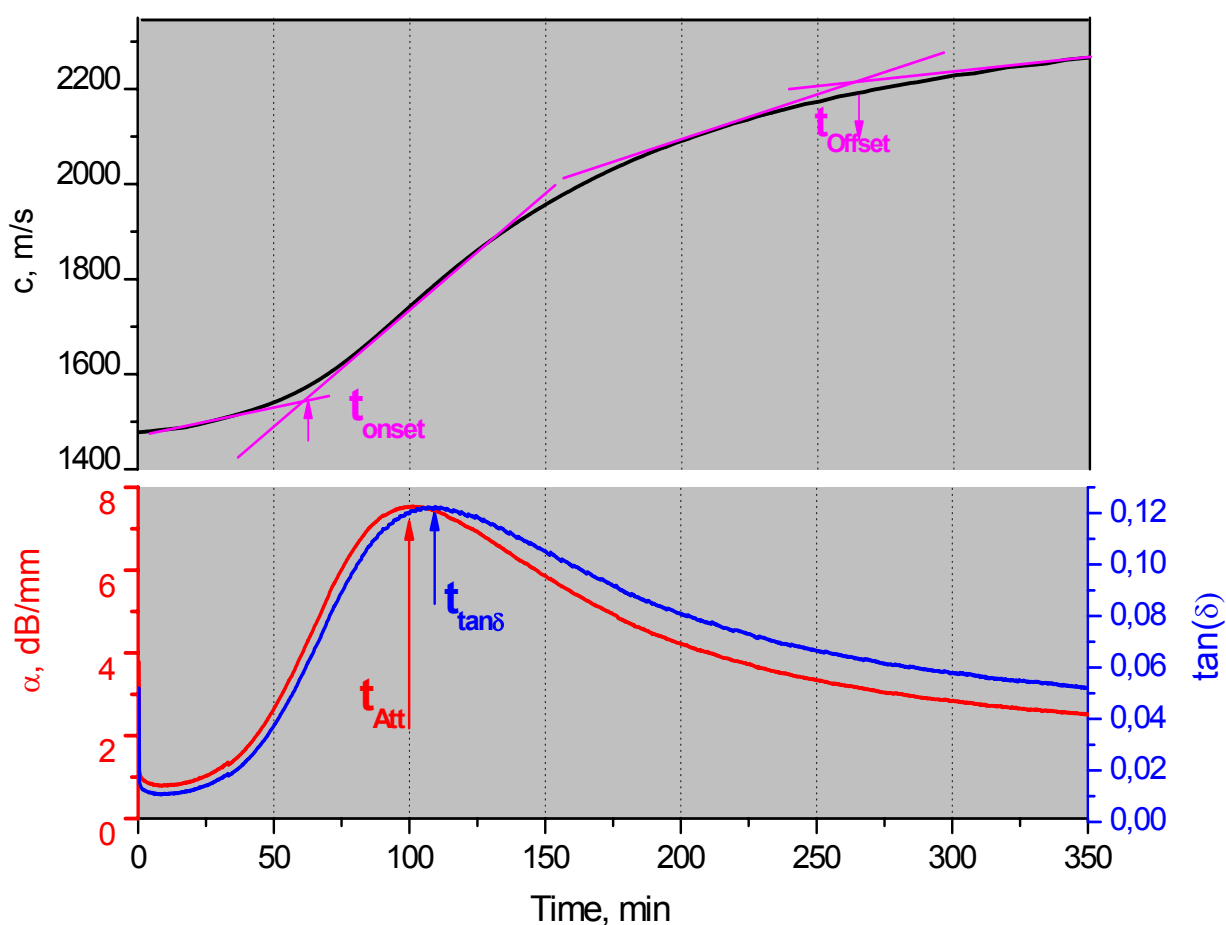
Fig. 5.15 S*ound velocity, attenuation and tan(δ) versus time plot for isothermal cure at 60 °C. The arrows designate reference points used to describe cure behaviour*
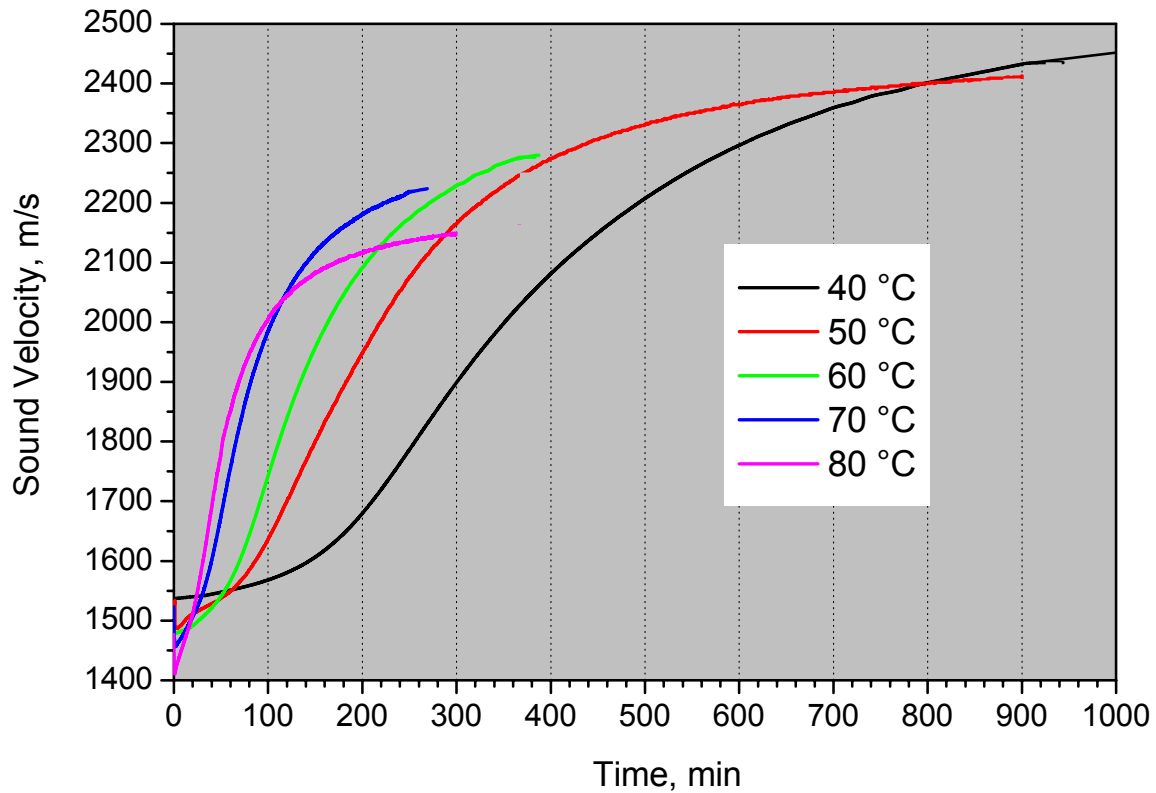
Fig. 5.16: *Sound velocity versus cure time plot for a range of isothermal temperatures*
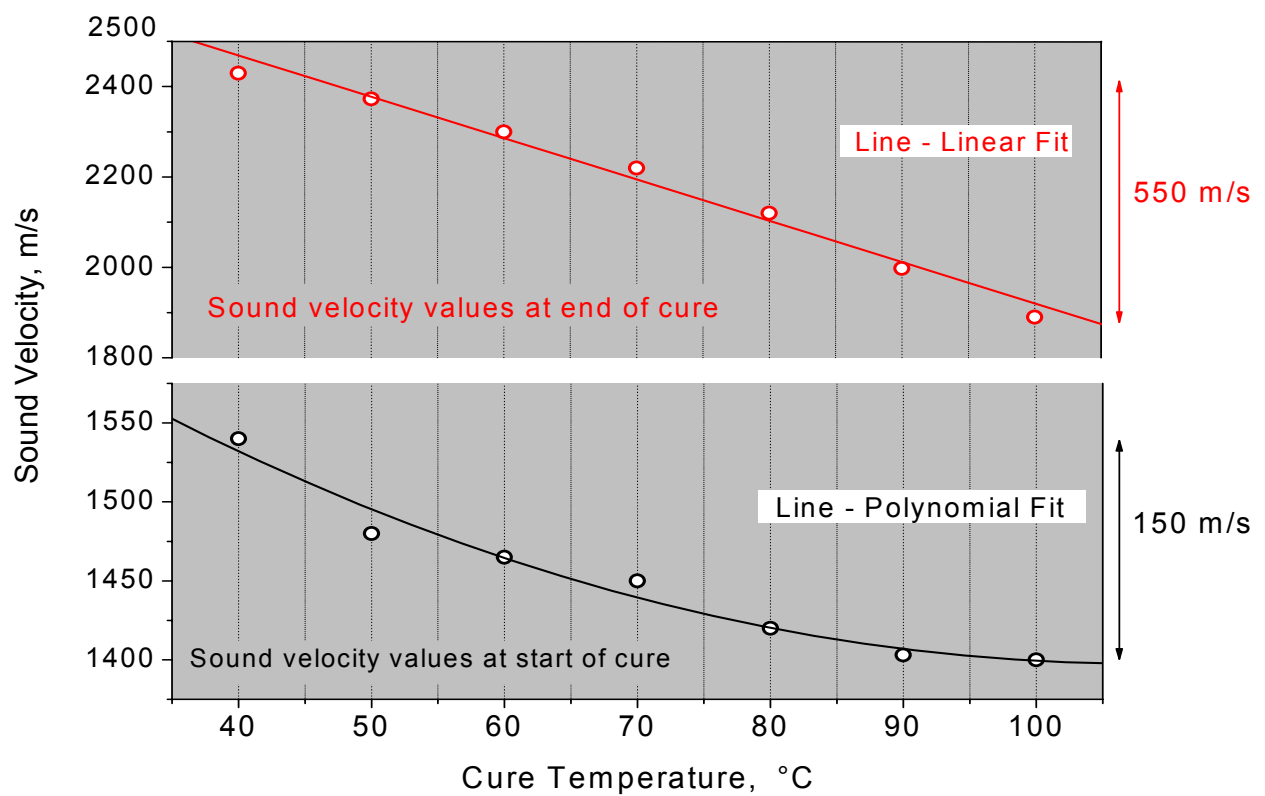
Fig. 5.17 *Magnitude of sound velocity measured at the start and at the end of cure plotted against cure temperature*

In Fig. 5.17 the sound velocity values measured at cure begin decrease with increasing cure temperature and could be best fitted using a polynomial curve that reaches almost constant minimum values of about 1420 m/s at temperatures greater than 80 °C. This behaviour can be explained by considering the viscosity or modulus values of the resin system at the start of cure. As the mould temperature increases the viscosity of the resin will decrease, reflected by the almost linear decrease in sound velocity up to 80 °C. At higher temperatures the sound velocity levels off at a minimum value of 1420 m/s which is equivalent to the sound velocity of fresh water (Krautkrämer `86). In other words the resin reaches a minimum viscosity at temperatures higher than 80 °C explaining the polynomial form of the fitted sound velocity values at cure begin. On the other hand, the sound velocity values at the end of cure exhibit a linear decrease up to 100 °C. To explain this behaviour information obtained in Chapter 5.1 (investigations on a fully cured epoxy) needs to be applied. **(1)** The glass transition temperature defined by the maximum in tan(δ) is observed at approx. 115 °C in the 3 to 5 MHz region as shown in Fig. 5.8. **(2)** At temperatures higher than 115 °C the material will not vitrify and the sound velocity decreases from about 1650 m/s at T_g to about 1300 m/s at 180 °C as shown in Fig. 5.5. Therefore for acoustic measurements at constant cure temperatures below 100 °C vitrification will always occur ($T_{cure} < T_{g\infty}$) i.e. the epoxy will cure in the glass state. In addition the high sound velocity values at the end of cure are clearly larger than 1650 m/s obtained at T_g and confirming this interpretation. Using this explanation then the linear decrease in sound velocity observed at the end of cure (red line in Fig. 5.17) is almost certainly caused by the temperature dependence of the modulus of the cured epoxy.

Presently only sound velocity profiles have been considered, however as shown in Fig. 5.18, tan(δ) can also be employed to obtain important additional information facilitating a general interpretation of the material state at different cure temperatures. At cure temperatures between 40 and 100 °C a peak maximum in tan(δ) can be identified. However, this peak maximum becomes less pronounced at 90 °C and is difficult to distinguish at 100 °C. If at cure temperatures $T_{cure} \geq T_{g\infty}$ (see TTT diagram in Fig.3.3) then vitrification cannot occur and the material will cure in the rubber state whereby no peak in tan(δ) should be observed. At temperatures greater than 115 °C the epoxy will not vitrify, remaining in the rubber state until being cooled. 115 °C describes a specific transition temperature region but in fact the transition occurs in a temperature range and the influence of the glass transition will be observed first at lower temperatures as shown in Fig. 5.18 whereby the tan(δ) maximum becomes less distinct at high cure temperature < 100 °C.
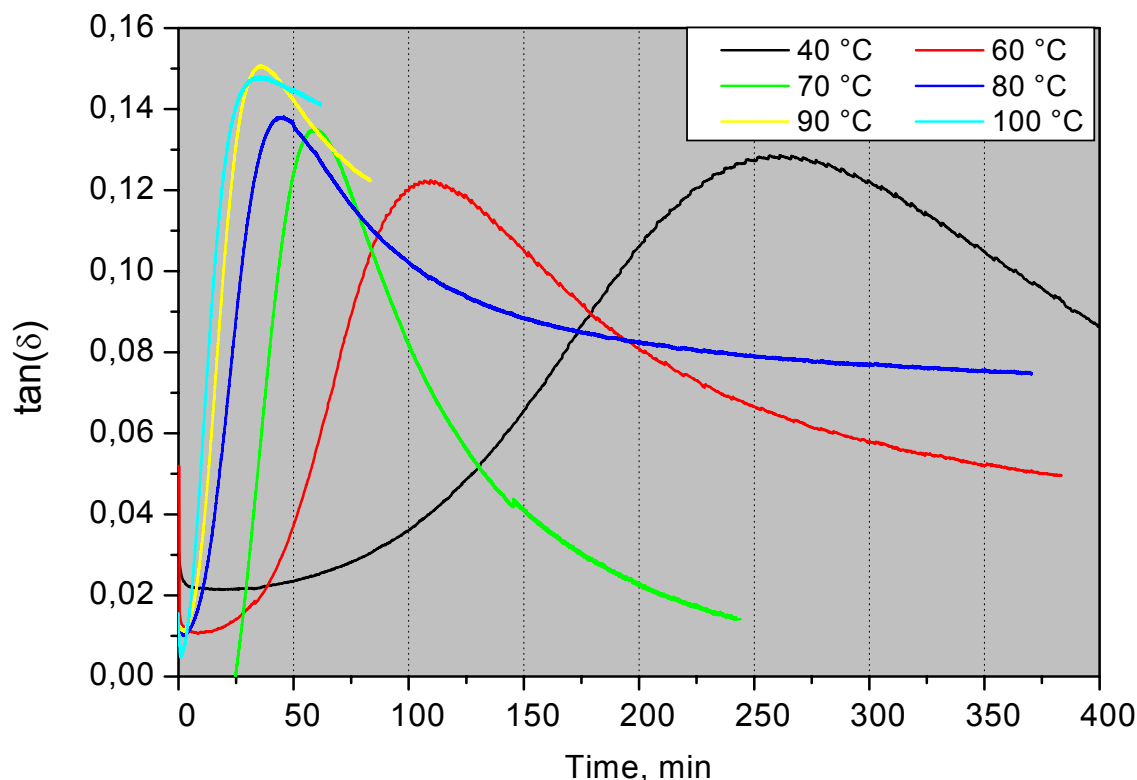
Fig. 5.18 *tan(δ) versus cure time plot for a range of isothermal temperatures*

5.3.3 Rheometry

5.3.3.1 Interpretation of Cure Profile

A rheometer using 20 mm parallel plates as described in Chapter 4.4 is employed to measure the development of shear storage G´ and loss modulus G´´ as well as tan(δ) at constant temperatures between 40 and 100 °C. All measurements take place at 1 Hz with a sample thickness of 0.5 mm. Before the measurement results are interpreted it is useful to consider information gathered from conventional low frequency DMA experiments at the beginning of this chapter. From these experiments it is know that the ultimate glass transition temperature of the fully cured epoxy $T_{g\infty}$ is approximately 86 °C using low frequency measurement techniques. As already discussed, determination of the glass transition is strongly frequency dependent and this value is only valid at low frequencies such as with a rheometer. e.g. 1 Hz. Interpreting this information in terms of the TTT principles (Chapter 3.2) means that this epoxy will gel and vitrify for all cure temperatures at or below 80 °C and at higher

temperatures just gelation will be observed and not vitrification. An example of a typical cure profile at 60 °C is shown in Fig. 5.19. Accurate measurement values for the rheometric parameters (G´, G´´ and tan(δ)) were first obtained after 85 minutes and a shear storage modulus G´ of approximately 10 Pa. This is typical for this particular rheometer measurement setup (20 mm parallel plates) which provides a compromise between sensitivity over a very large modulus magnitude range (typically 8 orders) and low resolution under 10 Pa. Even within these limitations most relevant information relating to viscoelastic behaviour and in particular gelation and vitrification can be obtained from the measured cure profile.

***Gelation*:** After 85 minutes G´ starts to increase rapidly from about 10 Pa and after 90 mins G´ and G´´ crossover occurs which is equivalent to tan(δ) = 1. For dynamic oscillatory measurements this is the most established definition (Winter `97) of the gelation point. According to the author determination of gelation times should be independent of measurement frequency. Gelation is a critical phenomenon which obeys percolation laws i.e. gelation will take place at constant conversion and constant T_g; both of which will depend on the epoxy employed (Gillham `73). This information can be used later in this chapter.
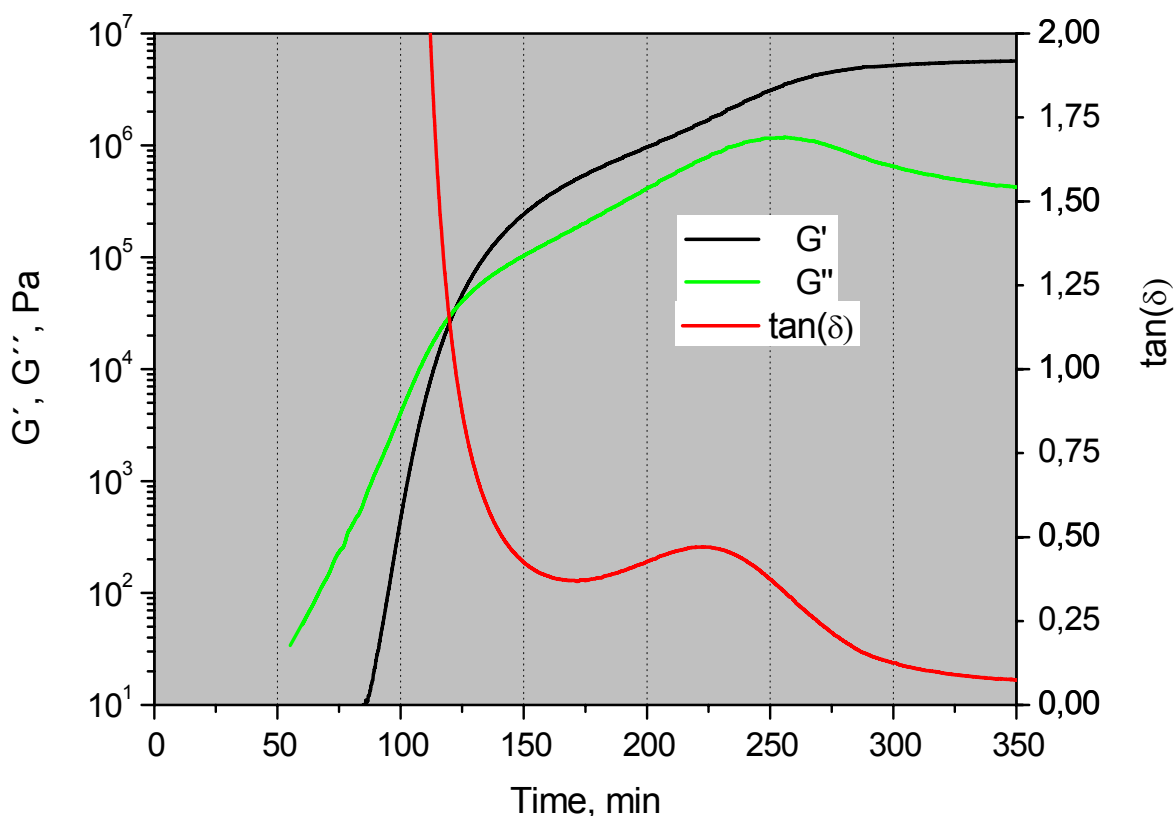

Fig. 5.19: *Modulus (G´ and G´´) and tanδ versus cure time at 60 °C*

Vitrification: Corresponds to the irreversible liquid or sol/gel rubber to sol gel/glass transition and occurs when the glass transition temperature of the epoxy resin approaches the curing temperature (i.e. $T_g = T_{cure}$), discussed in detail in Chapter 3.1. No general criterion has been defined or accepted so far for the determination of the vitrification point and several methods based on different criteria are used arbitrarily. When rheometric techniques are used two common criteria to determine the vitrification point are used either taking peak values of $\tan(\delta)$ or G'' at 1 Hz (Teil `04; Lange `00). As suggested by the fact that measurement frequency is stated, vitrification is a dynamic transition and for commercial cure cycles most typically describes the rubber (gel) to glass transition and as such its location on an isothermal cure time scale will depend on the measurement frequency employed.

5.3.3.2 Cure Behaviour as a function of Temperature

Isothermal cure measurements at a frequency of 1 Hz were performed in the temperature range 40 to 100 °C. The results are shown in Figure 5.20. At 40 °C isothermal cure, gelation (G', G'' crossover) and vitrification occur at similar times after 535 and 575 minutes. A clear peak in G'' is observed but due to the fact that gelation and vitrification occur after similar cure times, only a shoulder and no clear $\tan(\delta)$ peak can be identified. Gelation will occur at fixed conversion (Wisanrakkit `90) and as shown in the following section using DSC experiments, the curing reaction has to proceed to about 60 % conversion before gelation will take place. At T_{cure} <40 °C, the critical 60 % value may not be reached and vitrification can occur without gelation. For this reason, the lower the cure temperature (well below $T_{g\infty}$) the more difficult it becomes to separate the two transitions. This has been explained using the TTT diagram in Fig. 3.3. As the cure temperature is increased the two transformations become more clearly separated and a peak in both G'' and $\tan(\delta)$ is observed at temperatures up to 80 °C. At 80 °C a rather flat ill defined peak is observed and indicating that the epoxy does not vitrify i.e. the cure temperature $T_{cure} = T_g$. This is confirmed by cure at 100 °C where no vitrification peak is observed. There is a large scientific interest in defining gelation times describing the formation of a macroscopic network as a result of the crosslinking reaction. As shown in Fig. 5.20 at lower cure temperatures (40 and 50 °C) gelation occurs some time after a clear increase in viscosity is observed. In the past authors described gelation using viscosity measurements as the point at which the viscosity increases exponentially due to the abrupt increase in molecular weight. Using this technique the gelation point was normally defined by

some critical viscosity value such as 10 kPas (Karkanas `98). Past experience has shown that material processors are not particularly interested in determining gelation times, instead their main concern is acquiring cure times at which a strong increase in viscosity or modulus is observed. For example, in the Resin Transfer Moulding RTM process fibre impregnation must be completed well before the gel point is reached while the consolidating pressure is first applied after the resin has gelled. For this reason and also to compare the sensitivity of the different analytical techniques, the cure time required t_{onset} until a low critical value of $G´ = 10$ Pa has been reached was chosen. $G´ = 10$ Pa is the first trustworthy value that can be obtained using the present 20 mm plate set-up and has been chosen for this reason. t_{onset} describes the first clear increase in shear modulus corresponding roughly to a viscosity of $\eta = 35$ Pas. The relationship between oscillatory and steady flow experiments performed in rotation is described by the Cox-Merz rule (Cox `58; Chapter 4.4). Critical values as well as gelation and vitrification times are documented in Table 5.1 at the end of this chapter.
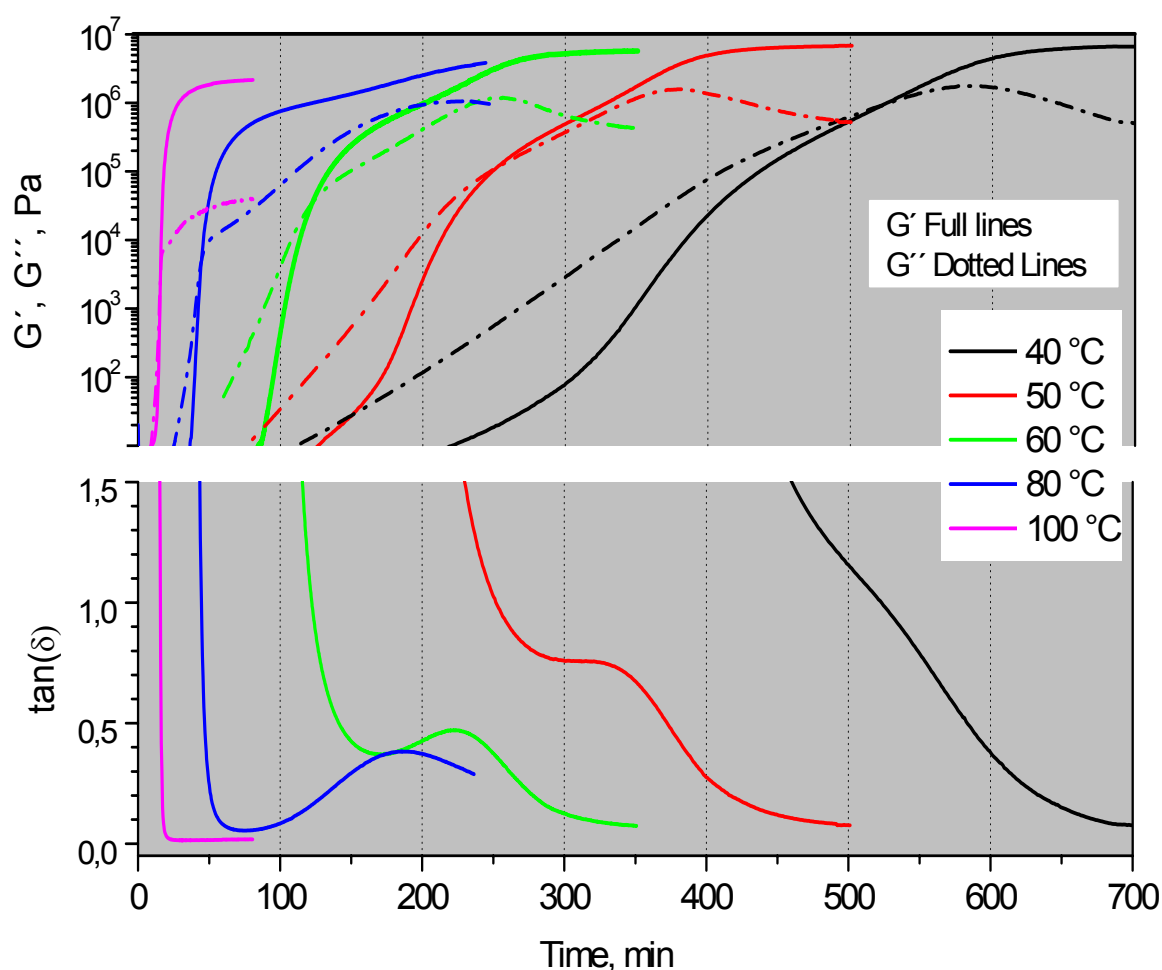
Fig. 5.20 *Modulus (top graph) and tan(δ) versus cure time for a range of constant cure temperatures*

5.3.4 Dynamic Scanning Calorimetry DSC

5.3.4.1 Degree of Cure and Cure Profile

DSC provides information on the extent of the curing reaction in terms of evolution of the fractional degree of cure (most often referred to as fractional conversion α). By heating the epoxy sample to 300 °C in a dynamic heating run at 10 K/min, it is possible to obtain the total exothermic heat of reaction released during the curing reaction from the area enclosed under a thermogram (see Eq. 4.27, p64). It can be confirmed that the reaction has proceeded to 100 % by a consecutive heating run or rescan. By determining the exothermic heat of reaction for either isothermal or dynamic cure runs and placing it in relationship to total cure it is possible to determine fractional conversion for a particular cure cycle (see Figure 5.22). More detailed example is provided in Fig. 4.14 and with help of Eqs. 4.23 to 4.24.
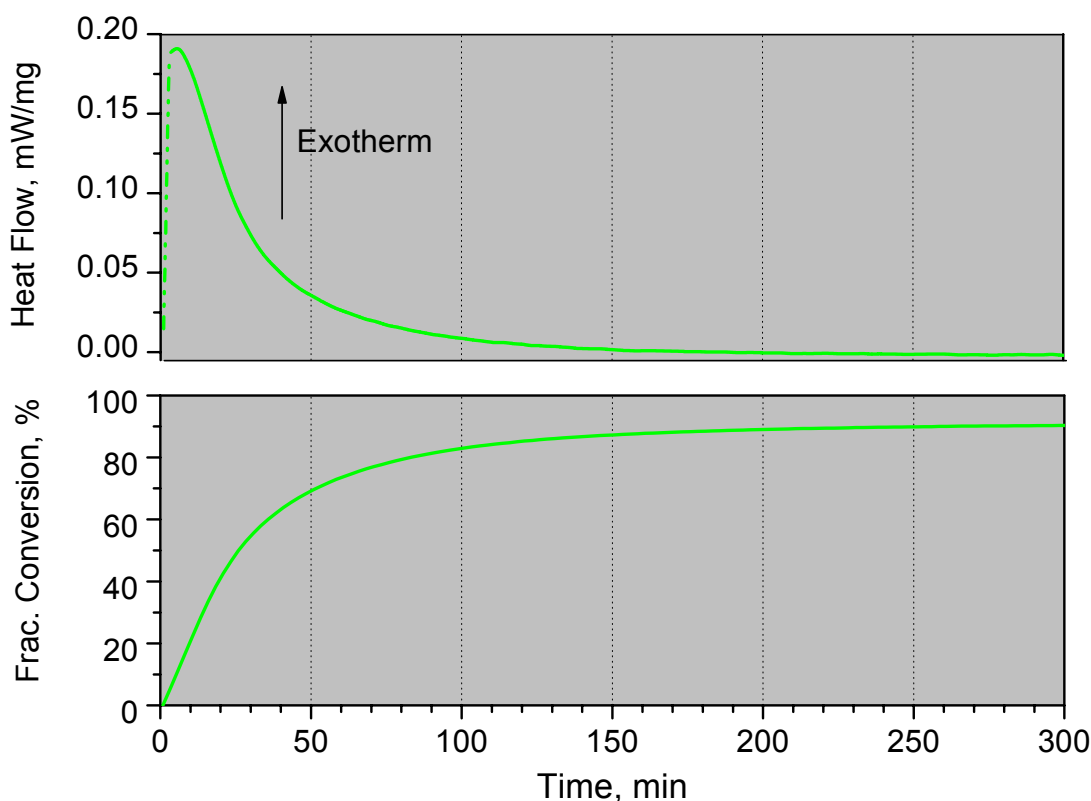
Fig. 5.22 *Exothermic heat flow for cure at 80 °C (top half). The area under the curve is determined by integration and presented as percentage of the total heat of reaction in terms of conversion*

5.3.4.2 Fractional Conversion as a function of Temperature

In Fig. 5.23 the fractional conversion is presented at cure temperatures between 60 and 100 °C. Interesting to note is that the highest degree of cure reached is approx. 95 %. This is because the initial phase of reaction cannot be measured precisely. On introducing the room temperature sample into the instrument it requires a certain undefined period of time before the sample reaches the set instrument temperature. Even though samples weight less than 10 mg it takes time until steady state conditions are reached and during this time it is not possible to determine heat of reaction. On the other hand, the reference heat of reaction for total cure using a dynamic heating run starting at low temperatures is not affected by this initial error. For this reason it is unlikely that 100 % cure will be reached using this definition. As shown by the isothermal conversion curves the reaction rate increases by about 40 % for every 10 K increase in cure temperature. This is a general observation and a quantitative value such as the activation energy describing the minimum energy for a reaction to occur is a very helpful reference.
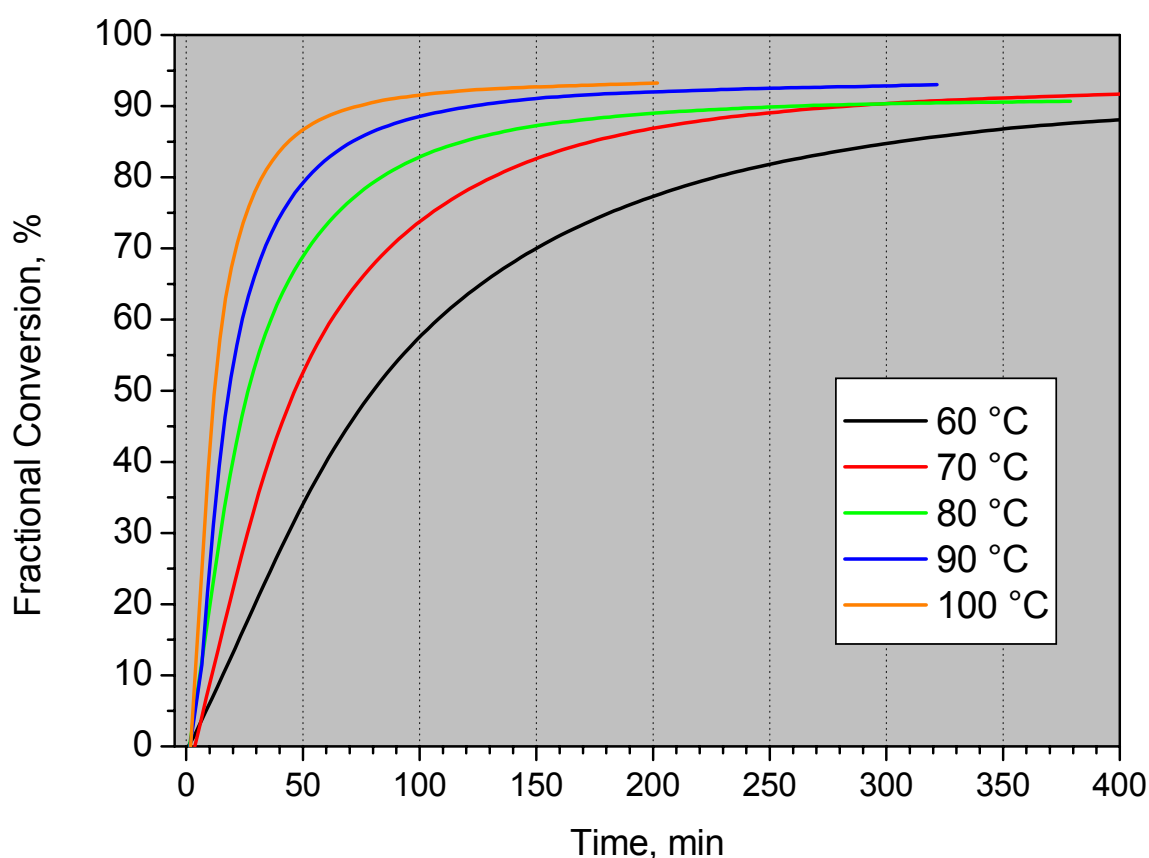
Fig. 5.23 *Degree of cure at different cure temperature between 60 and 100 °C*

Activation energy is typically determined using the Arrhenius relationship (Chapter 3.3.1 and Eq. 3.1). In order to describe the reaction rate as the product of two independent phenomena, one incorporating the temperature influence in the form of Arrhenius dependent reaction rate constant k obtained from Eq. 3.3, it is necessary that all the reactions involved be equally activated. The relationship therefore assumes that the polymerisation reaction is kinetically controlled with a single activation energy. The scientific validity of this statement for an epoxy amine reaction where both catalysed and non-catalysed reactions may occur simultaneously may be questioned, but as shown by several authors (Guibe `96; Pindinelli `02; Blumenstock `02) such rate laws can be satisfactorily used in the early stages of cure to obtain the activation energies for conversion values up to 65 or 70 %. As described in Chapter 3.3, the different reaction mechanisms can be divided into pure chemical or kinetic reactions and reactions controlled by the diffusion of the reactive species throughout the mixture. As the reaction advances, the autocatalysis reaction diminishes giving way to the non-catalytic epoxy amine addition reaction with a consequent increase in the activation energy of the reacting system and a transition to *diffusion control* occurs at vitrification. Vitrification induces a modification of reaction kinetics by prohibiting further reactions, although a very slow diffusion-controlled reaction may occur in the glassy state. As a result, the curing reaction kinetics goes from chemistry driven to diffusion controlled. One possibility of differentiating between the two mechanisms and defining the region in which the Arrhenius law may be employed uses Time Temperature Superposition TTS principles (described in Chapters 2.3.2 and 5.1.1). The technique used here is similar in principle to the description provided in Chapter 5.1. However, instead of shifting isothermal temperature curves along the frequency axis conversion α curves are shifted by a factor a_T along the logarithmic cure time axis to form a master curve with a selected reference temperature. For this epoxy a reference temperature of 100 °C was chosen and the master curve is illustrated in Fig. 5.24. The cure curves should superimpose to a master curve up to the vitrification point, since above this point the curing reaction is no longer kinetically controlled As shown in Fig. 5.24 an excellent superposition of the conversion curves is obtained up to about 65 % conversion. At higher conversion values the reaction becomes diffusion controlled and slows dramatically and the Arrhenius relationship is no longer valid. An Arrhenius plot can be formed by plotting the slope of the shift factor a_T versus reciprocal temperature. Under these conditions an activation energy of 47 kJ/mol was calculated from the slope as shown in the internal small diagram in Fig. 5.24.
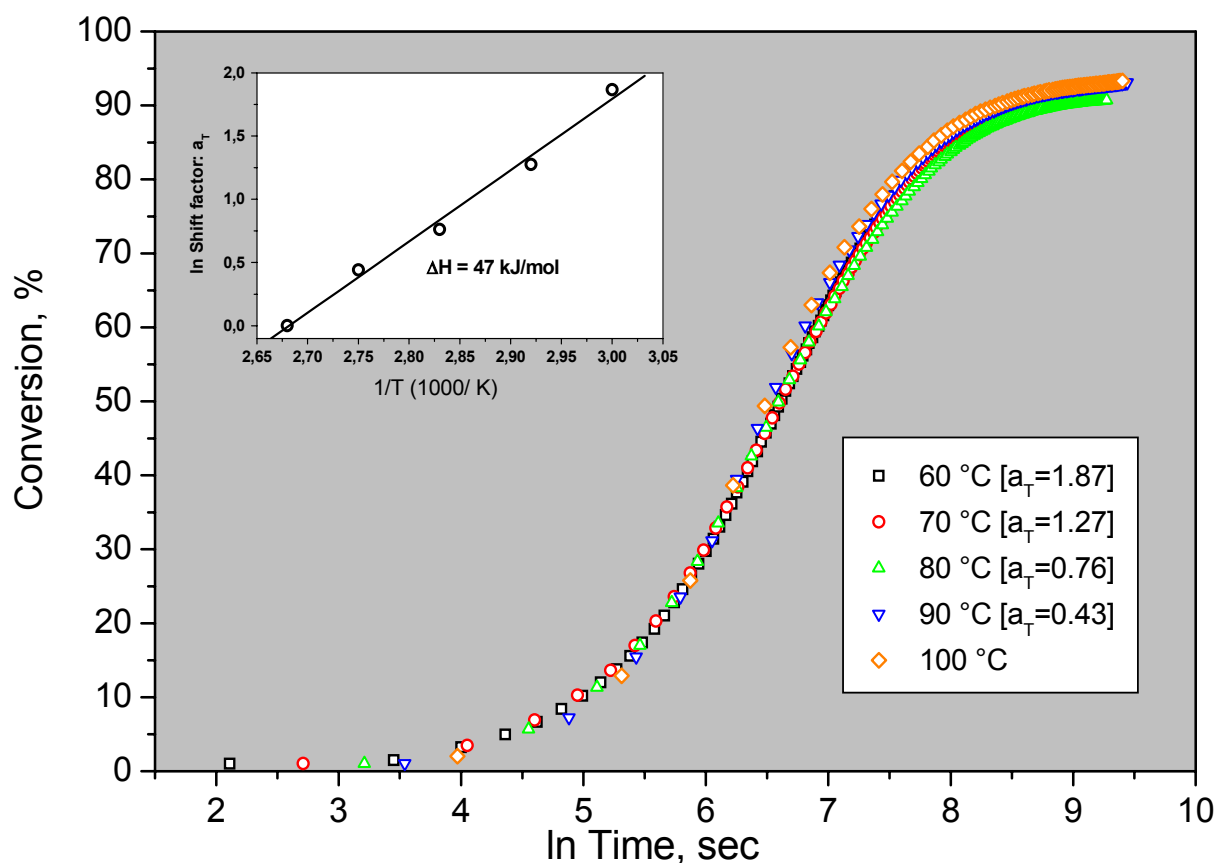
Fig. 5.24 *Superposition of conversion versus ln (time) data for isothermal cure data.*
Reference temperature is 100 °C. Top left: Arrhenius plot of the determined shift factor a_T

Karkanas (Karkanas `98) quotes activation energy for an epoxy amine resin of 55 kJ/mol in the kinetic or chemically controlled reaction region so that the stated value seems to be reasonable. Additional information may be obtained in regard to structure or network development during the curing reaction by determining the glass transition temperature T_g. T_g can be determined as a function of conversion by using dynamic heating runs to pre-specified temperatures, followed by rapid cooling and a subsequent rescan. T_g is then determined from the midpoint of the endothermic shifts observed during this rescan (Chapter 4.3.3). By employing this method the advancement of glass transition during cure can be illustrated by plotting T_g as a function of conversion as shown in Fig. 5.25. A one to one relationship between glass transition temperature T_g and conversion is observed up to approximately 60 to 70 % conversion. This observation corresponds with the region where conversion as a function of cure time can be superimposed to form a master curve. Deviations from the master curve illustrated in Fig. 5.24 as well as the non-linear dependence of T_g at conversions values greater than 70 % both occur as the reaction begins to slow and becomes diffusion controlled. In Fig. 5.25 the red circle at a conversion of 98 % and T_g of 69 °C indicates the degree of cure and T_g reached when the recommended curing conditions from the manufacturer are followed.

For a fully cured resin a maximum $T_{g\infty}$ of 76 °C is reached. This value is 10 °C lower than for T_g determined from the tan(δ) maximum in Fig. 5.1 by conventional DMA at 1 Hz. Two points need to be considered before evaluating this information. Firstly, the tan(δ) maximum will always be observed at higher temperatures than the maximum in tensile loss E'' also used to define a glass to rubber transition using DMA (see Fig. 2.2). Secondly the glass process is a relaxation or time dependent process and its determination must not only depend on measurement frequency but also on heating or cooling rates. Most authors agree that T_g determined as tan(δ) maximum (Mettler Applications; Rieger `01) will always be higher than for DSC experiments under normal conditions. According to the forenamed authors variations of 10 °C in the location of the observed glass transition between DSC and DMA are typical. However the authors warn that this value should not be taken as a general rule as large variations may occur depending on material investigated. Towards the end of cure at conversion values between 94 and 99 % (last three points in Fig. 5.25) an increase in T_g is observed. This is attributed to the relative insensitivity of DSC to low residual exotherms at low reaction rates (Wisanrakkit `90). On the other hand the crosslink density and modulus will increase significantly in this region leading to a distinct increase in glass transition temperature T_g.
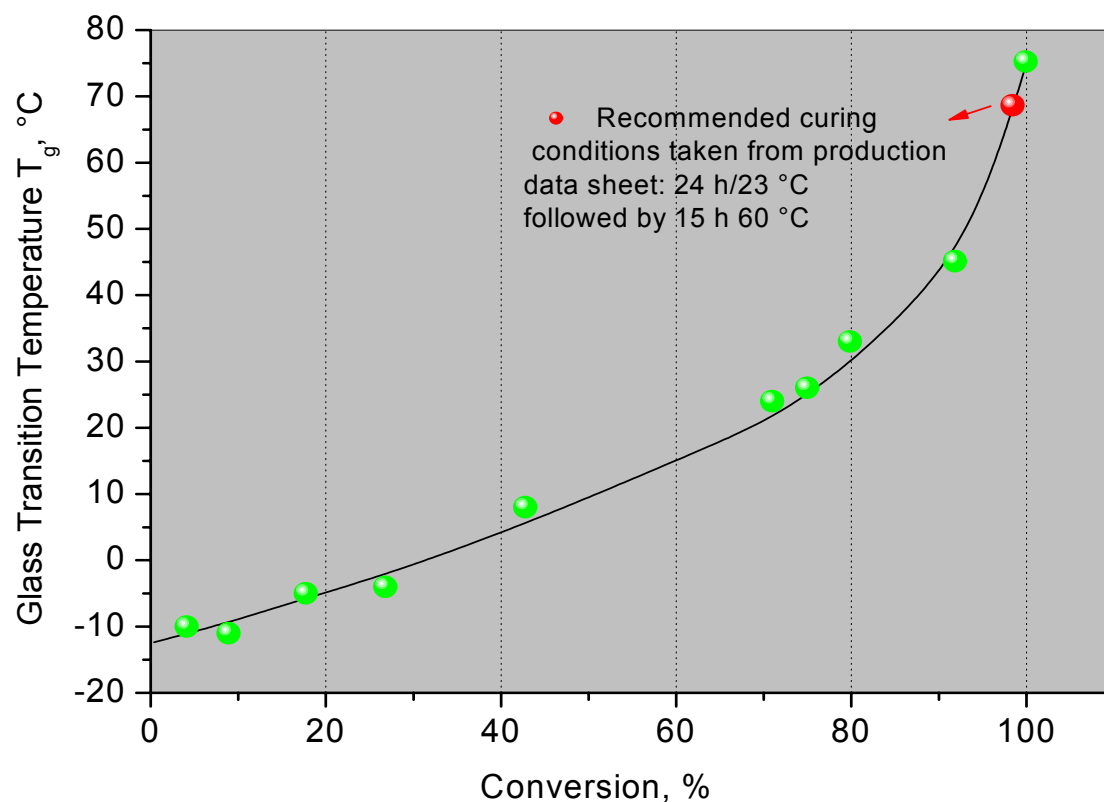
Fig. 5.25 *T_g versus conversion for prepared epoxy samples cured in an oven*

5.3.5 Summary: Sensitivity of Ultrasound to Cure Monitoring

In the following, the experimental results from the three techniques ultrasound, rheometry and DSC are summarised and compared. Although both rheometry and ultrasound are both based on dynamic mechanical measurement principles direct comparison is difficult mainly due to the large difference in measurement frequency employed. To aid in interpretation characteristic cure times have been chosen that define turnover points in the respective cure profiles. These characteristic cure times have been explained clearly and are taken from isothermal cure curves from both ultrasound (shown in Figs. 5.16 and 5.18) and rheometry (Figs. 5.20 and 5.21). Values are illustrated in Tables 5.1 and 5.2.

Ultrasound Data   **DSC Data**

Temperature		t_{onset}	t_{Offset}	* t_{Att}	* $t_{tan\delta}$	$\alpha = 30\%$
(°C)	$10^3/T$ (K)	(min)	(min)	(min)	(min)	(min)
40	3.19	145	910	251	262	
50	3.10	80	570	150	160	
60	3.00	55	300	100	106	43
70	2.92	29	200	56	60	24
80	2.83	19	160	42	44.5	14
90	2.75	12	75	32	34	10
100	2.68	6	52	27	32	7

* refers to peak maximum

Table 5.1 *Characteristic cure times taken from sound velocity and DSC (30 % conversion) profiles at isothermal cure temperatures*

Rheology Data

Temperature		t_{onset}	G'/G''_{Gel}	G''_{Peak}	$t_{tan\delta}$	t_{sat}
(°C)	$10^3/T$ (K)	(min)	(min)	(min)	(min)	(min)
30	3.30	446	885	930		997
40	3.19	218	524	582		650
50	3.10	130	255	372	336	430
60	3.00	88	122	252	222	300
70	2.92	52	76	236	206	240
80	2.83	38	46	220	184	210
100	2.68	10	16			51

Table 5.2 *Cure times taken from characteristic points from rheometry experiments (G´ and G´´) at isothermal cure temperatures*

As a brief reminder: depending on technique employed the notation t_{onset} refers to the strong increase during cure of sound velocity c, shear modulus G' or in the case of DSC when a conversion of 30 % is reached. The notation t_{Offset} refers to turnover cure time at which the strong increase in sound velocity slows and increases only gradually (Fig 5.15). For the analysis of rheometer data an offset or turnover point is not employed mainly because towards the end of cure a constant plateau or G' value is quickly reached and this is defined by a saturation term t_{sat}. The G' values measured in the t_{sat} range are typically between 1 and 10 MPa and are very close to the upper measurement tolerances of the Haake rheometer using this particular 20 mm plate setup. The terms $t_{tan\delta}$ and t_{Att} refer to cure times until the respective $\tan(\delta)$ or attenuation peak maxima are reached. To facilitate graphical comparison of the techniques employed the defined characteristic points determined during cure are illustrated in terms of conversion as shown in Fig. 5.26.
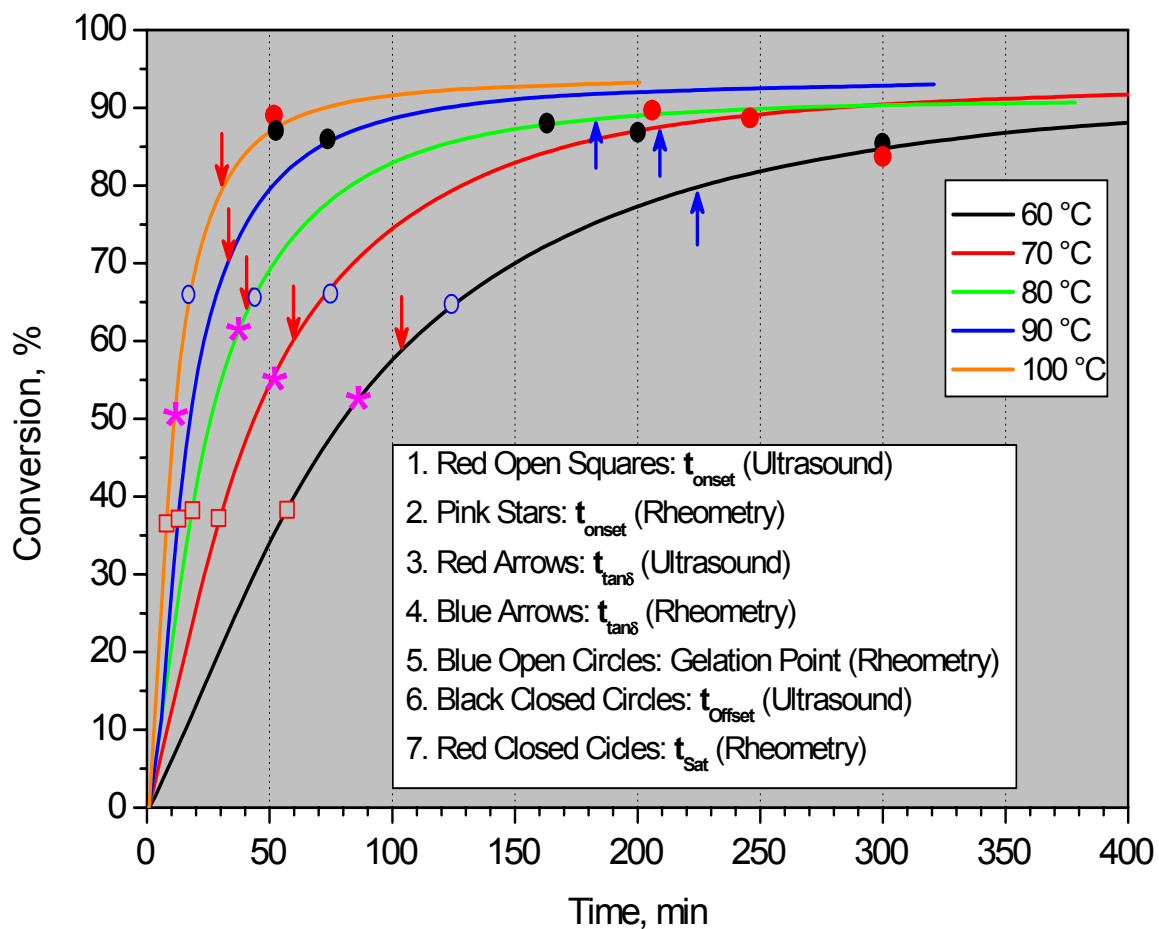
**Fig. 5.26** *Conversion versus cure time at various constant cure temperatures, data is taken from Fig. 5.23. Characteristic points in the cure profiles from ultrasound and rheometric measurements are marked with arrows and symbols.*

From this illustration following observations were made:

- *Cure Begin*: A large increase in sound velocity t_{onset} (red squares) is observed before any results could be evaluated from rheometric experiments. t_{onset} for rheometric experiments was chosen as G´ = 10 Pa representing the lower critical measurement limit for the 20 mm plates setup employed for this experiment. Accurate values for G´ below 10 Pa were not obtained as shown in Fig. 5.20. For ultrasound experiments t_{onset} represents the large increase in sound velocity defined in Fig. 5.15 and occurs for all cure temperatures at conversion values below 40 %. Even before t_{onset} is reached a gradual increase in sound velocity is observed. This is corroborated by Fig. 5.17 showing that even small changes in viscosity at the start of cure may be distinguished by differences in sound velocity magnitude.

- *Gelation point:* This point is defined by the crossover of G´ and G´´ in rheometry. Shortly after the increase in sound velocity, the shear modulus t_{onset} (rheometric measurements) increases dramatically and gelation occurs at approx. 62 to 65 % conversion. These values indicate the accuracy of the results, as according to publications discussed in Chapters 3.2 gelation should occur at constant conversion and T_g independent of cure temperature. Also, conversion values of about 60 % are typical for stoichiometric mixtures of epoxy systems (Mc Hugh `01; Nunez `05).

- *End of Cure*: The end of cure is defined as the region in which the reaction becomes diffusion controlled and was determined experimentally as shown in Fig.5.24. This occurs at 65 to 70 % conversion correlating well with gelation point. The saturation or plateau region of the conversion curves marks the cessation of the reaction. As shown both G´ and sound velocity can be measured close to the end of reaction at all cure temperatures. However for rheometric experiments it is no longer possible to obtain trustworthy results almost immediately after vitrification i.e. after tan(δ) maximum is reached as shown in Fig. 5.19. This is the upper measurement limit of this rheometer set-up. At similar cure times sound velocity also reaches t_{Offset} (black closed circles). After this turnover time is reached sound velocity only increases gradually as shown in Fig. 5.16. It was demonstrated using Fig. 5.25 that even a small increase in conversion of about 5 % towards the end of cure can cause a significant increase in T_g. Small changes in conversion occurring at the end of cure are hardly negligible using DSC but will lead to an increase in crosslink density and modulus. The results indicate that sound velocity is a highly sensitive parameter capable of detecting changes in modulus occurring after vitrification. .

Arrhenius plots of the data in Fig. 5.26: The empirical comparison in Fig. 5.26 provides a solid background for discussing the sensitivity of ultrasound. However, the same information may be presented in an Arrhenius plot providing a qualitative means for comparing analysis techniques based on different physical principles. The results are shown in Figs. 5.27 and 5.28. To compare the sensitivity of the techniques to the kinetically controlled reaction at cure begin, initial cure times t_i were chosen in the cure range between 40 and 100 °C, using the following criteria:

- *DSC*: isothermal cure times at 30 % conversion from Table 5.2 i.e. kinetic reaction

- *Ultrasound*: cure time to required to reach t_{onset} was chosen because as shown in Fig. 5.15 it is a clearly distinguishable point observed at all cure temperatures and marks the significant increase in sound velocity occurring at about 40 % conversion.

- *Rheometry*: cure time was taken as the time to the first clear increase in G´ at 10 Pa also referred to as t_{onset}. Gelation occurs at 63 % conversion with modulus values $\geq$ 10 kPa. All values chosen including those taken from ultrasound and DSC experiments clearly lower than gelation times and therefore in the kinetically controlled region.
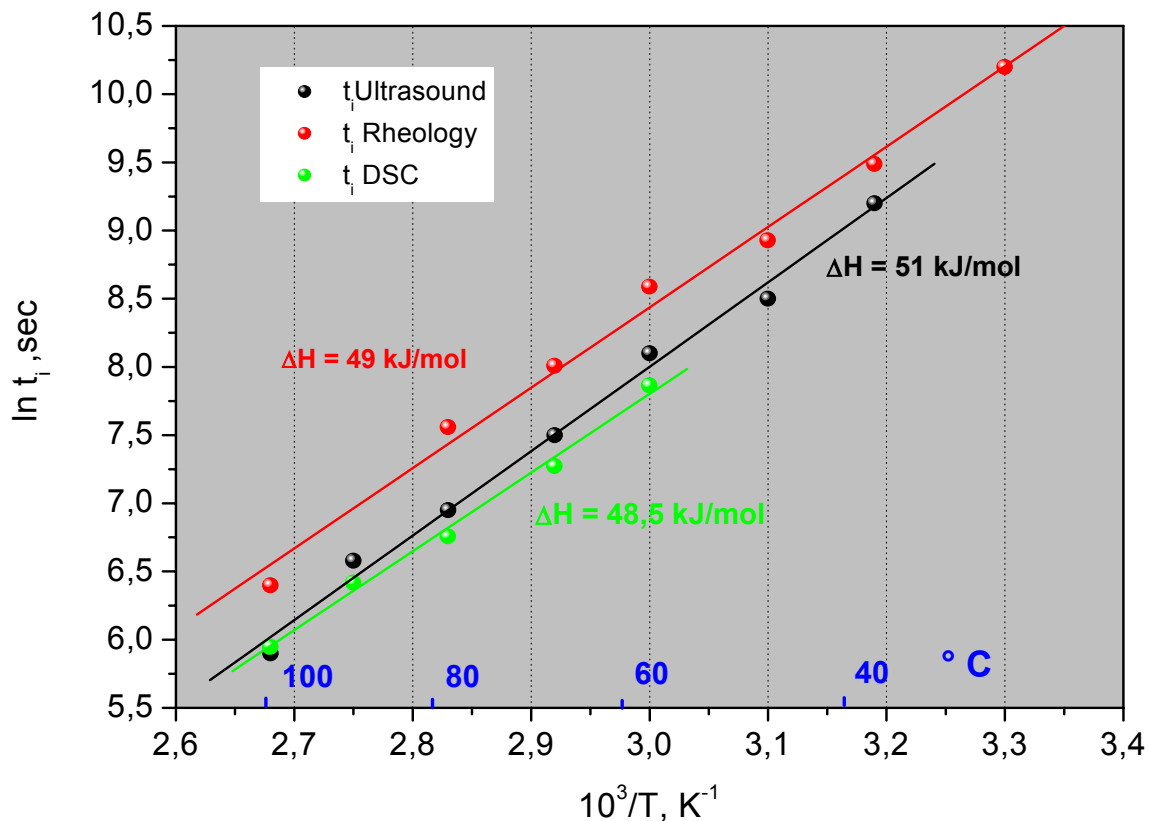
Figure 5.27 *Arrhenius plot taking characteristic cure times at t_{onset} from the different analytical techniques (Tables 5.1 and 5.2).*

The values obtained for t_{onset} using the various analytical techniques are shown in Fig. 5.27 and Tables 5.1 and 5.2 and are all close together close in terms of curing time. However, this fact mainly depends on the rather subjective selection criteria for t_{onset} as explained above and therefore has no greater physical meaning. As shown the data from all techniques can be fitted linearly, showing that they all obey Arrhenius behaviour. Calculated activation energies (between 48.5 and 51 kJ/mol) for the initial polymerisation reaction are very similar for all techniques revealing that all methods are sensitive to the same reaction. These values are also very close to the activation energies for the initial chemically controlled reaction for epoxy-amine cure typically about 54 kJ/mol (Eloundou `96a; Karkanas `98).

The Arrhenius law may be employed to describe any thermally activated process as long as conditions of linearity are upheld. Therefore the vitrification times defined by tan(δ) peak for both ultrasound and rheology were also compared using an Arrhenius plot for epoxy cured in the temperature range 40 to 100 °C and the results illustrated in Fig. 5.28. As additional information the cure times for loss peak in attenuation from ultrasound and shear loss modulus G´´ from rheometry were also plotted in the same diagram
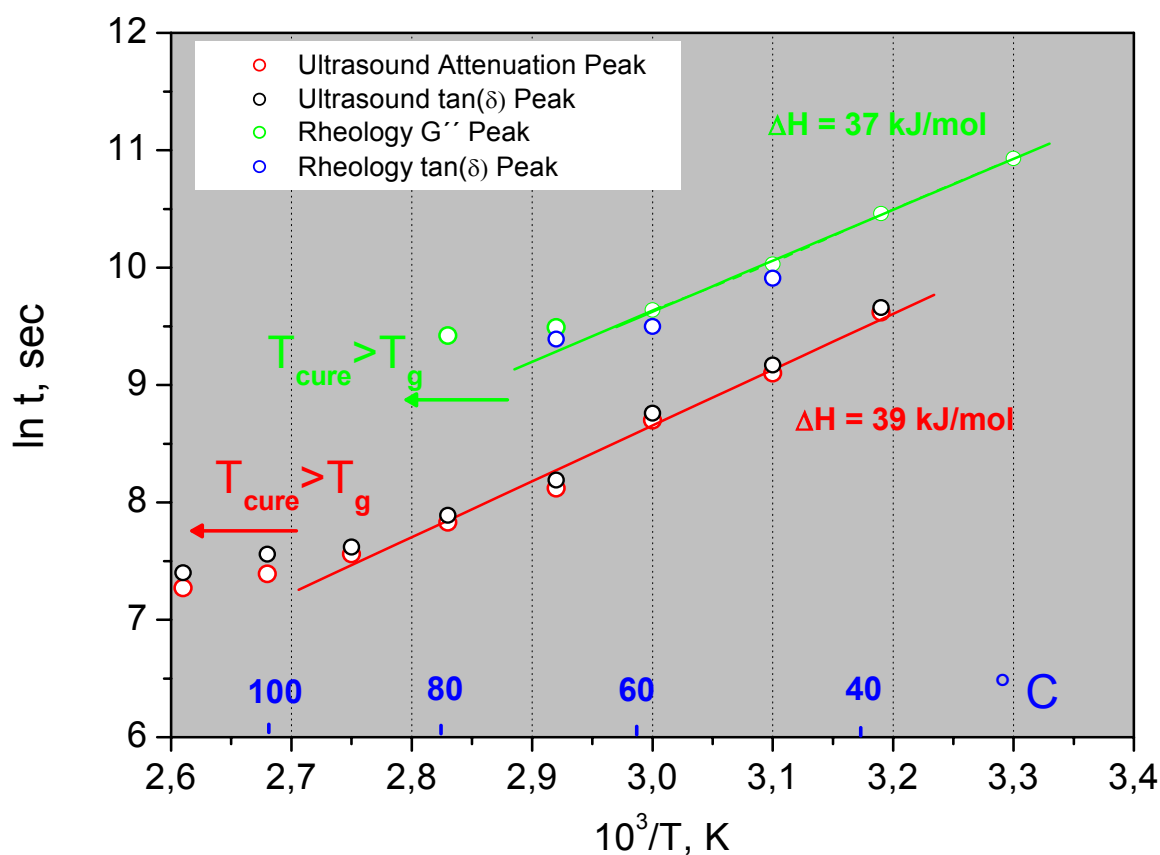
Fig. 5.28 *Arrhenius plot taking characteristic cure times until a loss peak is observed for cure temperatures between 40 and 100°C. Cure times are taken from Table 5.1 and 5.2.*

The activation energies calculated of 39 and 37 kJ/mol are very similar for both DMA techniques presented and correlate well with values obtained by Guibe (Guibe `96) using DSC experiments whereby the author describes vitrification time as cure time required until $T_{cure}=T_g$ (see Chapter 3.2). However, the determined values should not be confused with activation energy for the diffusion controlled reaction and the estimated energies simply provide a good means to compare two different analysis techniques. The actual physical meaning of the absolute values and their application is unclear at present. The time scale of the experiment illustrates that the loss peak associated with vitrification will be observed first with the ultrasound technique. As shown in Chapter 5.1 determination of the temperature at which the glass transition is observed will depend strongly on the measurement frequency of the technique employed. Using ultrasound as DMA at 4 MHz and conventional DMA experiments at 1 Hz the respective $T_{g\infty}$ values determined were 115 °C and 86 °C as shown in Fig. 5.8. Therefore deviations from linearity occur at temperatures at which a glass rubber transition is no longer distinguished using the respective analysis technique i.e. at $T_{cure} \geq T_{g\infty}$ when the selected cure temperature approaches the maximum achievable $T_{g\infty}$ of the epoxy system.

Comments: Sensitivity of the Acoustic Parameters to Gelation

One recurring question with regard to ultrasound investigations on a curing resin has not been clearly answered. ***Is the measured sound velocity or attenuation sensitive to gelation taking place during epoxy cure?*** The simple answer is ***no!*** The reason that gelation point is conventionally taken as the crossover point G´and G´´ or tan(δ) = 1 and should be independent of measurement frequency at 1 Hz (Winter `87) although the same author admits that there are some exceptions to this rule (Winter `97). Ultrasound measurements have been performed to a high accuracy and throughout cure tan(δ) has remained smaller than 0.13 so that according to classical convention ultrasound parameters will not be influenced by gelation. Explanation for the insensitivity of ultrasound to gelation as defined by the percolation theory (not to be confused with increase in viscosity) may result from the nature of longitudinal waves. It is known that for longitudinal wave measurement that the following equation describes the relationship between longitudinal storage L´, bulk storage K´ and shear storage G´ module:

$$L'=K'+4/3G' \qquad\qquad \textit{see Eq.} \; 2.18$$

Shear waves do not propagate in liquids and are first observed after gelation (Parthun `95). Therefore before gelation $L'=K'$ meaning that only a compression wave can propagate in the polymer. Losses in polymers due to internal friction or damping will be significantly lower for dynamic compression than for tensile or shear loading experiments (Murayama `78). This is corroborated by the low intensity values for $\tan(\delta)$ values obtained for ultrasound measurements in comparison to values obtained by conventional DMA (see Figs. 5.1 and 5.20). For this reason the differences in storage modulus will not be as striking for a measured longitudinal modulus as for shear modulus that will change by several orders of magnitude during cure. Taking these points into consideration a definition of gelation as the crossover between L' and L'' or $\tan(\delta) =1$ is unlikely to be fulfilled for dynamic compression experiments.

Another possible explanation for this apparent insensitivity to gelation may be demonstrated using Fig. 5.26. In this figure the glass transition is observed for all cure temperatures either before or in close vicinity to gelation. Determination of gelation should be independent of frequency as explained above whereas the rubber-glass transition temperature taken as the $\tan(\delta)$ maximum is not and is observed much earlier at high acoustic measurement frequencies than for rheometer experiments (see Fig. 5.26) For this reason, in the temperature range employed even if this acoustic techniques were sensitive to gelation, it would most likely be overshadowed by vitrification.

Chapter Six

6 Conclusions

It is well know that acoustic wave propagation can be employed to determine the dynamic modulus of polymers. However, several questions remain open in regard to the sensitivity of the determined longitudinal modulus L′ particularly in comparison to more conventional modulus values e.g. shear G′ or tensile E′ storage modulus measured using conventional DMA performed at low frequencies. The academic potential of this acoustic technique is presently only limited by complications in an exact interpretation of results. If wave propagation techniques are employed for DMA of material properties several additional factors may influence quantitative determination of L′, L′′ or tan(δ). Amongst others, they include the high frequency of measurement, acoustic coupling of sensors, amplitude losses at boundaries and temperature stability of sensors. These points were taken into consideration as follows:

- A two sample measuring setup was constructed so that boundary effects (reflections) leading to a large decrease in amplitude could be neglected
- Fast Fourier Transformation analysis software was developed so that frequency specific sound velocity and attenuation could be determined
- In order to obtain data over a wider range of frequency high temperature sensors in the 2 to 6 MHz and 250 to 650 kHz range were employed.
- To study the influence of the glass rubber transition on measurement results, a commercial epoxy was chosen with a glass rubber transition T_g of 86 °C i.e. well within the limits of the ultrasound and DMA techniques measuring range.

Integration of these factors into experimental setup and evaluation strategy means that enough accurate acoustic data are available over a large frequency and temperature range to make credible conclusions on the application of ultrasound as a DMA technique.

The experimental results are divided into two main sections: firstly investigations on a fully cured epoxy and secondly on a curing epoxy resin. In the first section all investigations took place on a fully cured epoxy with a glass rubber transition at approximately 86 °C (defined by tan(δ) maximum at 1 Hz). The results from ultrasound longitudinal and in just one example for shear wave propagation were compared to conventional DMA. The main topics covered are briefly introduced and demonstrate the application of ultrasound as a high frequency DMA technique:

- *Acoustic Parameters*: L′, L′′ and tan(δ) were evaluated as a function of frequency from the ultrasound parameters sound velocity and attenuation. The term $\alpha c/\omega \ll 1$ was calculated and has a maximum value of 0.08 even in the α relaxation region that is associated with high damping. Therefore reduced equations will almost always be valid for unfilled polymers and can be employed to calculate L′, L′′ and tan(δ). Material damping properties are best described using tan(δ). This loss factor has the added advantage that it can easily calculated from acoustic parameters and is common to all DMA techniques. The elastic modulus is typically expressed using L′ but as the density of the sample only exhibits minor changes then sound velocity $c \propto \sqrt{L'}$ may also be used to express changes in viscoelastic properties.

- *Influence of Frequency*: By analysing the results from conventional DMA in the frequency range 0.1 to 50 Hz and using the Williams Landel Ferry WLF equation it was possible to predict the influence of high measurement frequencies on the determination of α relaxation. The model correlated well with experimental results evaluated at specific frequencies in the ranges 400 to 800 kHz and 2 to 5 MHz. It was clearly shown that the α relaxation observed at 86 °C at 1 Hz will be observed at 118 °C at 4 MHz or an approx. shift of 5 K per decade increase in measurement frequency.

- *Interrelation of Modulus:* By measuring both shear and longitudinal wave propagation for the epoxy system as a function of temperature in the range 20 to 200 °C their respective storage moduli G′ and L′ could be determined. From these parameters the bulk K′ and tensile E′ storage moduli as well as the real part of Poisson's ratio μ' can be calculated. This provides the background necessary to understand the interrelation of the different dynamic moduli as well as Poisson's ratio. More importantly it demonstrated the sensitivity of the longitudinal modulus to changes in the viscoelastic properties.

The second section of this thesis is concerned with determining the sensitivity of sound velocity and attenuation to changes in the viscoelastic properties of a curing resin i.e. application of ultrasound as a cure monitoring technique. Sound velocity and attenuation or tan(δ) are compared to the results from other laboratory analysis techniques, all measured over a range of constant cure temperatures between 40 and 100 °C. Differential Scanning Calorimeter DSC is employed to obtain information relating to the extent of the curing reaction and network formation. A rheometer is also employed as DMA technique to monitor variations in G′ and tan(δ) during the curing reaction. To discuss the sensitivity of the ultrasound technique the cure process is divided under the following four headings:

Start of Cure: Sound velocity increases gradually at the start of cure with a large increase occurring at approx. 40% conversion and referred to as t_{onset}. Using a rheometer measured values for the storage G′ modulus could first be determined after approx. 50 % conversion. As discussed, for conversion values below 60 % the reaction remains kinetically controlled which means that the activation energy for the reaction can be calculated using the Arrhenius equation. The respective activation energies calculated for Ultrasound, Rheometer and DSC techniques were 51, 49 and 48.5 KJ/mol providing a clear indication that all methods are sensitive to the same initial polymerisation reaction.

Gelation Point: No evidence indicates that sound velocity is sensitive to gelation according to conventional definitions such as tan(δ)=1. Possible reasons are that measured tan(δ) values obtained using compressional or longitudinal loading forces had a maximum value of 0.14 or well under the above gelation criteria. Another explanation for the apparent insensitivity of ultrasound to gelation was demonstrated using Fig. 5.26. In this figure the glass transition is observed for all cure temperatures either before or in close vicinity to gelation. Determination of gelation should be independent of frequency as explained above whereas the rubber-glass transition temperature taken as the tan(δ) maximum is not and is observed much earlier in the MHz frequency range than at low frequencies used for rheometer experiments. For this reason, even if acoustic techniques are sensitive to gelation for this epoxy it is most likely that gelation would be overshadowed by vitrification. Although, the results show that a specific gelation point could not be identified, the continued increase in sound velocity in this region indicates a high sensitivity to changes in viscosity or modulus as the curing reaction proceeds.

Vitrification: it was demonstrated that the ultrasound tan(δ) peak observed at different cure temperatures is caused by vitrification. Maximum values of tan(δ)=0.14 are obtained at vitrification and provide excellent correlation with values obtained for the glass rubber

transition for ultrasound investigations on the fully cured epoxy discussed in Chapter 5.1. At vitrification the reaction becomes diffusion controlled and a gradual change of material state from gel/rubber to a glassy state occurs. This rubber-glass transition is a dynamic transition and during cure will be observed at shorter cure times the higher the measurement frequency employed. For this reason the tan(δ) peak will be observed at shorter cure times for ultrasound than for rheometric experiments.

End of Cure: Vitrification induces a modification of the reaction kinetics by prohibiting further reactions, although a very slow diffusion controlled reaction may occur in the glassy state. DSC is relatively insensitive to this latter reaction as conversion reaches saturation shortly after vitrification. It is only with subsequent rescans that an increase in T_g can be detected proving the epoxy has reacted further. The results confirm that even small changes in conversion that are difficult to measure using DSC lead to an increase in crosslink density and modulus. At present the only DMA technique capable of providing quantitative storage modulus values over the whole curing reaction is the ultrasound wave propagation technique presented in this work. For isothermal cure, even the newer rheological instruments require at least one change of plates (large plates for liquid to rubberlike state and small plates for the rubber to glass-like state) or at least two separate experiments pro cure temperature before a change in modulus can be accurately measured throughout cure.

Application for Cure Monitoring: The main advantage of ultrasound over most laboratory based analysis techniques is that it is based on wave propagation principles so that only relatively small sensors are required to provide information on the viscoelastic state of polymers. The sensors employed here are temperature resistance to 190 °C and can easily be incorporated into most production processes. By using a dry coupling technique with copper foil as couple medium modern sensors can even be mounted behind the mould wall so that marking of the moulding does not take place. These factors combined with the high sensitivity of this technique for DMA of polymer materials demonstrates its potential for a range of applications.

Suggestions for Further Work

The ultrasound cure monitoring technique "US Plus" is currently in use for several commercial applications in the field of injection moulding of thermosetting powder compounds e.g. Phenol or Urea Formaldehyde. Other applications include flow front and cure monitoring of epoxy based compounds reinforced with carbon or glass fibre e.g Resin Transfer Moulding RTM. The work presented here is intended to aid interpretation of results and to fill existing gaps in knowledge regarding the accuracy of this technique in-particular to understand relationships between storage and loss modulus and tan(δ) and the measured ultrasound parameters. The experiments were performed on neat or virgin resin materials to avoid further complicating interpretation and to minimise sources of potential error. Futher work will continue particularly in directions relating to possible future commercial applications.

- Continued development of ultrasound system and evaluation techniques for new applications such as the characterisation of Carbon Fibre Reinforced Plastics CFRP. This will mean taking the information published here a step further and applying it to fibre reinforced composites whereby additional problems such as scattering on fibre interfaces, voids, or filler combinations may have to be considered.

- Future applications especially in the materials science field will most likely involve the combination of sound velocity analysis with kinetic models for the prediction of cure behaviour. Such predictive models are commonly used in combination with DSC but as mentioned in the literature review are not common for DMA techniques.

- The ultrasound technique has shown great potential for cure monitoring especially when employed in combination with other analysis techniques such as rheometry. One possibility would be to develop an ultrasound technique for laboratory application for example employing a larger frequency bandwidth than used here and with an additional oven enabling dynamic heating and cooling runs.

References

Adabbo, E., Williams, R. J .J., "The Evolution of Thermosetting Polymers in a Conversion-Temperature Phase Diagram", *Journal of Applied Polymer Science*, **27,** 1327, (1982)

Aklonis, J. J., MacKnight, W. J., Shen, M., "Introduction to Polymer Viscoelasticity", *Wiley-Interscience New York, London,* (1972)

Alig, I., Fedtke, M., Häusler, K. G., Tänzer, W., Wartewig, S., "Modified Epoxies as Studied by Ultrasonic Methods", *Progr. Colloid Poly. Sci.*, **78**, 54, (1988)

Alig, I., Häusler, K., Nancke, K., Tänzer, W., Wartewig, S., "Ultraschalluntersuchungen zur Bildung von diolmodifizierten Epoxidharznetzwerken", *Acta Polymerica*, **40**, 508, (1989)

Alig, I., "Ultrasonic Relaxation and Complex Heat Capacity", *Thermochimica Acta*, **35**, 304, (1997)

Alig, I., Lellinger, D., Tadjbakhsch, S., "Sonic Methods for Characterising Polymeric Materials''", *Polymeric Materials Science and Engineering*, **79**, 31, (1998)

Alig, I., Nancke, K., Johari, G. P., "Relaxation in Thermosets XXVI. Ultrasonic Studies of the Temperature Dependence of Curing Kinetics of Diglycidyl Ether of Bisphenol A with Catalyst", *Journal of Polymer Science: Part B*, **32**, 1465, (1994)

Alig, I., Tadjbakash, S., Zosel, A., "Comparison of Ultrasonic Shear Wave and Dynamic-Mechanical Measurement in Acrylic-Type Copolymers", *Journal of Polymer Science: Part B.*, **36**, 1793, (1998)

American Society for Testing and Materials ASTM E698: "Standard Test Method for Arrhenius Kinetic Constants for Thermally Unstable Materials", (1984)

Asay, J. R., Lamerson, D.L., Guenther, A.H., "Pressure and Temperature Dependence of Acoustic Velocities in Polymethylmethacrylate", *Journal of Applied Physics*, **40**, 1768, (1968)

Babayevsky, P. G., Gillham, J. K., "Epoxy Thermosetting Systems: Dynamic Mechanical Analysis of the Reactions of Aromatic Diamines with the Diglycidyl Ether of Bisphenol A", *Journal of Applied Polymer Science*, **17**, 2067, (1973)

Blumenstock, T., "Analyse der Eigenspannungen während der Aushärtung von Epoxidharz-massen", PhD Thesis, *University of Stuttgart*, (2002)

Borchardt, H.-J., Daniels, F. ,"The Application of Differential Thermal Analysis to the Study of Reaction Kinetics", *Journal American Chemical Society*, **79**, 41, (1957)

Brockman, N.L., Eisenberg, A., "The Bulk viscoelastic Properties of Poly(styrene –co-sodium styrene-p-carboxylate)", *Journal of Polymer Science: Polymer Physics Edition*, **23**, 1145, (1985)

Brown, E. C., Olley, P., Coates, P. D., "In Line Temperature Measurement during Real Time Ultrasound Monitoring of Single Screw Extrusion", *Plastics, Rubber and Composites,* **29**, 3, (2000)

Brydson, J. A., Plastics Materials, 6th Edition, *Butterworth-Heinemann*, Oxford, 1995

Challis, R. E., "Viscoelasticity of thin Adhesive Layers as a function of Cure and Service Temperature Measured by a Novel Technique", *Journal of Applied Polymer Science*, **44**, 65, (1992)

Challis, R. E., Cocker, R. P., Chadwick, D. L., Dare, D. J., Martin, C., Mahendrasingam, A., Fuller, W., "Ultrasonic Measurements related to Evolution of Structure in Curing Epoxy Resins", *Plastics, Rubber and Composites*, **29**, 110, (2000)

Challis, R. E., Unwin, M. E., Chadwick, D. L., Freemantle, R. J., Partridge, I. K., Dare, D. J., Karkanas, P. I., "Following Network Formation in an Epoxy/Amine by Ultrasound, Dielectric and Nuclear Magnetic Resonance Measurements: A Comparative Study, *Journal of Applied Polymer Science*, **88**, 1665, (2003)

Choy, I. C, Plazek, D. J, "The Physical Properties of Bisphenol—Based Epoxy Resins during and after Curing", *Journal of Polymer Science: Part B: Polymer Physics*, **24**, 1303, (1986)

Chow, A.W., Bellin, J. L., "Simultaneous Acoustic Wave Propagation and Dynamic Mechanical Analysis of Curing of Thermoset Resins", *Polymer Engineering and Science*, **32**, 182, (1992)

Cowie, J. M. G., "Polymers Chemistry & Physics of Modern Materials", 2nd Edt., *Blackie Glasgow and London,* (1991)

Cox, W.P., Merz, E.H., **"**Correlation of Dynamic and Steady Flow Viscosities", *Journal of Polymer Science*, **28**, 619, (1958)

Cunningham, J. R., Ivey, D.G., "Dynamic Properties of Various Rubbers at High Frequencies", *Journal of Applied Physics,* **27**, 967, (1956)

DiBenedetto, A. T., "Prediction of the Glass Transition Temperature of Polymer: A Model based on the Principle of Corresponding States", *Journal of Polymer Science, Part B: Polymer Physics*, **25**, 1949, (1987).

DIN 53 479 (German Standard): "Bestimmung der Dichte", Verfahren A, (1976)

DIN 53 529 (German Standard): "Vulkametrie: Bestimmung des Vulkanisationsverlaufes und reaktionskinetische Auswertung von Vernetzungsisothermen", Teil 2, (1983)

Döring, J., Stark, W., "Untersuchung zur Aushärtung von Duroplasten", *Zerstörungsfreie Materialprüfung, Jahrestagung, Lindau*, (1996)

Döring, J., Stark, W., Bartusch, J., Mc Hugh, J., "Contribution to Ultrasound Cure Control for Composite Manufacturing", *15th World Congress of Non-Destructive Testing, Rome*, (2000)

Döring, J., Stark, W., "Produktionskontrolle mit Ultraschall", *Kunststoffe*, **91**, 83, (2001)

Döring, J., Mc Hugh, J., Schmachtenberg, E., Töpker, J., "RTM Process Optimization Using Incorporated Ultrasonic Sensors", *5. International AVK-TV Conference, Baden-Baden, Germany*, (2002)

Döring, J., McHugh, J., Bartusch, J., Stark, W., "Process Monitoring using Incorporated Ultrasound Sensors" *6th International Conference for Reinforced Plastics, Baden–Baden, Germany,* (2003)

Eckstein, A., Suhm, J., Friedrich, C., Maier, R.D., Sassmannshausen, J., Bochmann, M., Müllhaupt, R., "Determination of Plateau Moduli and Entanglement Molecular Weights of Isotactic, Syndiotactic and Atactic Polypropylenes Synthesised with Metallocene Catalysts", *Macromolecules*, **31**, 1335, (1998)

Eisele, U., "Introduction to Polymer Physics", *Springer-Verlag, Berlin, Heidelberg*, (1990)

Ellis, B., "Chemistry and Technology of Epoxy Resins", *Blackie Academic and Professional, Glasgow*, (1993)

Enns, J. B., Gillham, J. K., "Time-Temperature-Transformation (TTT) Cure Diagram: Modelling the Cure Behaviour of Thermosets", *Journal of Applied Polymer Science,* **28**, 2567 (1983)

Eloundou, J.P., Gerard, J.F, Harran, D., Pascault, J. P., "Temperature Dependence of the Behavior of a Reactive Epoxy-Amine system near the Gel point through Viscoelastic Study 1: Low Tg Epoxy Amine System", *Macromolecules*, **29**, 6207, (1996a)

Eloundou, J.P., Gerard, J.F, Harran, D., Pascault, J. P., "Temperature Dependence of the Behavior of a Reactive Epoxy-Amine system by means of Dynamic Rheology 2: High Tg Epoxy Amine System", *Macromolecules*, **29**, 6917, (1996b)

Flory, J., "Principles of Polymer Chemistry", *Chap IX, Cornell University Press, Ithaca, New York*, (1953)

Flammersheim H. J., Opferman, J., "Kinetic evaluation of DSC curves for reacting systems with variable stoichiometric compositions", *Themochemica Acta,* **388***,* 389, (2002)

Fitzgerald, E. R., Ferry, J. D., "Method for determining the Dynamic Mechanical Behaviour of Gels and Solids at Audio Frequencies: Comparison of Mechanical and Electric Poperties", *Journal of Colloid Science*, **8**, 1, (1953)

Ferry, J. D., "Viscoelastic Properties of Polymers", 3rd edt, *John Wiley and Sons Inc.*, (1980)

Ferry, J. D., Fitzgerald E**, "**Mechanical and electrical relaxation distribution functions of two compositions of polyvinyl chloride and dimethylthianthrene", *Journal of Colloid Science*, **8**, 244, (1953)

Freemantle, R. J., Challis, R. E., "Combined Compression and Shear Wave Ultrasonic Measurements on Curing Adhesive", *Measurement Science & Technology*, **9**, 148, (1998)

Frigione, M., Maffezzoli, A., Acierno, A., Luprano, V.A.M., Montagna, G., "Non-destructive and in-situ Monitoring of Mechanical Property Build-Up in Epoxy Adhesives for Civil Applications by Propagation of Ultrasonic Waves", *Polymer Engineering and Science*, **40**, 656, (2000)

Gemant, A., "The Measurement of Solid Frictions of Plastics: Friction in Solids", *Journal of Applied Physics*, **11**, 647, (1940)

Gillham, J. K., "The Time-Temperature-Transformation (TTT) State Diagram" in the Role of the Polymeric Matrix in the Processing and Structural Properties of Composite Materials", Edts. Seferis, J.C., Nicolais, L., *Plenum Press, New York and London*, (1988)

Gillham, J. K., "Formation and Properties of Network Polymeric Materials", *Polymer Engineering and Science*, **19**, 676, (1979)

Gordon, M., Scantlebury, G. R., "The Theory of Branching Processes and Kinetically Controlled Ring–Chain Competition Processes", *Journal of Polymer Science: Part C,* **16,** 3933, (1968)

Guibe, C., Frabcillette, J., "Time-Temperature-Transformation (TTT) Cure Diagrams: Relationships between T_g, Cure Temperature, and Time for DGEBA/DETA Systems", *Journal of Applied Polymer Science*, **62**, 1941, (1996)

Harismendy, I, Gomez, C. M., Del Rio, M., Mondragon, I., "Cure Monitoring of Catalysed Cyanate Ester Resins", *Polymer International*, **49**, 735, (2000)

Hartmann, B., Jarzynski, J., "Ultrasonic Hysteresis Absorption in Polymers", *Journal of Applied Physics*, **43**, 4304, (1972)

Höhne, G. W. H., Hemminger, W. F., Flammersheim, H. J., "Differential Scanning Calorimetry", *Springer-Verlag Berlin*, (2003)

Hou, T.H., Huang, J. Y. Z., Hinkley, J. A., "Chemorheology of an Epoxy Resin System under Isothermal Curing", *Journal of Applied Polymer Science*, **41**, 819, (1990)

Hoffman, M., Krömer, H., Kuhn, R., "Polymeranalytik", *George Thieme Verlag*, *Stuttgart*, (1977)

Hueter, T. F., Bolt, R. H., "Sonics: Techniques for the use of Sound and Ultrasound in Engineering and Science", *John Wiley and Sons, Inc*, (1955)

Ivey, D.G, Mrowca, B.A., Guth, E., "Propagation of Ultrasonic Bulk Waves in High Polymers", *Journal of Applied Physics*, **20**, 486, (1949)

Karkanas, P. I., Partridge, I. K., Attwood, D., "Modelling the Cure of a Commercial Epoxy Resin for Applications in Resin Transfer Moulding", *Polymer International,* **41,**183, (1996)

Karkanas, P. I., "Cure Modelling and Monitoring of Epoxy/Amine Resin Systems", PhD Thesis, *Cranfield University, England,* (1998)

Karkanas, P. I., Partridge, I. K., "Cure Modelling and Monitoring of Epoxy/Amine Resin Systems:I. Cure Kinetics Modeling", *Journal of Appl. Polym. Sci.*, **77**, 1419, (2000a)

Karkanas, P. I., Partridge, I. K., "Cure Modelling and Monitoring of Epoxy/Amine Resin Systems: II. Network Formation and Chemoviscosity Modelling", *Journal of Appl. Polym. Sci.*, **77**, 2178, (2000b).

Karrenberg, U., "Signale Prozesse Systeme", 2. Auflage, *Springer Verlag, Berlin, Heidelberg, New York*, (2001)

Kolsky, H., "Stress Waves in Solids", *Dover Publications, New York*, (1963)

Kono, R., "The Dynamic Bulk Viscosities of Polystyrene and Polymethylmethacrylate", *Journal of the Physical Society of Japan*, **15**, 718, (1960)

Kono, R., "The Dynamic Bulk and Shear Viscosities of PVC", *Journal of the Physical Society of Japan*, **16**, 1793, (1961)

Kroll, J., Alshuth, T., Shuster, R. H., "Dynamische Moduli von Elastomeren in Ultraschall und Dynamisch-Mechanischer-Analyse" *Kautschuk, Gummi, Kunststoffe*, **4**, 49, (2006)

Krautkrämer, J., Krautkrämer, H., "Werkstoffprüfung mit Ultraschall", *Springer Verlag, Berlin*, (1986)

Landi, V.R., "Determining the Cure of Phenolics by Ultrasonic Sound Transmission during Molding", *1ˢᵗ Tagung der Arbeitsgemeinschaft verstärkter Kunststoffe-Technische Vereinigung (AVK-TV)*, *Baden-Baden, Germany*, (1998)

Lange, J., Altmann, N., Kelly, C.T., Halley, P. J., "Understanding Vitrification during Cure of Epoxy Resins using Dynamic Scanning Calorimetry and Rheological Techniques", *Polymer*, **41**, 5949, (2000)

Leaderman, H., "Elastic and Creep Properties of Filamentious Materials and other High Polymers", *The Textile Foundation*, *Washington*, (1943)

Li, G., Lee-Sullivan, P., Thring, R.W., "Determination of the Activation Energies for Glass Transition of an Epoxide Adhesive using Dynamic Mechanical Analysis", *Journal of Thermal Analysis and Calorimetry*, **60**, 377, (2000)

Lionetto, F., Maffezzoli, A*.,* "Relaxations during the Postcure of Unsaturated Polyester Networks by Ultrasonic Wave Propagation, Dynamic Mechanical Analysis, and Dielectric Analysis", *Journal of Polymer Science Part B*, **43**, 596, (2004a)

Lionetto, F., Rizzo, R., Luprano, V. A .M., Maffezzoli, A*.,* "Phase Transformations during the Cure of Unsaturated Polyester Resins", *Materials Science and Engineering A,*" **370**, 284, (2004b)

Love, A. E. H., "Mathematical Theory of Elasticity", *Cambridge University Press, London*, (1927)

Maeda, Y., "Ultrasonic Studies of high Polymers", *Journal of Polymer Science*, **18**, 87, (1955)

Maffezoli, A., Quarta, E., Luprano, A. M., Montagna, G., Nicolais, L., " Cure Monitoring of Epoxy Matrices for Composites by Ultrasonic Wave Propagation", *Journal of Applied Polymer Science,* **73**, (1999)

Mettler Toledo, "DMA Application Notes: DMA Glass Transition Compared to DSC", www.Thermal-Easy.com

McCrum, N. G., Read, B. E.,Williams. G, "Anelastic and Dielectric Effects in Polymeric Solids", *John Wiley and Sons, Inc. New York*, (1967)

Mc Hugh, J., Döring, J., Stark, W., Guey, J. L., "Relationship between the Mechanical and Ultrasound Properties of Polymer Materials", *9th European Conference on NDT*, *Deutsche Gesellschaft für Zerstörungsfreie Prüfung e.V Berlin*, (2006)

Mc Hugh, J., Döring, J., Bartusch, J., "EU Project: Phased Array Ultrasonic Transducers for Inspection of Tubing: Project Report on Materials Selection, *PROJECT N^{O}: GRD1-2001-4053"1, Acronym: PharusIT*, (2005)

Mc Hugh, J., Döring, J., Stark, W., "Einsatz der Ultraschalltechnik bei der Produktion von Faserverbundteilen", *Deutsche Gesellschaft für Zerstörungsfreie Prüfung: Jahrestagung DGZfP, Mainz,* (2003)

Mc Hugh, J., Stark, W., Döring, J., "Evaluation of the Cure Behaviour of Epoxy Resin Using Rheometric and Ultrasonic Techniques", Nondestructive Characterization of Materials XI (2003), 651-658; Edt. Robert E. Green, *Springer-Verlag,* (2003)

Mc Hugh, J., "Ultrasonic Process Monitoring for Thermosetting Polymers", MSc Research Thesis, *SIMS, Cranfield University, Cranfield, England*, (2001)

McIntire, P., "Nondestructive Testing Handbook-Ultrasonic Testing", 2nd Edition, **7**, *American Society for Nondestructive Testing*, (1991)

McSkimin H. J, "Ultrasonic methods for measuring the mechanical properties of liquids and solids" *Physical Acoustics* vol 1, edt. Warren P. Mason, *New York: Academic* (1964)

Mijovic, J, Lee, C. H., "Modelling of Chemorheology of Thermoset Cure by Modified WLF Equation", *Journal of Applied Polymer Science*, **37**, 889, (1989)

Murayama, T, "Dynamic Mechanical Analysis of Polymer Material", *Elsevier North Holland*, (1978)

Nguyen, N. T., Lethiecq, M., Gerard, J. F.,"Glass Transition Characterisation of Homogenous and Heterogenous Polymers by an Ultrasonic Method", *Ultrasonics*, **33**, 323, (1995)

Nolle, A. W., "Acoustic Determination of the Physical Properties of Rubber-like Materials" *J. Acoustic Society of America*, **19**, 194, (1946)

Nolle, A. W., Mowry, S.C., "Measurement of Ultrasonic Bulk-Wave Propagation in High Polymers", *J. Acoustical Society of America,* **20**, 432, (1948)

Nolle, A. W., Sieck, P. W., "Longitudinal and Transverse Ultrasonic Waves in a Synthetic Rubber", *J. Applied Physics,* **23**, 888, (1952)

North, A.M., Pethrick, R. A., Philips, D. W., "Ultrasonic Studies of solid poly(akyl methacrylates)", *Polymer*, **18**, 324, (1977)

Nunez-Regueira, L., Gracia-Fernandez, C. A., Gomez-Barreiro, S., "Use of Rheology, Dielectric Analysis for Gel Time Determination of a Thermoset", **46**, 5979, (2005)

Ochi, M., Okazaki, M., Masaki, S., "Mechanical Relaxation of Epoxide Resins Cured with Aliphatic Diamines", *Journal of Polymer Science*, **20**, 689, (1982).

O' Connell, P. A., Mc Kenna, G. B., "Arrhenius Type Temperature Dependence of the Segmental Relaxation below Tg", *Journal of Chemical Physics*, **110**, 11054, (1999)

O'Donnell, M., Jaynes, E.T., Miller J. G., "Kramers-Kronig Relationship between Ultrasonic Attenuation and Phase Velocity", *Journal of the Acoustical Society of America*, **69**, 696, (1981)

Papadakis, E.P., "Monitoring the Moduli of Polymers with Ultrasound", *Journal of Applied Physics*, **45**, (1974)

Parthun, M.G., "Dynamics of a Molecules Growth: Ultrasonic Relaxation Studies", *Journal of Chemical Physics*, **15**, 6301, (1994).

Parthun, M.G., Johari, "Dynamics of a Molecules Growth: Ultrasonic Relaxation Studies", *Journal of Chemical Physics*, **102**, 6301, (1995)

Pethrick, R.A., "Ultrasonic Studies of Macromolecules", *Prog. Polymer Science*. **9**, 197-295, (1983)

Pain, H.J., "The Physics of Vibrations and Waves", 4th Edition, *Wiley & Sons, New York*, (1993)

Ping, H., "Direct Measurement of Ultrasonic Dispersion using a Broadband Transmission Technique", *Ultrasonics*, **37**, 67, (1999)

Pindenelli, C., Montagna, G., Luprano, V. A. M., Maffezoli, A., "Network Development During Epoxy Curing: Experimental Ultrasonic Data and Theoretical Predictions", *Macromoles Symp.*, **180**, 73, (2002)

Rabinowitch, E., "Collision, Co-ordination, Diffusion and Reaction Velocity in Condensed Systems", *Transactions Faraday Society,* **33**, 1225, (1937)

Rath, M., Döring, J., Stark, W., Hinrichsen, G., "Process Monitoring of Moulding Compounds by Ultrasonic Measurements in a Compression Mould", *NDT&E International*, **33,** 123, (2000)

Rawabdeh, I. A., Petersen, P. F., "In-line Ultrasonic Monitoring of Injection Moulding Operations: A literature Review", *Journal Injection Molding Technology*, **3,** 47, (1999)

Retting, W., "Mechanik der Kunststoffe", *Hanser Verlag, München*, (1990)

Richeton, J., Schlatter, G., Vecchio, K. S., Remond, Y., Ahzi, S., "A Unified Model of the Stiffness of Amorphous Polymers across Transition Temperatures and Strain Rates", *Polymer*, **46**, 8194, (2005)

Sachse, W., Pao, Y-H., "On the determination of Phase and Group Velocities of Dispersive Waves in Solids", *Journal of Applied Physics*, **49**, 4320, (1978)

Rohklin, S. I., Lewis, D. I., Graff, K. F., Laszlo, A., "Real-Time Study of Frequency Dependence of Attenuation and Velocity of Ultrasonic Waves During the Curing Reaction of Epoxy Resin", *Journal of the Acoustical Society of America*, **79**, 1786, (1986)

Rieger, J., "The Glass Transition Temperature Tg of Polymers – Comparison of the values from Differential Thermal Analysis (DTA, DSC) and Dynamic Mechanical Measurements", *Polymer Testing,* **20**, 199, (2001)

Sahoune, A., Massine, F., Piche, L., "Ultrasonic Measurement of Relaxation Behaviour in Polystyrene", *Journal of Polymer Science: Polymer Physics*, **34**, 341, (1996)

Schmachtenberg, E., Töpker, J., Bartusch, J., Mc Hugh, J., "Online-Prozesskontrolle bei der Herstellung von Faserverbundkunststoffen", *GAK: Gummi, Fasern, Kunststoffe,* **56**, 84, (2003)

Schnorrenberg, W., "Messen und Testen: Frequenzanalyse durch FFT", *Elektronik*, 26, **54**,(1989)

Kremer, F., Schönhals, A. "Broadband Dielectric Spectroscopy" *Springer Verlag, Heidelberg, Germany,* (2002)

Shephard, D. D., Smith, K. R., "A Complete Ultrasonic Measurement System for In-Process Cure Monitoring and Control of Composites", http://www.ndt.net/article/aero1197/shephard/shephard.htm, (1997)

Shimbo, M., Ochi, M., Iesako, H., "Mechanical Relaxation of Epoxide Resins Cured with Acid Anhydrides, *Journal of Polymer Science: Polymer Physics Edition*, **22**, 1461, (1984)

Simon, S. L., Gilham, J. K., „Reaction Kinetics and TTT Cure Diagrams for Off-Stoichiometric Ratios of a High Tg Epoxy/Amine System", *Journal Applied Polymer Science*, **46**, 1245, (1992)

Skordos, A.A., "Modelling and Monitoring of Resin Transfer Moulding", PHD Thesis, *Cranfield University, Bedfordshire, England*, (2000)

Smythe, C., Kudryashov, E.D., Buckin, V., "High frequency shear and viscoelastic moduli measurement of casein particle Gel", *Colloids and Surfaces*, **183**, 517, (2001)

Sourour, S., Kamal, M. R., "Differential Scanning Calorimetry of Epoxy Cure: Isothermal Cure Kinetics", *Thermochemica Acta*, **14**, 41, (1976)

Sperling, L. H., "Introduction to Physical Polymer Science", 2nd Edition, *New York-Chichester, John Wiley & Sons Inc.*, (1992)

Starkweather, H. W., "Distribution of Activation Enthalpies in Viscoelastic Relaxations", *Macromolecules*, **23**, 328, (1993)

Stark, W., Döring, J., Kelm, J., "Measuring the State of Cure of Elastomers by using an Ultrasonic Technique" *Kautschuk-Gummi-Kunststoffe KGK,* (2002)

Stark, W., Döring, J., McHugh, J., Rath, M., "Fließ-härtungsverhalten von vernetzenden Systemen- das neue BAM Verfahren im kritischen Vergleich", *2. Int. Jahrestagung der AVK/TV, Baden-Baden, Tagungsband,* (1999)

Stark, W., "Thermoanalytische Charakterisierung Duroplastischer Formassen", *Materialprüfung*, **41**, 115, (1999b)

Stark, W., Döring, J., "Aushärtung von Duroplasten mit Ultraschall messen", *Materialprüfung*, **39**, 308, (1997)

Starke, C., "Ultraschall- Analyse des Formteilbildungsprozesses beim Thermoplast- Spritzgießen", PhD Thesis, *Institut für Kunststoffverarbeitung, Aachen*, (2005)

Straet, T., Bayerl., H., Stark, W., Kürten, C., "Ultraschallmessungen an Duroplastischen Formassen", *Kunststoffe*, **7**, 73, (2005)

Strobl, G., "The Physics of Polymers", *Springer Verlag, Berlin Heidelberg*, (1996)

Stutz, H., Mertes, J., Neubecker, K., "Kinetics of Thermoset Cure and Polymerisation in the Glass Transition Region", *Journal of Polymer Science: Part A*, **13**, 1879, (1933)

Sutherland, H. J., Lingle, R., "An Acoustic Characterization of Polymethylmethacrylate and Three Epoxy Formulations", *Journal of Applied Polymer Physics*, **43**, 4022, (1972)

Teil, H., Page, S. A., Michaud, V., Manson J-A. E., "TTT Cure Diagram of an Anhydride- Cured Epoxy System Including Gelation, Vitrification, Curing Kinetics Model and Monitoring of the Glass Transition Temperature", *Journal of Applied Polymer Science*, **93**, 1774, (2004)

Ting, S., Sachse, W., "Measurement of Ultrasonic Dispersion by Phase Comparison of Continious Harmonic Waves", *Journal Acoustic Society of America*, **64**, 852, (1978)

Tobolsky, A.V., Catsiff, E., "Elastoviscous Properties of Polyisobutylene (and other amorphous polymers) from Stress-Relaxation Studies: IX. A Summary of Results", *Journal of Polymer Science*, **19**, 111, (1956)

Vogel, K., "Untersuchung der Spannungsrelaxations-verhaltens von Hochpolymeren Kunststoffen bei verschiedene einfachen Beanspruchungsarten", Dissertation im Naturwissenschaften, *TH-Braunschweig*, (1966)

Waterman, H. A., "Determination of the Complex Moduli of Viscoelastic Materials with the Ultrasonic Pulse Method (Part 1 & Part 2), *Kolloid-Zeitschrift & Zeitschrift für Polymere*, **192**, 1-16, (1963)

Waterman, H. A., "Relations between Loss Angles in Isotropic Viscoelastic Materials", *Rheologica Acta*, **16**, 31, (1977)

Wen, S.-S. L, Jen, C. K., Nguyen, K. T., "Advances in On-line Monitoring of the Injection Moulding Process using Ultrasonic Techniques", *International Polymer Processing XIV*, **2**, 175, (1999)

Williams, P. R., William, R. L.,"Rheometrical Aspects of the viscoelastic dispersion of shear waves in gel-like mechanical networks", Journal of Newtonian Fluid Mechanics, **78**, 203, (1998)

Williams, M. L., Landel, R. F., Ferry, J. D., "The Temperature Dependence of Relaxation Mechanisms in Amorphous Polymers and other Glass-forming Liquids*", Journal American Chemical Society*, **77**, 3701, (1955)

Wintle, H. J., "Kramer-Konig Analysis of Polymer Acoustic data", Journal *of Applied Physics*, **85**, 44, (1999)

Winter, H. H., "Can the Gel Point of a Cross-linking Polymer be Detected by the G´-G´´ Cross-Over?", *Polymer Engineering Science*, **27**, 1698, (1987)

Winter, H. H., Mours, M., "Rheology of Polymers Near Liquid-Solid Transitions", *Advances in Polymer Science*, **134**, 166, (1997)

Witte, R. S., Mrowca, B.A., Guth, E., "Propagation of Audiofrequency Sound in High Polymers" *Journal of Applied Physics*, **20**, 481, (1949)

Wisanrakkit, G., Gillham, J. K., "The Glass Transition Temperature (Tg) as an Index of Chemical Conversion for a High Tg Amine Epoxy System: Chemical and Diffusion Controlled Reaction Kinetics", *Journal of Applied Polymer Scence,* **41**, 2885, (1990)

Wise, C. W., Cook, W. D., Goodwin, A.A., "Chemico-Diffusion Kinetics of Model Epoxy-Amine Resins", *Polymer*, **38**, 3251, (1997)

Yoon, S. S., Yu, W. J., Kim, H. C., "Phase Transition of Epoxy Resin during Isothermal Curing Monitored by Ultrasonic Velocity Measurements", *Journal Materials Science Letters*, **11**, 1392, (1992)

Zellouf, D., Jayet, Y., Saint-Pierre, N., Tatibouet, J., Baboux, J. C., "Ultrasonic Spectroscopy in Polymeric Materials: Application of the Kramers-Konig Relations", *Journal of Applied. Physics,* **80**, 2728, (1996)